Oncology and Translational Medicine

Volume 8 • Number 5 • October 2022

Oncology and Translational Medicine Volume 8 • Number 5 • October 2022 pp 209-266

邮发代号：38-121
ISSN 2095-9621

GENERAL INFORMATION
≫otm.tjh.com.cn

ISSN 2095-9621
CN 42-1865/R

Oncology and Translational Medicine

肿瘤学与转化医学（英文）

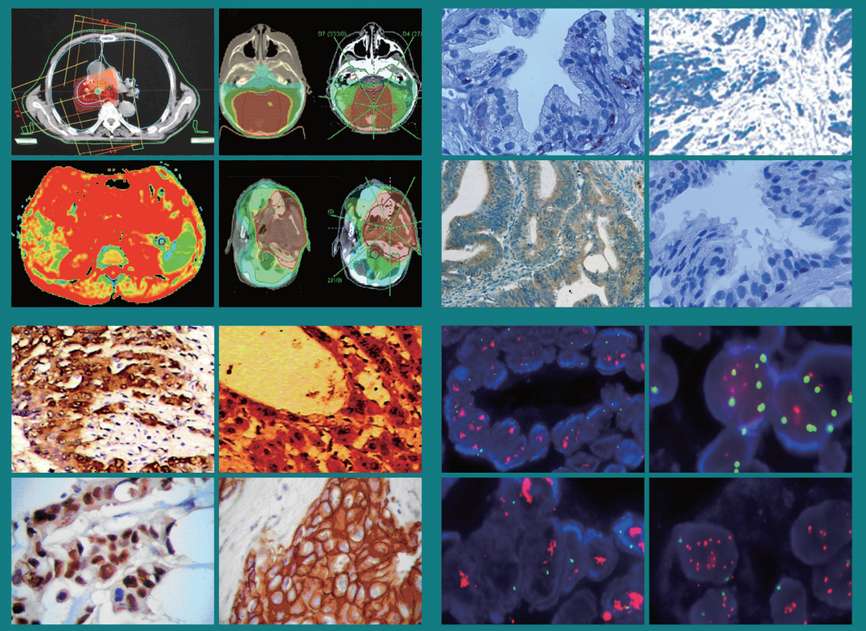

Volume 8
Number 5
October 2022

Oncology and Translational Medicine

Oncology and Translational Medicine
October 2022 Volume 8 Number 5

Contents

Oncology and Translational Medicine

Volume 8 • Number 5 • October 2022

Aims & Scope

Oncology and Translational Medicine is an international professional academic periodical. The Journal is designed to report progress in research and the latest findings in domestic and international oncology and translational medicine, to facilitate international academic exchanges, and to promote research in oncology and translational medicine as well as levels of service in clinical practice. The entire journal is published in English for a domestic and international readership.

Copyright

Supervised by

Ministry of Education of the People's Republic of China.

Administered by

Tongji Medical College, Huazhong University of Science and Technology.

Submission information

Manuscripts should be submitted to:
http://otm.tjh.com.cn
dmedizin@sina.com

Subscription information

ISSN edition: 2095-9621
CN: 42-1865/R

■ Subscription rates
Subscription may begin at any time. Remittances made by check, draft or express money order should be made payable to this journal. The price for 2022 is as follows: US $ 30 per issue; RMB ￥28.00 per issue.

Database

Oncology and Translational Medicine is abstracted and indexed in EMBASE, Index Copernicus, Chinese Science and Technology Paper Citation Database (CSTPCD), Chinese Core Journals Database, Chinese Journal Full-text Database (CJFD), Wanfang Data; Weipu Data; Chinese Academic Journal Comprehensive Evaluation Database.

Business correspondence

All matters relating to orders, subscriptions, back issues, offprints, advertisement booking and general enquiries should be addressed to the editorial office.

Mailing address
Editorial office of
Oncology and Translational Medicine
Tongji Hospital
Tongji Medical College
Huazhong University of Science and Technology
Jie Fang Da Dao 1095
430030 Wuhan, China
Tel.: +86-27-69378388
Email: dmedizin@sina.com

Printer
Changjiang Spatial Information Technology Engineering Co., Ltd. (Wuhan) Hangce Information Cartorgraphy Printing Filial, Wuhan, China
Printed in People's Republic of China

Editors-in-Chief

Managing director

Executive editors

Oncology and Translational Medicine
DOI 10.1007/s10330-022-0582-2

October 2022, Vol. 8, No. 5, P209–P216

ORIGINAL ARTICLE

Differential centrifugation enhances the anti-tumor immune effect of tumor lysate-pulsed dendritic cell vaccine against glioblastoma*

Xiaojin Liu, Yiwei Qi (Co-first author), Feng Hu, Kai Shu, Ting Lei (✉)

Sino-German Neuro-Oncology Molecular Laboratory, Department of Neurosurgery, Tongji Hospital, Tongji Medical College, Huazhong University of Science and Technology, Wuhan 430030, China

Abstract

Objective This study aimed to improve the antitumor immunocompetence of a tumor lysate-pulsed dendritic cell (DC) vaccine through differential centrifugation and provide a theoretical basis for its clinical application in glioblastoma.

Methods Peripheral blood mononuclear cells were extracted using Ficoll-Paque PLUS and induced into mature DCs *in vitro* with a cytokine cocktail. The modified tumor lysate was generated by differential centrifugation. The maturity markers of DCs in each group, namely the modified tumor lysate, tumor lysate, and negative and positive control groups, were assessed using flow cytometry. Furthermore, their ability to stimulate lymphocyte proliferation and *in vitro* antitumor effects were assessed using Cell Trace TM CFSE. IFN-γ secretion levels were measured with ELISA. Intracellular reactive oxygen species were measured using 2',7'-dichlorofluorescein diacetate (DCFDA) staining. The results were statistically analyzed using an unpaired Student's *t*-test and were considered significant at $P < 0.05$.

Results Compared with tumor lysate-pulsed DCs, modified tumor lysate-pulsed DCs had a higher expression of maturity markers: CD1a (7.38 ± 0.53% *vs*. 4.47 ± 0.75%) and CD83 (19.81 ± 4.09% *vs*. 9.64 ± 1.50%), were better capable of stimulating lymphocyte proliferation [proliferation index (PI): 8.54 ± 0.16 *vs*. 7.35 ± 0.05], secreting IFN-γ, and inducing stronger *in-vitro* cytotoxic T lymphocyte (CTL) cytotoxicity against glioblastoma cells. In addition, we found that the level of ROS in modified tumor lysate-pulsed DCs was lower than that in tumor lysate-pulsed DCs.

Conclusion Differential centrifugation of tumor lysates can improve the antitumor immunocompetence of DC vaccines, and reactive oxygen species may be the key to affecting DC function in the whole tumor lysate.

Received: 15 June 2022
Revised: 17 August 2022
Accepted: 22 September 2022

Key words: glioblastoma; immunotherapy; dendritic cell (DC) vaccine; reactive oxygen species

Glioblastoma is the most common primary malignant tumor of the central nervous system with an annual incidence rate of 3–5/100 000 and a poor prognosis of 14.6 months, accounting for about 50% of all gliomas [1–2]. Although there are numerous studies on glioblastoma, the anatomical location of the central nervous system limits the application of locoregional treatment. In addition, the tumor is characterized by endogenous radio- and chemoresistance, heterogeneity, and an immunosuppressive microenvironment; these factors limit the progress of glioblastoma treatment. The standard treatment is to safely maximize surgical resection with adjuvant radiotherapy and chemotherapy [3–4]. Other adjuvant treatments include tumor treating fields, immunotherapy, gene therapy, and molecular targeted therapy, among which immunotherapy has great potential in the treatment of glioblastoma.

As the most effective antigen-presenting cells, dendritic cells (DCs), bridge the innate and adaptive immune system [5–7]. DCs are cultured *in vitro* for maturation, sensitized with tumor-associated antigens or tumor-specific antigens, and then injected back into

✉ Correspondence to: Ting Lei. Email: tlei@tjh.tjmu.edu.cn
* Supported by the National Natural Science Foundation of China (No. 81602202 and 82173136).

the patient to elicit an antitumor immune response [8–11]. Many clinical studies have shown that DC vaccines are safe and rarely have autoimmune-related side effects, but their clinical efficacy remains limited [12–15]. Therefore, maximizing the effectiveness of DC vaccines is a hot topic in the field of immunotherapy. Considering the tumor heterogeneity of glioblastoma, it is difficult to induce an effective antitumor immune response by sensitizing DCs with a single antigen. Although tumor lysates contain multiple epitopes of tumor antigens, many components released from tumor cell lysis may inhibit DC maturation, thereby affecting their ability to effectively present antigens. Most studies have improved the anti-tumor immune effect of the DC vaccine through combination with immune adjuvants [16–18] but few have attempted to eliminate the possible components of whole tumor lysate that may inhibit the maturation of DCs to improve the clinical efficacy of DC vaccines.

Reactive oxygen species is a collective term for the superoxide anion (O_2^-), hydroxyl radical (HO•), and hydrogen peroxide (H_2O_2), which are mainly released from the electron transport chain in the mitochondria and membrane-bound NADPH oxidase complexes (NOXs). They are involved in the pathogenesis of many diseases such as tumors, aging, diabetes, neurodegenerative diseases, and atherosclerosis [19]. Many studies have shown that reactive oxygen species have a sophisticated effect on the function of DCs and can elicit bidirectional regulation of their maturation. Studies have shown that the reactive oxygen species in the tumor microenvironment can induce endoplasmic reticulum stress in ovarian tumor-associated DCs, causing abnormal deposition of lipid peroxides in DCs, resulting in a decrease in their ability to activate T cells, leading to immune tolerance [20]. Oxidized lipid products can affect antigen presentation by DCs, subsequently compromising their ability to stimulate adaptive immunity [21–22].

Differential centrifugation is a well-developed biological method for separating organelles, through which organelles with differences in sedimentation coefficients are separated from each other. We attempted to sequentially remove the main sources of reactive oxygen, including mitochondria, lysosomes, and peroxisomes, from the whole tumor lysate through differential centrifugation, reducing the level of reactive oxygen species in DCs sensitized by tumor lysate to boost their maturity. We found that modified tumor lysate-pulsed DCs have a higher expression of surface markers, such as CD1a and CD83, which are more capable of stimulating lymphocytes and inducing stronger *in vitro* cytotoxic T lymphocyte (CTL) cytotoxicity against glioblastoma cells.

Materials and methods

Cell culture

The glioma cell lines U87 and U251 were cultured in DMEM supplemented with 10% FBS, 2 mM l-glutamine, 100 units/ml penicillin, and 100 μg/mL streptomycin.

In vitro generation of human monocyte-derived DCs

Peripheral blood mononuclear cells (PBMCs) were obtained from healthy donor blood using Ficoll-Paque PLUS according to the manufacturer's instructions. The cells were incubated for 2 h at 37 °C at a concentration of 5×10^6 cells/mL in RPMI 1640 (Gibco, NY, USA). Non-adherent cells were removed, and adherent PBMCs were cultured in RPMI 1640 supplemented with 10% FBS, 2 mM L-glutamine, 100 units/mL penicillin, 100 μg/mL streptomycin, recombinant human granulocyte-macrophage colony-stimulating factor /rhGM-CSF (800 units/mL; R&D system, MN, USA), and recombinant human interleukin (IL)-4 /rhIL-4 (400 units/mL; R&D). DCs were activated by lipopolysaccharide (LPS; 0.5 μg/mL) and TNF-α (200 units/mL).

Tumor lysate preparation and DC loading

Glioma cell lines were harvested, washed twice in PBS, and resuspended at a density of 2×10^6 cells/mL in serum-free medium. The cell suspensions were frozen at 80 °C and thawed at 37 °C for four freeze-thaw cycles. To remove cell debris, the lysate was centrifuged at 1000 × *g* for 10 min. The supernatant was collected as a classic tumor lysate and passed through a 0.2 μm filter. The modified tumor lysate was prepared by differential centrifugation. Briefly, the lysate was centrifuged at 1000 × *g* for 10 min to remove debris and cell nuclei, the supernatant centrifuged at 10000 × *g* for 10 min to remove mitochondria, then at 15300 × *g* for 20 min to remove lysosomes and peroxisomes. Finally, the supernatant was collected as a modified tumor lysate containing microvesicles and soluble proteins. The protein concentration of the lysate was determined using the BCA kit (NCM Biotech, Suzhou, China). DCs were pulsed with the tumor lysate and modified tumor lysate at a concentration of 100 μg/mL.

Flow cytometric analysis

DCs and lymphocytes were removed from the plate and centrifuged at 1500 × *g* for 5 min. The pelleted cells were washed with RPMI-1640 and incubated at 4 °C for 30 min with FITC-anti-CD1a (catalog No. 300103), FITC-anti-CD83 (catalog No. 305305), PE/CY5-anti-CD86 (catalog No. 305407), PE-anti-HLA-DR (catalog No. 307605), and PE-anti-CD3 (catalog No. 300309), PE-anti-CD4 (catalog No. 317409), FITC-CD8 (catalog No. 344703). Species-

and isotype-matched monoclonal antibodies were used as controls. All antibodies were purchased from BioLegend, San Diego, CA, USA. The cells were washed twice with PBS and analyzed using a FACSort flow cytometer (BD Bioscience, San Jose, CA, USA). Flow cytometry data were analyzed using FlowJo v.9 (TreeStar, Ashland, OR).

Proliferative T cell response and cytokine measurement

Human blood samples were collected from healthy donors under the principles of the ethical committee of Tongji Hospital, Tongji Medical College, Huazhong University of Science and Technology, China. PBMCs were isolated by Ficoll-Paque PLUS density gradient centrifugation and depleted of red blood cells using ammonium chloride. The cells were incubated for 2 h at 37 °C at a concentration of 5×10^6 cells/mL in RPMI 1640 (Gibco, NY, USA). Non-adherent cells were collected and cultured in RPMI 1640 medium supplemented with 10% FBS, 100 units/mL penicillin, 100 μg/mL streptomycin, and 100 U/mL IL-2 (R&D system, MN, USA). These cells were co-cultured with autologous DCs in four parallel groups consisting of PBS-pulsed, LPS-pulsed, tumor lysate-pulsed, or modified tumor lysate-pulsed DCs at a ratio of 10:1 in RPMI 1640 culture medium containing IL-2 (50 U/mL). On day 5, the culture media were collected for the measurement of IFN-γ secretion using an ELISA kit (Proteintech, Rosemont, IL, USA). The capacity of the DC-induced proliferative T cell response was determined using Cell Trace™ CFSE (Invitrogen, Waltham, MA, USA) according to the manufacturer's instructions.

Determination of CTL cytotoxicity

After DC-T cell co-culture, the cells were collected as effector cells on day 5. The glioma cell lines U87 and U251 were labeled with CFSE (Invitrogen, Waltham, MA, USA), cultured in 6-well plates, and used as target cells for cytotoxicity assays. After 24 h, the medium was removed, and effector cells were added to CFSE-labeled target cells at an E:T ratio ["E" means effector cells (CTLs), "T" means target cells (U87 and U251)] of 50:1 in RPMI 1640 supplemented with 10% FBS, 100 units/mL penicillin, 100 μg/mL streptomycin, and 100 U/ml IL-2 (R&D system, MN, USA).

Measurement of ROS

Intracellular ROS was measured using 2',7'-dichlorofluorescein diacetate (DCFDA) staining (Abcam, Cambridge, UK) according to the manufacturer's instructions.

Statistical analysis

All statistical analyses were performed using GraphPad Prism 5.0 (GraphPad Software Inc., CA, USA). Differences between the means of experimental groups were statistically compared using unpaired Student's *t*-test, and significance was set at $P < 0.05$.

Results

DC morphology and expression of surface markers

Human blood mononuclear cells were induced and cultured *in vitro*. Small adherent round mononuclear cells and precursor cells were visible on day 2 under an inverted phase contrast microscope (Fig. 1a) and had a low expression of surface molecules such as CD1a (2.78 ± 0.88%), CD83 (3.74 ± 0.93%), and CD86 (50.70 ± 0.98%) (Fig. 1c and 1e). As the stimulation time increased, the cells became irregular, bulged, and larger. Around the 5th day, DC colonies began to form. The cell volume continued to grow and the bulges became more prominent. At this time, the cells remained immature. After stimulation with LPS and TNF-α for 24–48 h, the DCs were gradually separated from the colonies, presenting an irregular morphology of increased volume and elongated bulge. The PBMCs were finally induced into mature irregular DCs with clear protrusions *in vitro* on day 7 (Fig. 1b), which had a higher expression of CD1a (7.43 ± 0.44%), CD83 (18.16 ± 5.91%), and CD86 (92.35 ± 2.56%) (Fig. 1d and 1e).

Upregulation of maturation markers on modified tumor lysate-primed DCs

Through differential centrifugation, the tumor lysate was modified to contain microvesicles and soluble proteins (Fig. 2a). DCs were loaded with tumor lysate, modified tumor lysate, PBS (negative control group), and LPS (positive control group) on day 5. The expression of surface markers on DCs stimulated by different antigens was analyzed by flow cytometry on day 7. The result showed that the modified tumor lysate-pulsed DCs had a significantly higher expression of CD1a (7.38 ± 0.53% *vs.* 4.47 ± 0.75%) and CD83 (19.81 ± 4.09% *vs.* 9.64 ± 1.50%), compared with that of the tumor lysate group. CD86 (92.07 ± 0.355% *vs.* 91.72 ± 1.748%) and HLA-DR (98.04 ± 2.02% *vs.* 95.19 ± 2.06%) remained at a high level, and there was no statistical significance between the two groups (Fig. 2b).

Modified tumor lysate-pulsed DCs stimulated lymphocyte proliferation and secretion of IFN-γ

Lymphocytes were successfully isolated from PBMCs and identified using flow cytometry (Fig. 3a–3c). To measure proliferative T cell responses, we co-cultured T cells with DCs for 1, 3, and 5 d. We found that T cells

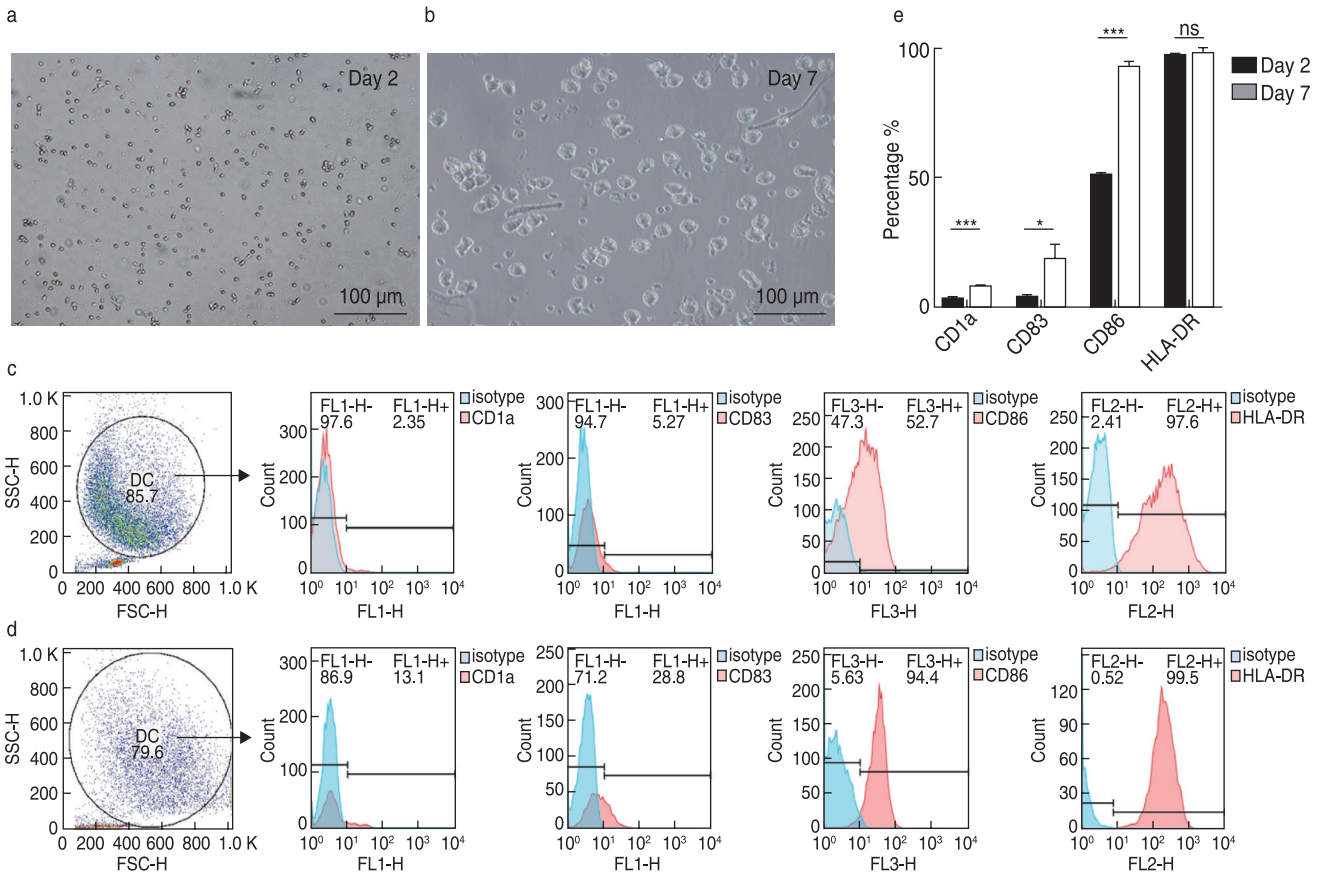

Fig. 1 Dendritic cell (DC) morphology and surface markers. (a) and (b) show DC morphology on Day 2 and Day 7, respectively. (c) and (d) represent the expression of DC surface markers (CD1a, CD83, CD86, and HLA-DR) on Day 2 and Day 7, respectively. (e) represents the statistic histogram of the expression of DC surface markers. Scale bar = 100 μm. * $P < 0.1$; ** $P < 0.01$; *** $P < 0.001$

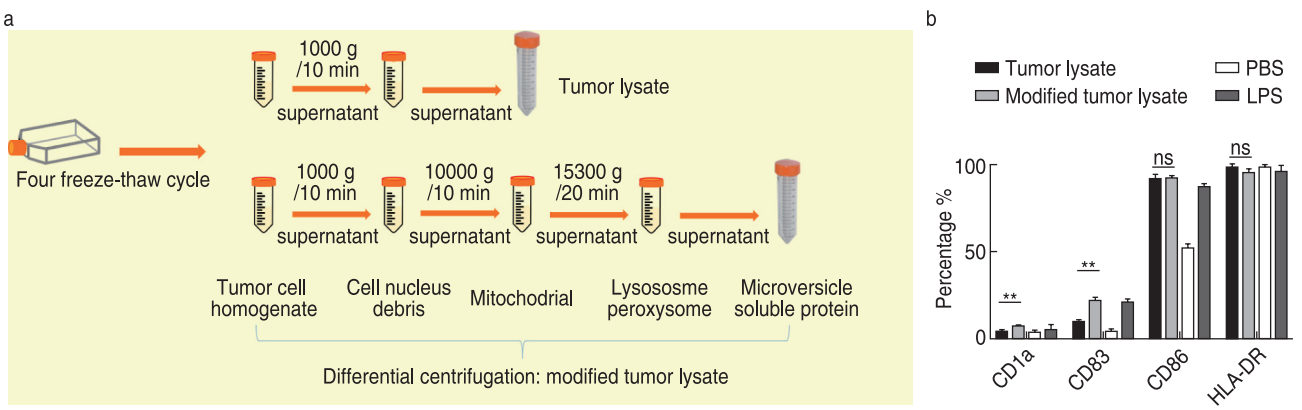

Fig. 2 Upregulation of maturation markers in modified tumor lysate-primed DCs. (a) illustrates the preparation of the modified tumor lysate through differential centrifugation. (b) shows that modified tumor-lysate-primed DCs have a higher expression of maturation markers. ** $P < 0.01$

were not activated and began to proliferate after 1 and 3 d of co-culture, and no differences between these four co-culture groups in terms of proliferation index, compared to T cells alone were found (Fig. 3d and 3e). After 5 d of co-culture, we showed that modified tumor lysate-pulsed DCs were better capable of stimulating T cells and triggered stronger proliferative responses than that of the other three groups (Fig. 3f and 3g). Furthermore, we confirmed that T cells had a higher ratio of $CD8^+$ / $CD4^+$ cells after co-culture with DCs; however, there

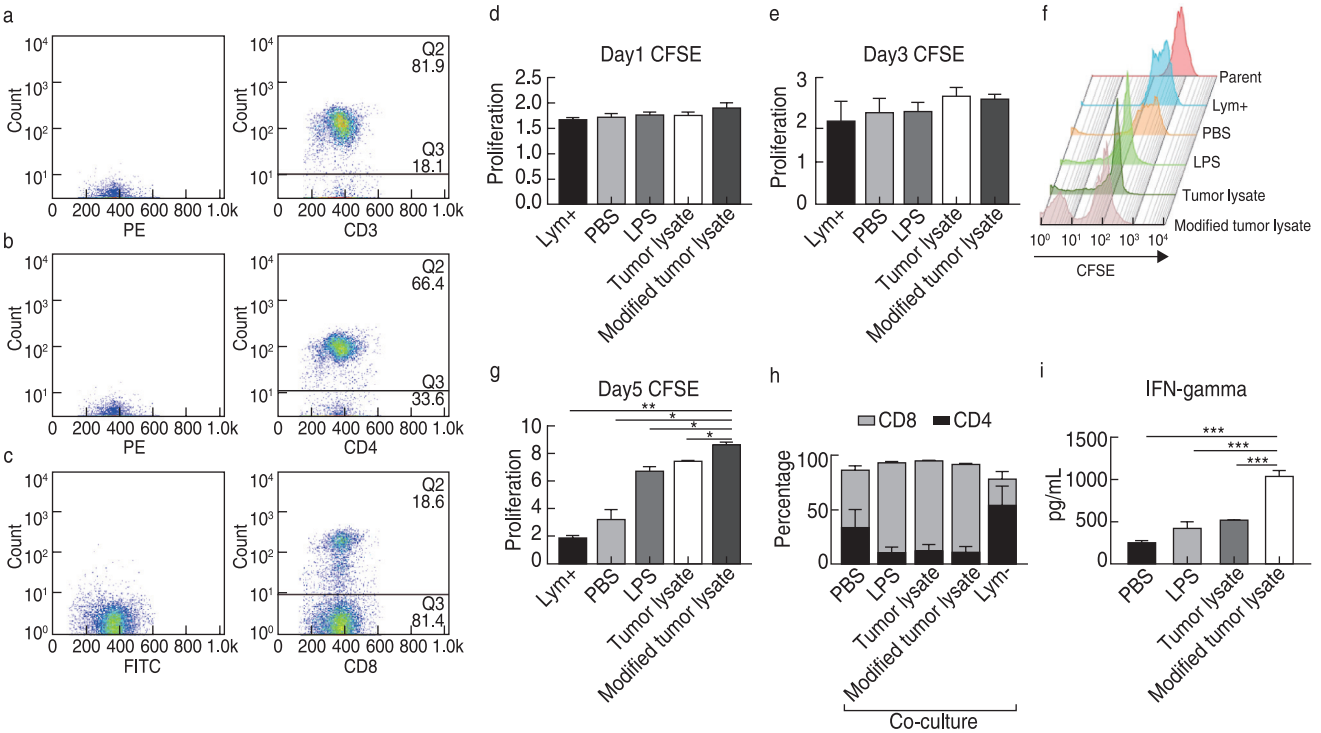

Fig. 3 T cell proliferation and IFN-γ secretion. (a), (b), and (c) show the flow cytometry scatter plot of CD3, CD4, and CD8, respectively on lymphocytes isolated from PBMCs. (d) and (e) represent the statistical histogram of the proliferative T cell responses on Day 1 and Day 3, respectively, after co-culture with tumor lysate, modified tumor lysate, PBS, and LPS pulsed DCs. (f) and (g) exhibit the flow cytometry overlay histogram plot and statistical histogram, respectively, which represents the proliferative T cell response on Day 5 after co-culture with the four groups of DCs. Lym+ stands for the group of T cells without co-culture. (h) indicates the ratio of $CD8^+/CD4^+$ T cells after co-culture with the four groups of DCs. Lym– stands for the group of T cells before co-culture. (i) represent the statistical histogram of the IFN-γ secretion level in the four groups. * $P < 0.1$; ** $P < 0.01$; *** $P < 0.001$

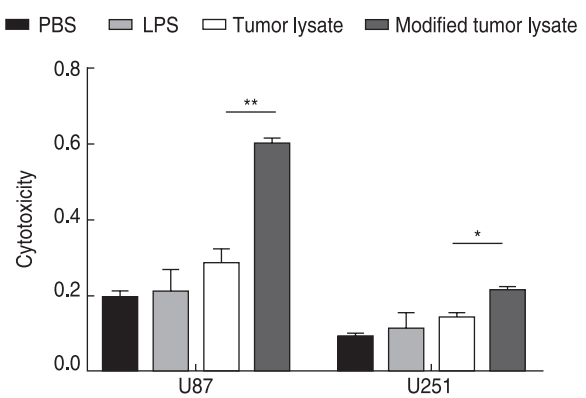

Fig. 4 Cytotoxicity of CTLs pulsed with DC vaccines. CTLs pulsed with modified tumor lysate-primed DCs showed the strongest cytotoxicity against tumor cells (U87 and U251). * $P < 0.1$; ** $P < 0.01$

were no differences between tumor lysate-pulsed DCs and modified tumor lysate-pulsed DCs in terms of the ratio of $CD8^+/CD4^+$ T cells (Fig. 3h). After co-culture of T cells with DCs for 5 d, we collected the culture media and measured the secretion level of IFN-γ using an ELISA kit. We demonstrated that the level of IFN-γ was significantly higher in the modified tumor lysate-pulsed DCs than that in the tumor lysate, PBS, or LPS-pulsed DCs (Fig. 3i).

Modified tumor lysate-pulsed DCs induced CTL cytotoxicity against glioblastoma cells

To determine the cytotoxicity of T cells stimulated by modified tumor lysate-pulsed DCs, we used the CFSE-labeled glioma cell lines U87 and U251 as target cells. The cytotoxicity of T cells activated by modified tumor lysate-pulsed DCs was significantly greater than that of PBS, LPS, and tumor lysate-pulsed DCs (Fig. 4).

ROS in modified tumor lysate-pulsed DCs

To explore the mechanism involved in the improvement of the *in vitro* antitumor immunocompetence of the modified DC vaccine, we measured ROS in the tumor lysate and modified tumor lysate-pulsed DCs. We found that the level of ROS in modified tumor lysate-pulsed DCs was lower than that in tumor lysate-pulsed DCs (Fig. 5).

Discussion

Immunotherapy is one of the most promising adjuvant treatments for glioblastoma following surgery, radiotherapy, and chemotherapy. DC vaccines play vital

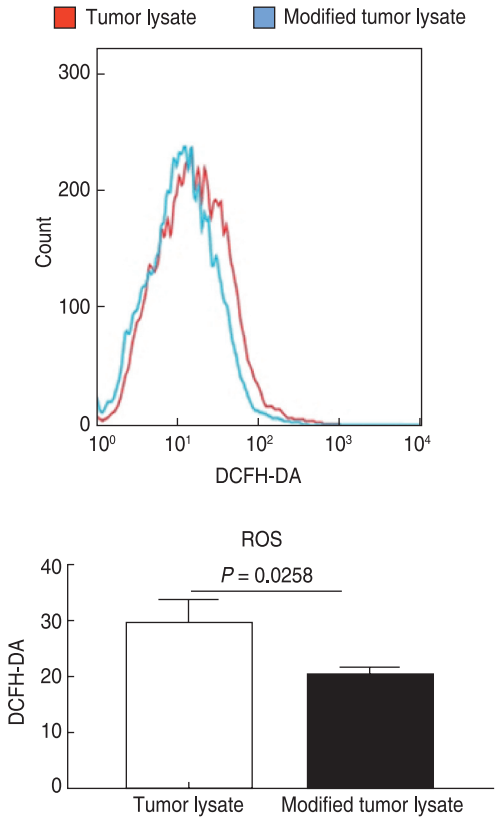

Fig. 5 ROS in different lysate-primed DCs

roles in immunotherapy [23–24]. The high heterogeneity of glioblastomas limits the antitumor effect of a single antigen-sensitized DC vaccine. Although the whole tumor lysate contains multiple epitopes of tumor antigens, many components released during cell lysis may affect the normal function of DCs. This study highlights that by using differential centrifugation to sequentially remove the sources of ROS, including mitochondria, lysosomes, and peroxisomes, from the whole tumor lysate, we increased the maturity of DCs and their ability to stimulate lymphocyte proliferation and secrete IFN-γ. Meanwhile, the number of $CD8^+$ lymphocytes increased, contributing to a more effective antitumor immune response.

The maturity of DCs determines their ability to stimulate lymphocytes and their antitumor effects. Mature DCs can elicit an effective adaptive immune response, whereas immature DCs induce immune tolerance [25–26]. In this study, differential centrifugation was used to remove the source of ROS, which may affect the maturation of DCs from the whole tumor lysate. We showed that the modified tumor lysate-pulsed DCs had a higher expression of surface markers such as CD83 and CD1a, and a better ability to stimulate lymphocyte proliferation and IFN-γ secretion, which indicates a more efficacious adaptive immune response. The cross-presentation of foreign antigens by DCs to $CD8^+$ T lymphocytes underpins anti-tumor immunity [23, 27]. Chen *et al* proposed that DCs present foreign antigens to naive $CD8^+$ T cells through cross-activation in the form of MHC-I-antigen complexes and stimulate them into CTLs, which exert a strong and specific anti-tumor immune response [28]. Studies have shown that infiltrating T lymphocytes in the tumor microenvironment, especially $CD8^+$ T cells, are closely related to the anti-tumor immune effect, and a higher infiltration of T cells suggests a relatively better prognosis for patients with malignant tumors [29–30]. The modified DC vaccine prepared in this study triggered an evident lymphocyte ratio conversion after co-culture with lymphocytes *in vitro*. There was no significant difference in the ratio of $CD8^+/CD4^+$ lymphocytes between the tumor lysate and modified tumor lysate-pulsed DCs; nonetheless, the latter was better capable of stimulating the proliferation of lymphocytes. Therefore, the number of $CD8^+$ T cells stimulated by the modified tumor lysate-pulsed DCs was considerably increased, indicating that the modified DC vaccine can trigger a more powerful anti-tumor immune response. We further confirmed that the modified DC vaccine was more effective in triggering CTL cytotoxicity against glioma cells.

Many studies have shown that the effect of ROS on DC function is complex. The maturation and antigen-presenting ability of DCs are bidirectionally regulated through different mechanisms [31–33]. Rutault *et al* found that the maturity of DCs increased after H_2O_2 intervention [34]. However, studies have shown that reactive oxygen species inhibit the maturation of DCs by inducing endoplasmic reticulum stress [35]. Herber *et al* found that the abnormal deposition of oxidized liposomes in DCs reduced their ability to process and present tumor-related antigens, compromising their ability to trigger anti-tumor immune responses, which was restored after the reduction of oxidized liposomes through drug intervention in lipid synthesis [36]. Moreover, Herrera *et al* showed that abnormal oxidative stress in breast cancer patients indicates an increased risk of tumor recurrence [37]. In 2015, Juan *et al* confirmed that ROS in the tumor microenvironment inhibits the ability of DCs to stimulate T cells by inducing abnormally activated endoplasmic reticulum stress in ovarian tumor-associated DCs. Intervention in the endoplasmic reticulum stress signaling pathway restores the ability of tumor-associated DCs to activate T cells and elicit efficacious anti-tumor immune responses [20]. As one of the main sources of ROS, mitochondria play a key role in maintaining cellular redox balance [38]. Studies have shown that mitochondria continue to release ROS for 48 h, even after dysfunction of the electron transport chain [39]. Chougnet *et al* confirmed that mitochondrial-derived ROS inhibit the ability of

bone marrow-derived DCs to cross-present antigens in mice [32]. In this study, the main sources of ROS, including mitochondria, lysosomes, and peroxisomes, from the whole tumor lysate without a drug intervention, eliminated possible components that may inhibit the function of DCs through differential centrifugation. We found that the modified tumor lysate-pulsed DCs had a significant decrease in the level of intracellular ROS, which may explain, to a certain extent, the mechanism by which the modified tumor lysate stimulates DCs to further mature and trigger a more effective anti-tumor immune response.

Nevertheless, this study has some limitations and provides direction for further exploration and improvement. First, all experiments were *in vitro* cell experiments, which cannot reflect the role of the immune system as a whole and the impact of the tumor microenvironment. Second, although this study detected a decrease in the level of ROS in DCs sensitized by modified tumor lysate, we could not clarify whether ROS are involved in the mechanism of the modified DC vaccine to elicit more effective antitumor immune responses. Therefore, further studies are required. Third, considering that the components of the whole tumor lysate are complex, it is still necessary to further clarify which specific components affect the anti-tumor immune activity of the whole tumor lysate-sensitized DC vaccine.

Conclusion

In summary, this study improved the *in vitro* antitumor immunocompetence of the whole tumor lysate-pulsed DC vaccine against glioblastoma through differential centrifugation without a drug intervention. Meanwhile, we proposed that reactive oxygen species may be the key to affecting DC function in whole tumor lysates, providing a theoretical basis for the clinical application of a modified tumor lysate-pulsed DC vaccine in glioblastoma.

Acknowledgments

Not applicable.

Funding

Supported by the National Natural Science Foundation of China (No. 81602202 and 82173136).

Conflicts of interest

The authors indicated no potential conflicts of interest.

Author contributions

All authors contributed to data acquisition and interpretation and reviewed and approved the final version of this manuscript.

Data availability statement

The datasets used and/or analyzed in the current study are available from the corresponding author upon reasonable request.

Ethical approval

This study was conducted in accordance with the standards of the Human Ethics Committee of Tongji Hospital, Tongji Medical College, Huazhong University of Science and Technology, China.

References

1. Ostrom QT, Gittleman H, de Blank PM, et al. American Brain Tumor Association adolescent and young adult primary brain and central nervous system tumors diagnosed in the United States in 2008–2012. Neuro Oncol. 2016;18(Suppl 1):i1-i50.
2. Ostrom QT, Gittleman H, Fulop J, et al. CBTRUS statistical report: primary brain and central nervous system tumors diagnosed in the United States in 2008–2012. Neuro Oncol. 2015;17(Suppl 4):iv1-iv62.
3. Batash R, Asna N, Schaffer P, et al. Glioblastoma multiforme, diagnosis and treatment; recent literature review. Curr Med Chem. 2017;24(27):3002-3009.
4. Bush NA, Chang SM, Berger MS. Current and future strategies for treatment of glioma. Neurosurg Rev. 2017;40(1):1-14.
5. Poltorak MP, Schraml BU. Fate mapping of dendritic cells. Front Immunol. 2015;6:199.
6. Collin M, Bigley V. Human dendritic cell subsets: an update. Immunology. 2018;154(1):3-20.
7. Qian C, Cao X. Dendritic cells in the regulation of immunity and inflammation. Semin Immunol. 2018;35:3-11.
8. Filley AC, Dey M. Dendritic cell based vaccination strategy: an evolving paradigm. J Neurooncol. 2017;133(2):223-235.
9. Garg AD, Coulie PG, Van den Eynde BJ, et al. Integrating next-generation dendritic cell vaccines into the current cancer immunotherapy landscape. Trends Immunol. 2017;38(8):577-593.
10. Saxena M, Bhardwaj N. Re-emergence of dendritic cell vaccines for cancer treatment. Trends Cancer. 2018;4(2):119-137.
11. Wang Y, Xie RF, Niu HQ, et al. IL-13Ra2- and glioma stem cell-pulsed dendritic cells induce glioma cell death *in vitro*. Oncol Transl Med. 2016;2(5):210-215.
12. Phuphanich S, Wheeler CJ, Rudnick JD, et al. Phase I trial of a multi-epitope-pulsed dendritic cell vaccine for patients with newly diagnosed glioblastoma. Cancer Immunol Immunother. 2013;62(1):125-135.
13. Vik-Mo EO, Nyakas M, Mikkelsen BV, et al. Therapeutic vaccination against autologous cancer stem cells with mRNA-transfected dendritic cells in patients with glioblastoma. Cancer Immunol Immunother. 2013;62(9):1499-1509.
14. Constantino J, Gomes C, Falcão A, et al. Antitumor dendritic cell-based vaccines: lessons from 20 years of clinical trials and future perspectives. Transl Res. 2016;168:74-95.
15. Liau LM, Ashkan K, Tran DD, et al. First results on survival from a large Phase 3 clinical trial of an autologous dendritic cell vaccine in newly diagnosed glioblastoma. J Transl Med. 2018;16(1):142.
16. Lee AW, Truong T, Bickham K, et al. A clinical grade cocktail of cytokines and PGE2 results in uniform maturation of human monocyte-derived dendritic cells: implications for immunotherapy. Vaccine. 2002;20 Suppl 4:A8-A22.

17. Boullart AC, Aarntzen EH, Verdijk P, et al. Maturation of monocyte-derived dendritic cells with Toll-like receptor 3 and 7/8 ligands combined with prostaglandin E2 results in high interleukin-12 production and cell migration. Cancer Immunol Immunother. 2008;57(11):1589-1597.
18. Van Lint S, Wilgenhof S, Heirman C, et al. Optimized dendritic cell-based immunotherapy for melanoma: the TriMix-formula. Cancer Immunol Immunother. 2014;63(9):959-967.
19. Chio IIC, Tuveson DA. ROS in cancer: the burning question. Trends Mol Med. 2017;23(5):411-429.
20. Cubillos-Ruiz JR, Silberman PC, Rutkowski MR, et al. ER stress sensor XBP1 controls anti-tumor immunity by disrupting dendritic cell homeostasis. Cell. 2015;161(7):1527-1538.
21. Ramakrishnan R, Tyurin VA, Veglia F, et al. Oxidized lipids block antigen cross-presentation by dendritic cells in cancer. J Immunol. 2014;192(6):2920-2931.
22. Veglia F, Tyurin VA, Mohammadyani D, et al. Lipid bodies containing oxidatively truncated lipids block antigen cross-presentation by dendritic cells in cancer. Nat Commun. 2017;8(1):2122.
23. Le Gall CM, Weiden J, Eggermont LJ, et al. Dendritic cells in cancer immunotherapy. Nat Mater. 2018;17(6):474-475.
24. Lim M, Xia Y, Bettegowda C, et al. Current state of immunotherapy for glioblastoma. Nat Rev Clin Oncol. 2018;15(7):422-442.
25. Steinman RM. The dendritic cell system and its role in immunogenicity. Annu Rev Immunol. 1991;9:271-296.
26. Steinman RM, Nussenzweig MC. Avoiding horror autotoxicus: the importance of dendritic cells in peripheral T cell tolerance. Proc Natl Acad Sci USA. 2002;99(1):351-358.
27. Kurts C, Robinson BW, Knolle PA. Cross-priming in health and disease. Nat Rev Immunol. 2010;10(6):403-414.
28. Chen DS, Mellman I. Oncology meets immunology: the cancer-immunity cycle. Immunity. 2013;39(1):1-10.
29. Fridman WH, Pagès F, Sautès-Fridman C, et al. The immune contexture in human tumours: impact on clinical outcome. Nat Rev Cancer. 2012;12(4):298-306.
30. Reiser J, Banerjee A. Effector, memory, and dysfunctional CD8(+) T cell fates in the antitumor immune response. J Immunol Res. 2016;2016:8941260.
31. Paardekooper LM, Vos W, van den Bogaart G. Oxygen in the tumor microenvironment: effects on dendritic cell function. Oncotarget. 2019;10(8):883-896.
32. Chougnet CA, Thacker RI, Shehata HM, et al. Loss of phagocytic and antigen cross-presenting capacity in aging dendritic cells is associated with mitochondrial dysfunction. J Immunol. 2015;195(6):2624-2632.
33. Dingjan I, Paardekooper LM, Verboogen DRJ, et al. VAMP8-mediated NOX2 recruitment to endosomes is necessary for antigen release. Eur J Cell Biol. 2017;96(7):705-714.
34. Rutault K, Alderman C, Chain BM, et al. Reactive oxygen species activate human peripheral blood dendritic cells. Free Radic Biol Med. 1999;26(1-2):232-238.
35. Luís A, Martins JD, Silva A, et al. Oxidative stress-dependent activation of the eIF2α–ATF4 unfolded protein response branch by skin sensitizer 1-fluoro-2,4-dinitrobenzene modulates dendritic-like cell maturation and inflammatory status in a biphasic manner [corrected]. Free Radic Biol Med. 2014;77:217-229.
36. Herber DL, Cao W, Nefedova Y, et al. Lipid accumulation and dendritic cell dysfunction in cancer. Nat Med. 2010;16(8):880-886.
37. Herrera AC, Victorino VJ, Campos FC, et al. Impact of tumor removal on the systemic oxidative profile of patients with breast cancer discloses lipid peroxidation at diagnosis as a putative marker of disease recurrence. Clin Breast Cancer. 2014;14(6):451-459.
38. Angajala A, Lim S, Phillips JB, et al. Diverse roles of mitochondria in immune responses: novel insights into immuno-metabolism. Front Immunol. 2018;9:1605.
39. Qian W, Kumar N, Roginskaya V, et al. Chemoptogenetic damage to mitochondria causes rapid telomere dysfunction. Proc Natl Acad Sci USA. 2019;116(37):18435-18444.

DOI 10.1007/s10330-022-0582-2
Cite this article as: Liu XJ, Qi YW, Hu F, et al. Differential centrifugation enhances the anti-tumor immune effect of tumor lysate-pulsed dendritic cell vaccine against glioblastoma. Oncol Transl Med. 2022;8(5):209–216.

Oncology and Translational Medicine
DOI 10.1007/s10330-021-0527-7

October 2022, Vol. 8, No. 5, P217–P225

ORIGINAL ARTICLE

Relationship between *IKZF1* polymorphisms and the risk of acute lymphoblastic leukemia: a meta-analysis*

Sisi Wang, Chuyang Lin (Co-first author), Tingting Xi, Yu Tong, Jinlin Wu (✉)

Department of Pediatrics; Key Laboratory of Birth Defects and Related Disease of Women and Children, Ministry of Education; West China Second University Hospital, Sichuan University, Chengdu 610041, China

Abstract

Objective The aim of the study was to systematically evaluate the correlation between *IKZF1* polymorphisms and the risk of acute lymphoblastic leukemia.

Methods Computer databases including PubMed, EMBASE, and Web of Science were searched for case-control studies on the association between *IKZF1* polymorphisms and the risk of acute lymphoblastic leukemia. The retrieval period was from the establishment of the database to November 2020. Two researchers independently screened the literature, extracted the data, evaluated the risk of bias in the included studies, and used Stata 14.0 software for meta-analysis.

Results A total of 48 case-control studies were included, with 10 520 and 44 049 cases in the case and control groups, respectively. The meta-analysis results showed that rs4132061 and rs11978267 of *IKZF1* were significantly correlated with the risk of acute lymphoblastic leukemia (ALL).

Conclusion Current evidence indicates that rs4132061 and rs11978267 of *IKZF1* are significantly associated with the risk of B-cell ALL.

Received: 11 October 2021
Revised: 25 April 2022
Accepted: 6 July 2022

Key words: *IKZF1*; gene polymorphism; acute lymphoblastic leukemia (ALL); meta-analysis; systematic reviews; case-control study

Childhood leukemia is the most common malignancy in childhood, accounting for 1/4 of all childhood malignancies [1]. Acute lymphoblastic leukemia (ALL) accounts for approximately 80% of all childhood leukemia cases, with a peak prevalence at the age of 2 to 5 [1–2]. According to the immunophenotype, ALL can be divided into B-cell ALL (B-ALL) and T-cell ALL (T-ALL), accounting for 85% and 15% of the cases, respectively [3]. The pathogenesis of ALL remains inconclusive, but in recent years, great progress has been made in understanding the genetic factors related to the pathogenesis of ALL. With the development of sequencing technology and genome-wide association studies, more polymorphism sites associated with ALL have been identified [4–8], most of which encode hematopoietic transcription factors. An increasing number of studies have found that alteration of *IKZF1* (IKAROS zinc finger 1) is correlated with the occurrence of ALL. The *IKZF1* gene is located on the long arm of chromosome 7 and encodes the early lymphoid transcription factor IKAROS, a DNA-bound zinc finger transcription factor that plays an important role in hematopoiesis, particularly in the maturation and differentiation of lymphoid progenitor cells [9]. Studies have confirmed that the loss of *IKZF1* expression is an independent risk factor for ALL recurrence and poor prognosis [10]. However, the results of the association between single nucleotide polymorphisms (SNPs) in the *IKZF1* gene and ALL risk were inconsistent. There are some SNPs in the *IKZF1* gene, including rs6964823, rs4132601, rs6944602, and rs11978267. Previous studies have revealed that rs4132601 and rs11978267 polymorphic sites of *IKZF1* in different ethnic groups are associated with the occurrence of ALL; however, the conclusion remains unclear, and this contradiction may

✉ Correspondence to: Jinlin Wu. Email: wujl_2000@sina.com
* Supported by the National Key Project of Neonatal Children (No. 1311200003303), Grants from the Science and Technology Bureau of Sichuan Province (No. 2021YJ0211), and Grants from the Health Planning Committee of Sichuan Province (No. 20PJ070).

be at least partially attributed to the small sample size and ethnic differences in the whole study. Therefore, this study adopted a meta-analysis method to systematically summarize all qualified data to provide more reliable evidence and explore the relationship between *IKZF1* polymorphisms and the risk of ALL to provide a basis for clinical decision-making.

Materials and methods

The present meta-analysis was performed in accordance with the Preferred Reporting Items for Systematic reviews and Meta-Analyses (PRISMA) statement (S1 File) and Meta-Analysis on Genetic Association Studies Checklist (S2 File).

Eligibility criteria

Inclusion criteria: (1) Case-control-designed studies. (2) The association between *IKZF1* polymorphisms and ALL risk was evaluated. (3) Sufficient data on allele or genotype distribution in patients and controls. (4) Met the Hardy-Weinberg equilibrium (HWE). (5) Full-text English.

Exclusion criteria: (1) Editorials and review articles. (2) Republished papers. (3) Lack of complete data or sufficient information.

Search strategy

A systematic electronic search of the PubMed, EMBASE, and Web of Science databases for original articles was performed to identify potentially relevant articles and abstracts to collect case-control studies on the correlation between *IKZF1* polymorphisms and the risk of ALL. The search time limit was set from the establishment of the database to November 2020. The search terms included *IKZF1*, IKAROS zinc finger 1, acute leukemia, acute lymphoblastic leukemia, ALL, rs4132601, rs11978267, polymorphism, variant, mutation, 7p12.2, allele, genotype, case, and control. The language was restricted to English. PubMed was used as an example (Fig. 1).

Data extraction and quality assessment

Two investigators independently screened the literature, extracted the data from the selected eligible studies, and cross-checked them. Disagreements were resolved through discussion or by a third reviewer. In the literature screening, the title was first read, followed by the abstract and full text to determine whether to include the study once irrelevant literature had been excluded. If necessary, the original study author was contacted via email or telephone to obtain undetermined but important information for the study. Data extraction content included (1) basic information of the included studies: study title, first author, publication time, ethnicity, etc.; (2) baseline characteristics, allele frequency, and gene detection methods of the study subjects; (3) key elements of bias risk assessment; and (4) outcome indicators and outcome measurements of concern. The Newcastle-Ottawa Scale was used to evaluate the risk of bias in the included case-control studies, with a score ≥ 5 included in the meta-analysis[11]. The results of the quality assessments are shown in the S3 File.

Statistical analysis

All statistical tests were performed using Stata version 14.0. The HWE was calculated using the Chi-squared test for each study in the control groups ($P < 0.05$, defined as departure from HWE). The pooled odds ratios (ORs) with 95% confidence intervals (CIs) to assess the strength of the association of the *IKZF1* polymorphism with ALL risk in five genetic models were evaluated using the Z test. Heterogeneity was evaluated using the Chi-squared Q-test and I^2. If $I^2 > 50\%$ or $P < 0.05$, significant heterogeneity was indicated. A random-effects model was used to calculate the ORs and 95% CIs. Otherwise, a fixed-effects model was used. Stratified analyses were performed based on ethnicity and subtype of leukemia. The Begg's test was used to estimate potential publication bias. Statistical significance was set at $P < 0.05$. Sensitivity tests carried out by omitting each of the studies discussed the association of rs4132061 or rs11978267 with ALL susceptibility. The pooled OR and 95% CI were not significantly different, which in turn confirmed the robustness of the relationship between rs4132061 or rs11978267 and ALL predisposition.

Results

Literature screening results

The initial database search identified 79 potentially relevant studies. Based on the selection in accordance with the inclusion criteria, 27 articles were included. The genotype distributions in the controls of the 27 studies were fitted into the HWE, except for three [12–14]. After assessing the quality of the studies, three studies were excluded because they scored less than five points [15–17]. Finally, 48 studies from 21 publications were included [6–7, 12, 14, 18–34], comprising 10 520 cases and 44 049 controls.

#1 IKZF1 OR Ikaros zinc finger 1 OR rs4132601 OR rs11978267 OR 7p12.2

#2 acute lymphoblastic leukemia

#3 polymorphism OR variation OR allele OR genotype

#4 #1 AND #2 AND #3

Fig. 1 Search strategy on PubMed

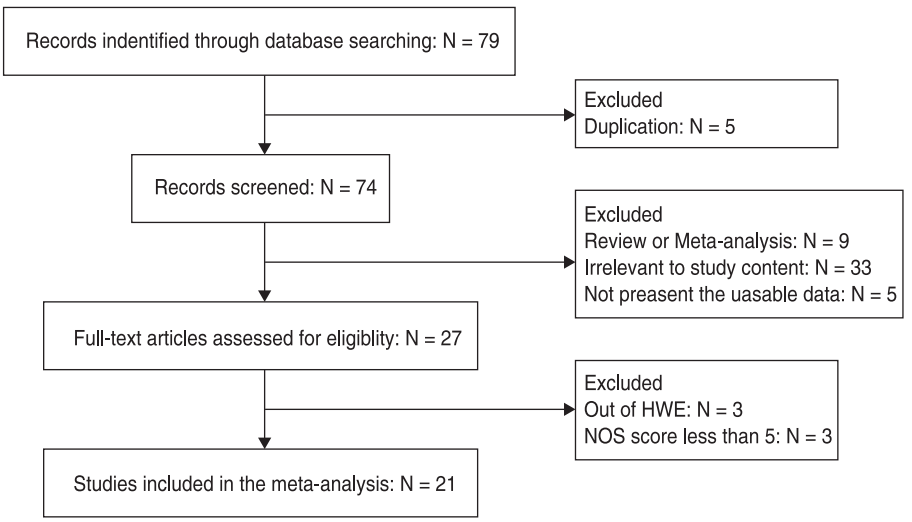

Fig. 2 Flow diagram of literature selection

There were 39 studies from Caucasians, seven studies from Asians, and two studies from Africans. The flowchart of the selection process is shown in Fig. 2. Detailed characteristics of the included studies are presented in Table 1.

Results of allele analysis

rs4132061

A total of 29 studies in the 18 included articles analyzed the correlation between the rs4132061 polymorphism and the risk of ALL. Heterogeneity was observed in the allele model (I^2 = 55.1%, P = 0.00), and we applied a random-effects model to conduct the meta-analysis. The G allele exhibited a significant 1.46-fold increased risk of developing ALL compared with the A allele (OR = 1.46, 95% CI: 1.36–1.57, P < 0.001). Through sensitivity analysis, the meta-analysis showed that rs4132061 G *vs.* T was significantly associated with the risk of ALL (I^2 = 0.0%, OR = 1.33, 95% CI: 1.29–1.38, P < 0.001) after exclusion of references [19, 23–25]. This demonstrates that the results obtained were statistically robust. The effect of the rs4132061 polymorphism on ALL was further evaluated using a stratification analysis of ethnicity and ALL type. A higher risk was detected in Europeans (OR = 1.54; 95% CI: 1.46–1.61, P < 0.001) or B-ALL (I^2 = 5.0%, OR = 1.56; 95% CI: 1.48–1.65, P < 0.001; Fig. 3).

rs11978267

A total of 12 articles and 19 studies were included (Table 1), and a significant association with the risk of ALL was found (I^2 = 64.3%, OR = 1.33, 95% CI: 1.21–1.45). Sensitivity analysis was performed to exclude studies that had a significant impact on heterogeneity [4, 8, 18–19, 24]. Meta-analysis showed a significant correlation, as described above. In subgroup analysis, a significantly increased ALL risk was found in the B-cell ALL subgroup (I^2 = 5.0%, OR = 1.39, 95% CI: 1.27–1.51, P < 0.001; Fig. 4).

Genotype analysis

rs4132061

A total of 23 studies in 15 articles reported the genotype distribution of rs4132061. The pooled OR revealed a significant association between ALL risk and the rs4132061 polymorphism in all comparisons (GG *vs.* TT: OR = 2.41, 95% CI: 2.10–2.77, P < 0.001; GT *vs.* TT: OR = 1.52, 95% CI: 1.37–1.69, P < 0.001; GG *vs.* TT + GT: OR = 1.94, 95% CI: 1.72–2.19, P < 0.001; GG + GT *vs.* TT: OR = 1.71, 95% CI: 1.52–1.93, P < 0.001). Stratification analysis according to ethnicity showed that the rs4132601 polymorphism was associated with a high risk of ALL in all genetic models in Caucasians. The GG, TG, and TT + GG genotypes may increase the risk of ALL in Asians (Table 2). The results of subgroup analysis by ALL subtype showed that ALL gene models were significantly associated with the risk of ALL in B-ALL. In T-ALL, there is no evidence that the rs4132061 polymorphism is associated with ALL risk.

rs11978267

Six of the eligible studies reported rs11978267 genotype distribution. A significantly increased risk of ALL was observed among individuals with the homozygous GG genotype (GG *vs.* AA: OR = 1.687, 95% CI: 1.311–2.171, P < 0.001; GG *vs.* AA + GG: OR = 1.687, 95% CI: 1.311–2.171, P < 0.001; Table 2).

Publication bias

Begg's test was used to detect publication bias in the included studies, and the results showed no significant publication bias (P = 0.205; Fig. 5).

Table 1 Characteristics of the included articles

(A) rs4132601

First author	Year	Country	Ethnicity	Disease	Case					Control					Case/Control	HWE *P* for controls
					TT	TG	GG	T	G	TT	TG	GG	T	G		
Mosaad. a	2020	Egyptian	Caucasian	B-ALL	55	72	15	182	102	249	162	25	660	212	142/436	0.841036
Mosaad. b	2020	Egyptian	Caucasian	T-ALL	15	12	4	42	20	249	162	25	660	212	31/436	0.841036
Urayama	2018	Japan	Asian	B-ALL	–	–	–	958	96	–	–	–	7050	714	527/3882	–
Lopes	2017	Brazilian	Caucasian	B-ALL	120	98	28	338	154	246	192	29	684	250	276/467	0.292591
Bhandari	2016	Indian	Asian	B-ALL	69	67	26	205	119	78	61	11	217	83	162/150	0.844204
Kreile	2014	Latvian	Caucasian	B-ALL	35	32	8	102	48	63	44	7	170	58	76/121	0.852246
Burmeister. a	2014	German	Caucasian	B-ALL	86	111	30	283	171	811	574	116	2196	806	227/1501	0.305358
Burmeister. b	2014	German	Caucasian	T-ALL	51	40	4	142	48	811	574	116	2196	806	95/1501	0.305358
Orsi. a	2012	France	Caucasian	B-ALL	148	166	47	462	260	817	632	93	2266	818	361/1542	0.043056
Orsi. b	2012	France	Caucasian	T-ALL	15	23	3	53	29	817	632	93	2266	818	41/1542	0.043056
Peyrouze. a	2012	France	Caucasian	B-ALL	–	–	–	97	55	–	–	–	252	108	76/180	–
Peyrouze. b	2012	France	Caucasian	T-ALL	–	–	–	108	40	–	–	–	252	108	74/180	–
Ellinghaus. a	2012	Germany	Caucasian	B-ALL				553	285				683	265	419/474	–
Ellinghaus. b	2012	Germany	Caucasian	B-ALL	–	–	–	528	284	–	–	–	2456	908	406/1682	–
Ellinghaus. c	2012	Italy	Caucasian	B-ALL	–	–	–	362	212	–	–	–	857	301	287/579	–
Vijayakrishnan. a	2010	Thailand	Asian	B-ALL	122	49	1	293	51	145	36	1	326	38	172/182	0.435546
Vijayakrishnan. b	2010	Thai	Asian	T-ALL	13	3	2	29	7	145	36	1	326	38	18/182	0.435546
Prasad. a	2010	German	Caucasian	B-ALL	471	552	166	1494	884	811	574	116	2196	806	1193/1516	0.305358
Prasad. b	2010	UK	Caucasian	B-ALL	60	96	32	216	160	206	133	21	545	175	191/361	0.938949
Papaemmanuil. a	2009	UK	Caucasian	B-ALL	172	205	82	549	369	751	564	123	2066	810	459/1438	0.244163
Papaemmanuil. b	2009	UK	Caucasian	T-ALL	19	16	9	54	34	751	564	123	2066	810	44/1438	0.244163
Papaemmanuil. c	2009	UK	Caucasian	B-ALL	129	191	45	449	281	533	358	69	1451	523	365/960	0.963117
Papaemmanuil. d	2009	UK	Caucasian	T-ALL	19	17	3	55	23	533	358	69	1451	523	39/960	0.963117
Mahjoub	2019	Tunisian	African	ALL	73	73	24	219	121	76	68	6	220	80	170/150	0.051360
Bahari	2016	Iranian	Asian	ALL	23	59	28	105	115	52	45	23	149	91	110/120	0.025812
Rudant	2015	France	Caucasian	ALL	175	202	57	552	316	211	167	37	589	241	434/415	0.631803
Wang	2013	China	Asian	ALL	415	141	12	971	165	504	159	9	1167	177	568/672	0.370420
Lautner-Csorba	2012	Hungary	Caucasian	ALL	246	229	68	721	365	307	181	41	795	263	543/529	0.053063
Pastorczak	2011	Poland	Caucasian	ALL	178	165	46	521	257	389	270	56	1048	382	389/715	0.341676

(B) rs11978267

First author	Year	Country	Ethnicity	Disease	Case					Control					Case/Control	HWE *P* for controls
					TT	TG	GG	T	G	TT	TG	GG	T	G		
Mosaad. a	2020	Egyptian	Caucasian	B-ALL	82	47	13	211	73	239	165	32	643	229	142/436	0.841036
Mosaad. b	2020	Egyptian	Caucasian	T-ALL	19	10	2	48	14	239	165	32	643	229	31/436	0.841036
Urayama	2018	Japanese	Asian	B-ALL	–	–	–	957	97	–	–	–	7010	753	527/3882	–
Lopes	2017	Brazilian	Caucasian	B-ALL	133	87	26	353	139	258	175	34	691	243	276/467	0.292591
Orsi. a	2012	France	Caucasian	B-ALL	–	–	–	462	260	–	–	–	2266	818	361/1542	0.043056
Orsi. b	2012	France	Caucasian	T-ALL	–	–	–	53	29	–	–	–	2266	818	41/1542	0.043056
Peyrouze. a	2012	France	Caucasian	B-ALL	–	–	–	99	53	–	–	–	252	108	76/180	–
Peyrouze. b	2012	France	Caucasian	T-ALL	–	–	–	108	40	–	–	–	252	108	74/180	–
Ellinghaus. a	2012	Germany	Caucasian	B-ALL	–	–	–	545	293	–	–	–	673	275	419/474	–
Ellinghaus. b	2012	Germany/ Australian	Caucasian	B-ALL	–	–	–	536	276	–	–	–	2456	908	406/1682	–
Ellinghaus. c	2012	Italy	Caucasian	B-ALL	–	–	–	189	385	–	–	–	868	290	287/579	–
Mariana	2014	brazilian	Caucasian	ALL	80	62	12	222	86	271	182	37	724	256	154/490	0.404219
Linabery	2013	U.S	Caucasian	ALL	321	299	110	941	519	204	152	28	560	208	574/384	0.965647
Heng Xu. a	2013	USA	Caucasian	ALL	–	–	–	1186	758	–	–	–	1996	776	574/2601	–
Heng Xu. b	2013	USA	African	ALL	–	–	–	130	48	–	–	–	2208	518	128/1075	–
Heng Xu. c	2013	USA	Caucasian	ALL	–	–	–	421	189	–	–	–	1492	524	143/640	–
Ross	2013	USA	Caucasian	ALL	53	31	12	137	55	204	152	28	560	208	96/384	0.965647
Lautner-Csorba	2012	Hungary	Caucasian	ALL	248	230	65	726	360	308	181	40	797	261	543/529	0.067779
Treviño	2009	USA	Caucasian	ALL	–	–	–	387	247	–	–	–	26219	9697	317/17958	–

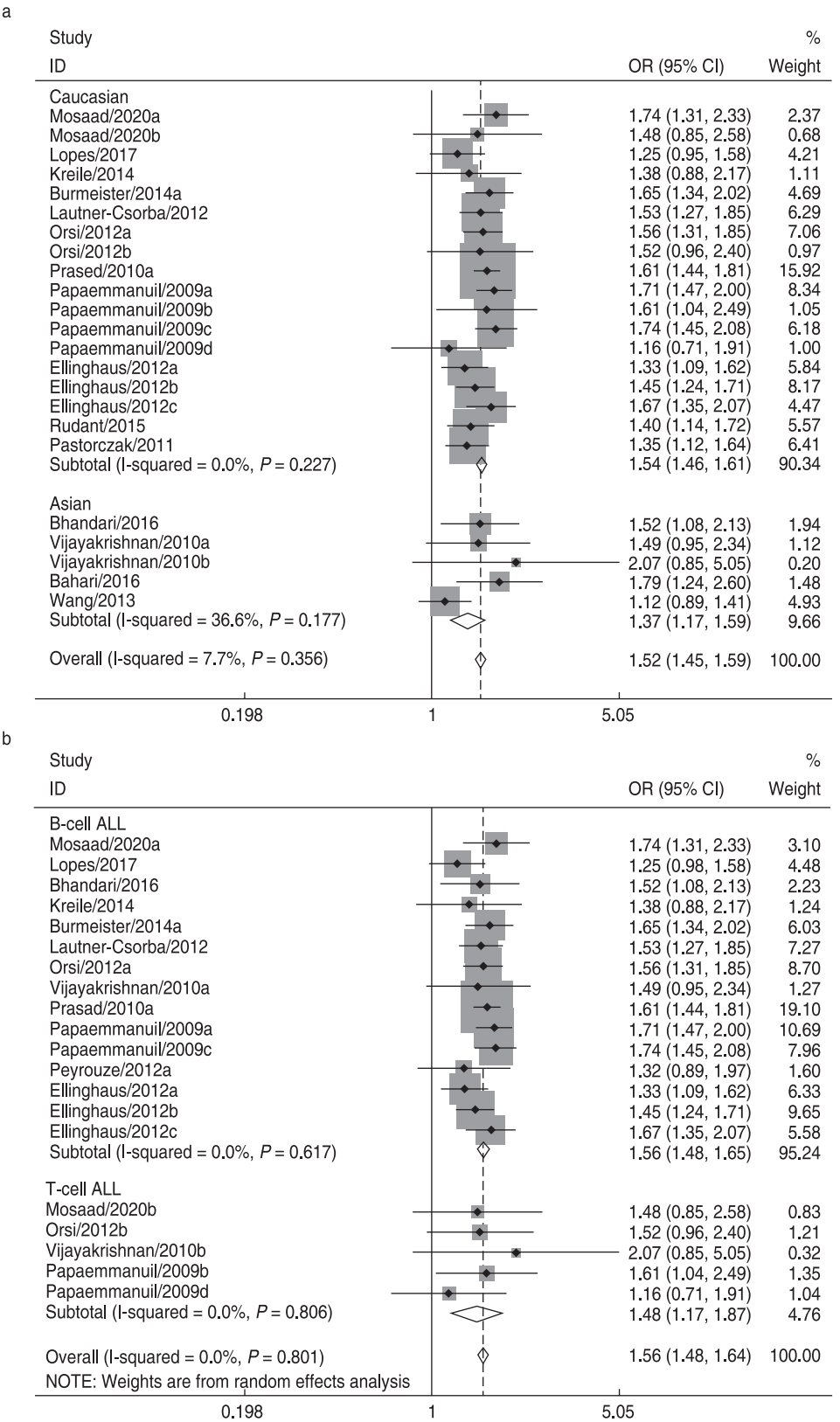

Fig. 3 Forest plots of ALL predisposition associated with rs4132061 polymorphism under genetic models. (a) Allelic model analysis (G vs. A) of rs4132061 and ALL risk among ethnicity. (b) Allelic model analysis (G vs. A) of rs4132061 and ALL risk among disease type

Table 2 Pooled ORs and 95% CIs for associations between *IKZF1* rs4132601 and rs11978267 polymorphisms and ALL risk

Genetic mode	Test of association			Test of heterogeneity		Genetic mode	Test of association			Test of heterogeneity	
	OR (95%)	*Z*	*P*	I^2	*P*		OR (95%)	*Z*	*P*	I^2	*P*
	rs4132061						rs11978267				
G *vs.* T	1.46 (1.36, 1.56)	10.44	0.000	55.1%	0.000	G *vs.* A	1.33 (1.21, 1.45)	6.19	0.000	64.3%	0.000
GT *vs.* TT	1.52 (1.37, 1.69)	7.71	0.000	48.6%	0.005	GA *vs.* AA	1.09 (0.88, 1.34)	0.77	0.441	54.2%	0.041
GG *vs.*TT	2.41 (2.10, 2.77)	12.43	0.000	19.0%	0.194	GG *vs.* AA	1.69 (1.31, 2.171)	4.07	0.000	16.8%	0.302
GG *vs.* TT + GT	1.94 (1.72, 2.19)	10.70	0.000	10.9%	0.312	GG *vs.* AA + AG	1.63 (1.31, 2.02)	4.41	0.000	0.0%	0.509
GG + GT *vs.* TT	1.71 (1.52, 1.93)	8.78	0.000	45.0%	0.023	GG + AG *vs.* AA	1.16 (0.95, 1.43)	1.45	0.147	58.7%	0.024

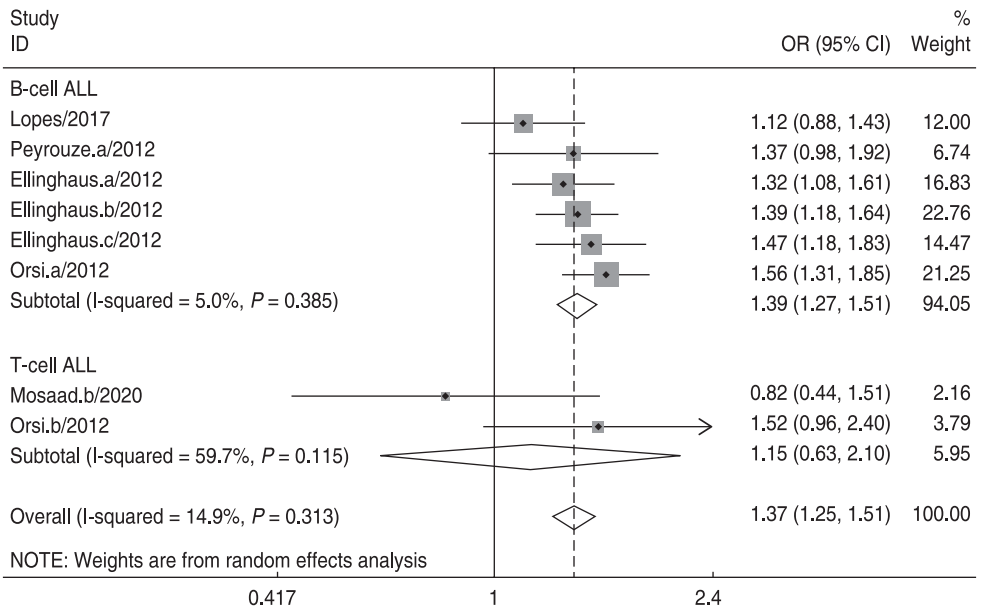

Fig. 4 Forest plots of ALL predisposition associated with rs11978267 polymorphism under genetic models

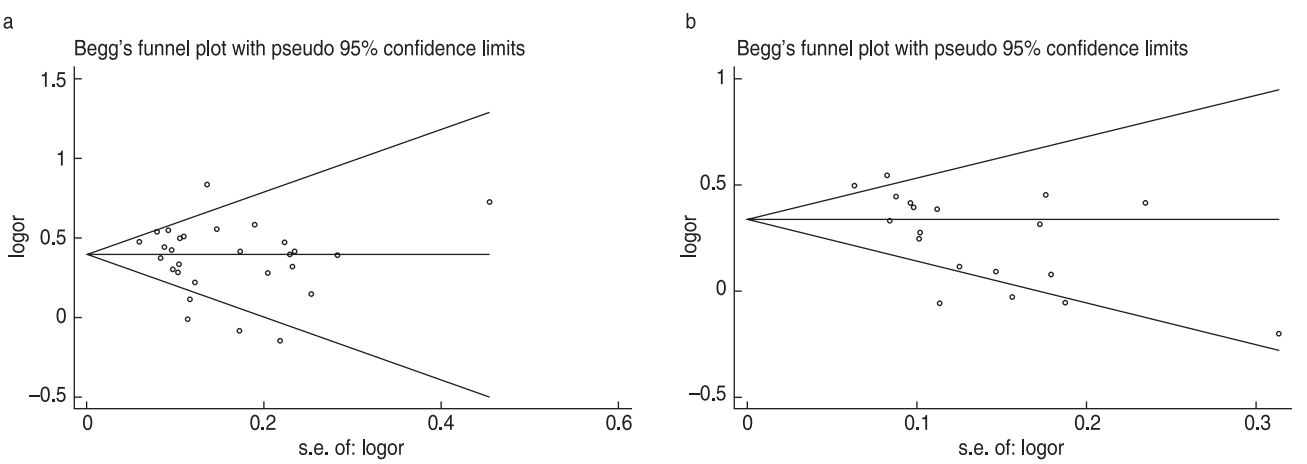

Fig. 5 Publication bias in studies of the association between *IKZF1* polymorphism and ALL risk assessed by Begg's Funnel plot (a, rs4132061; b, rs11978267)

Discussion

Regulation of oncogene expression through transcription factors that act as tumor suppressors is one of the main mechanisms regulating leukemia. Understanding this complex process is crucial for understanding the pathogenesis of leukemia and developing targeted therapies. IKAROS, encoded by *IKZF1*, is a DNA-binding

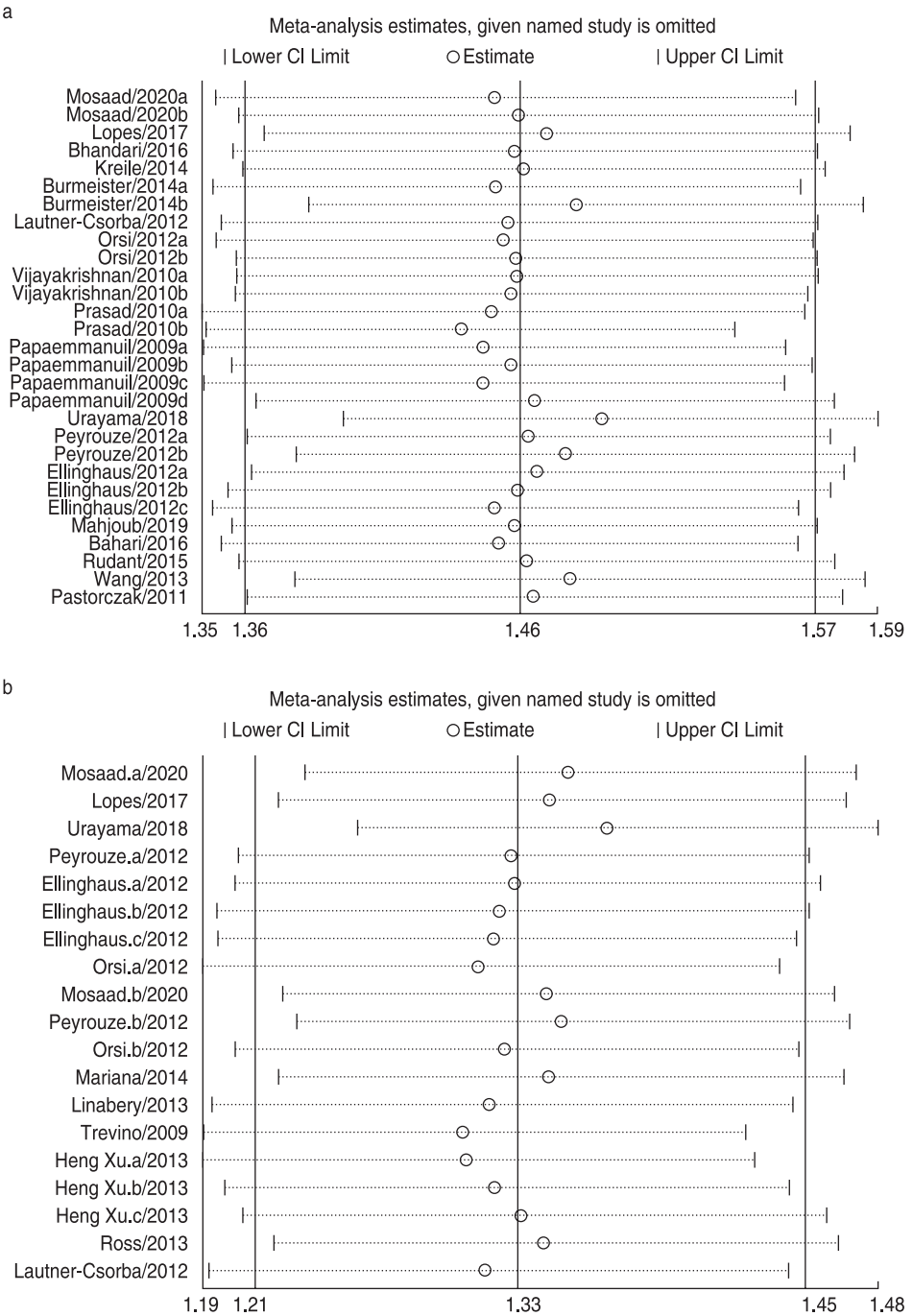

Fig. 6 Sensitivity analyses for studies on rs4132061 and rs11978267 polymorphism and ALL risk. (a) rs4132061 (G *vs.* T); (b) rs11978267 (G *vs.* A)

protein. IKAROS binds specific common binding motifs on the upstream regulatory elements of its target genes to recruit chromatin remodeling complexes to activate or inhibit transcription and plays a role in regulating lymphocyte differentiation and development [35].

In this study, a meta-analysis was performed to determine the correlation between the rs4132061 and rs11978267 loci of *IKZF1* and ALL. We observed that rs4132061 was associated with the risk of ALL in all genetic models, especially B-ALL. However, there is insufficient evidence to prove that rs4132061 is associated with the risk of T-ALL. The rs11978267 locus was associated with the risk of ALL in the GG *vs.* AA + AG and GG *vs.* AA models. Subgroup analysis showed that rs4132061 and rs11978267 were associated with the risk of ALL in the European population. In Asian populations,

rs4132061 has been associated with an increased risk of ALL. A combined analysis of 48 further studies grouped by two loci showed heterogeneity (rs4132061: I^2 = 55.1%, P = 0.00; rs11978267: I^2 = 64.3%, P = 0.00). Subgroup analysis showed that the heterogeneity of the rs4132061 locus was mainly concentrated in B-ALL (I^2 = 58.4%, P = 0.002) and Asian populations (I^2 = 57.4%, P = 0.038), and the heterogeneity of the rs11978267 locus was mainly concentrated in T-ALL (I^2 = 59.7%, P = 0.0115). In addition, sensitivity analysis (Fig. 6) was conducted, and seven documents that had a significant impact on the results were excluded [4, 8, 18–19, 23–25]. After the analysis, the results did not change, indicating that the findings are reliable.

This study had some limitations: (1) Most of the samples included in this study were from Caucasians, and the relationship between *IKZF1* polymorphisms and ALL in different ethnic groups still needs to be verified by further large-scale studies; (2) only published English literature was included in this study, which may have led to publication bias; (3) some studies have shown that the incidence of ALL is related to many environmental factors, but this study only considered genetic factors.

In conclusion, current evidence indicates that *IKZF1* polymorphisms are significantly associated with the risk of ALL, and their polymorphic loci may be effective and economical biomarkers for the diagnosis and treatment of ALL. Due to the limited quality of the included studies, the above conclusions need to be verified by further high-quality studies.

Acknowledgments

Not applicable.

Funding

This work was supported by the National Key Project of Neonatal Children (No. 1311200003303), Grants from the Science and Technology Bureau of Sichuan Province (No. 2021YJ0211 to Jinlin Wu), and Grants from the Health Planning Committee of Sichuan Province (No. 20PJ070 to Jinlin Wu).

Conflicts of interest

The authors declared no conflict of interest.

Author contributions

Sisi Wang and Chuyang Lin contributed equally to this work.

Data availability statement

Not applicable.

Ethical approval

Not applicable.

References

1. Ward E, DeSantis C, Robbins A, et al. Childhood and adolescent cancer statistics, 2014. CA Cancer J Clin. 2014;64(2):83-103.
2. Siegel DA, King J, Tai E, et al. Cancer incidence rates and trends among children and adolescents in the United States, 2001–2009. Pediatrics. 2014;134(4):e945-e955.
3. Hunger SP, Mullighan CG. Acute lymphoblastic leukemia in children. N Engl J Med. 2015;373(16):1541-1552.
4. Treviño LR, Yang W, French D, et al. Germline genomic variants associated with childhood acute lymphoblastic leukemia. Nat Genet. 2009;41(9):1001-1005.
5. Sherborne AL, Hosking FJ, Prasad RB, et al. Variation in *CDKN2A* at 9p21.3 influences childhood acute lymphoblastic leukemia risk. Nat Genet. 2010;42(6):492-494.
6. Papaemmanuil E, Hosking FJ, Vijayakrishnan J, et al. Loci on 7p12.2, 10q21.2 and 14q11.2 are associated with risk of childhood acute lymphoblastic leukemia. Nat Genet. 2009;41(9):1006-1010.
7. Rudant J, Orsi L, Bonaventure A, et al. *ARID5B*, *IKZF1* and non-genetic factors in the etiology of childhood acute lymphoblastic leukemia: the ESCALE study. PLoS One. 2015;10(3):e0121348.
8. Xu H, Yang W, Perez-Andreu V, et al. Novel susceptibility variants at 10p12.31-12.2 for childhood acute lymphoblastic leukemia in ethnically diverse populations. J Natl Cancer Inst. 2013;105(10):733-742.
9. Olsson L, Johansson B. Ikaros and leukaemia. Br J Haematol. 2015;169(4):479-491.
10. Olsson L, Castor A, Behrendtz M, et al. Deletions of *IKZF1* and *SPRED1* are associated with poor prognosis in a population-based series of pediatric B-cell precursor acute lymphoblastic leukemia diagnosed between 1992 and 2011. Leukemia. 2014;28(2):302-310.
11. Stang A. Critical evaluation of the Newcastle-Ottawa scale for the assessment of the quality of nonrandomized studies in meta-analyses. Eur J Epidemiol. 2010;25(9):603-605.
12. Bahari G, Hashemi M, Naderi M, et al. *IKZF1* gene polymorphisms increased the risk of childhood acute lymphoblastic leukemia in an Iranian population. Tumour Biol. 2016;37(7):9579-9586.
13. Gharbi H, Ben Hassine I, Soltani I, et al. Association of genetic variation in *IKZF1*, *ARID5B*, *CDKN2A*, and *CEBPE* with the risk of acute lymphoblastic leukemia in Tunisian children and their contribution to racial differences in leukemia incidence. Pediatr Hematol Oncol. 2016;33(3):157-167.
14. Mahjoub S, Chayeb V, Zitouni H, et al. *IKZF1* genetic variants rs4132601 and rs11978267 and acute lymphoblastic leukemia risk in Tunisian children: a case-control study. BMC Med Genet. 2019;20(1):159.
15. Al-Absi B, Razif MFM, Noor SM, et al. Contributions of *IKZF1*, *DDC*, *CDKN2A*, *CEBPE*, and *LMO1* gene polymorphisms to acute lymphoblastic leukemia in a Yemeni population. Genet Test Mol Biomarkers. 2017;21(10):592-599.
16. Lin CY, Li MJ, Chang JG, et al. High-resolution melting analyses for genetic variants in *ARID5B* and *IKZF1* with childhood acute lymphoblastic leukemia susceptibility loci in Taiwan. Blood Cells Mol Dis. 2014;52(2-3):140-145.
17. Liao F, Ye Y, Yin D, et al. Validations of top and novel susceptibility variants in all-age Chinese patients with acute lymphoblastic leukemia. Front Genet. 2020;11:1004.
18. Mosaad YM, El-Ziny MA, Darwish A, et al. *IKZF1* rs4132601 and rs11978267 gene polymorphisms and acute lymphoblastic leukemia: relation to disease susceptibility and outcome. J Pediatr Hematol

Oncol. 2020;42(7):420-428.
19. Urayama KY, Takagi M, Kawaguchi T, et al. Regional evaluation of childhood acute lymphoblastic leukemia genetic susceptibility loci among Japanese. Sci Rep. 2018;8(1):789.
20. Lopes BA, Barbosa TC, Souza BKS, et al. *IKZF1* gene in childhood B-cell precursor acute lymphoblastic leukemia: interplay between genetic susceptibility and somatic abnormalities. Cancer Prev Res (Phila). 2017;10(12):738-744.
21. Bhandari P, Ahmad F, Mandava S, et al. Association of genetic variants in *ARID5B*, *IKZF1* and *CEBPE* with risk of childhood de novo B-Lineage acute lymphoblastic leukemia in India. Asian Pac J Cancer Prev. 2016;17(8):3989-3995.
22. Kreile M, Piekuse L, Rots D, et al. Analysis of possible genetic risk factors contributing to development of childhood acute lymphoblastic leukaemia in the Latvian population. Arch Med Sci. 2016;12(3):479-485.
23. Burmeister T, Bartels G, Gröger D, et al. Germline variants in *IKZF1*, *ARID5B*, and *CEBPE* as risk factors for adult-onset acute lymphoblastic leukemia: an analysis from the GMALL study group. Haematologica. 2014;99(2):e23-e25.
24. Peyrouze P, Guihard S, Grardel N, et al. Genetic polymorphisms in *ARID5B*, *CEBPE*, *IKZF1* and *CDKN2A* in relation with risk of acute lymphoblastic leukaemia in adults: a Group for Research on Adult Acute Lymphoblastic Leukaemia (GRAALL) study. Br J Haematol. 2012;159(5):599-602.
25. Prasad RB, Hosking FJ, Vijayakrishnan J, et al. Verification of the susceptibility loci on 7p12.2, 10q21.2, and 14q11.2 in precursor B-cell acute lymphoblastic leukemia of childhood. Blood. 2010;115(9):1765-1767.
26. Orsi L, Rudant J, Bonaventure A, et al. Genetic polymorphisms and childhood acute lymphoblastic leukemia: GWAS of the ESCALE study (SFCE). Leukemia. 2012;26(12):2561-2564.
27. Ellinghaus E, Stanulla M, Richter G, et al. Identification of germline susceptibility loci in ETV6-RUNX1-rearranged childhood acute lymphoblastic leukemia. Leukemia. 2012;26(5):902-909.
28. Vijayakrishnan J, Sherborne AL, Sawangpanich R, et al. Variation at 7p12.2 and 10q21.2 influences childhood acute lymphoblastic leukemia risk in the Thai population and may contribute to racial differences in leukemia incidence. Leuk Lymphoma. 2010;51(10):1870-1874.
29. Wang Y, Chen J, Li J, et al. Association of three polymorphisms in *ARID5B*, *IKZF1* and *CEBPE* with the risk of childhood acute lymphoblastic leukemia in a Chinese population. Gene. 2013;524(2):203-207.
30. Ross JA, Linabery AM, Blommer CN, et al. Genetic variants modify susceptibility to leukemia in infants: a Children's Oncology Group report. Pediatr Blood Cancer. 2013;60(1):31-34.
31. Linabery AM, Blommer CN, Spector LG, et al. *ARID5B* and *IKZF1* variants, selected demographic factors, and childhood acute lymphoblastic leukemia: a report from the Children's Oncology Group. Leuk Res. 2013;37(8):936-942.
32. Emerenciano M, Barbosa TC, Lopes BA, et al. *ARID5B* polymorphism confers an increased risk to acquire specific MLL rearrangements in early childhood leukemia. BMC Cancer. 2014;14:127.
33. Pastorczak A, Górniak P, Sherborne A, et al. Role of 657del5 *NBN* mutation and 7p12.2 (*IKZF1*), 9p21 (*CDKN2A*), 10q21.2 (*ARID5B*) and 14q11.2 (*CEBPE*) variation and risk of childhood ALL in the Polish population. Leuk Res. 2011;35(11):1534-1536.
34. Lautner-Csorba O, Gézsi A, Semsei AF, et al. Candidate gene association study in pediatric acute lymphoblastic leukemia evaluated by Bayesian network based Bayesian multilevel analysis of relevance. BMC Med Genomics. 2012;5:42.
35. Iacobucci I, Iraci N, Messina M, et al. IKAROS deletions dictate a unique gene expression signature in patients with adult B-cell acute lymphoblastic leukemia. PLoS One. 2012;7(7):e40934.

DOI 10.1007/s10330-021-0527-7
Cite this article as: Wang SS, Lin CY, Xi TT, et al. Relationship between *IKZF1* polymorphisms and the risk of acute lymphoblastic leukemia: a meta-analysis. Oncol Transl Med. 2022;8(5):217–225.

Oncology and Translational Medicine
DOI 10.1007/s10330-021-0529-9

October 2022, Vol. 8, No. 5, P226–P231

ORIGINAL ARTICLE

Difference in the effects of three nutritional pathways on postoperative rehabilitation in patients with gastric cancer and type 2 diabetes mellitus*

Yan Li (✉), Yan Zhou, Mao Chen

Department of General Surgery, Mianyang Central Hospital, Mianyang 621000, China

Abstract

Objective To explore the difference in the effects of three nutritional pathways on the rehabilitation of patients with gastric cancer and diabetes mellitus after operation.

Methods Overall, 120 patients were randomly divided into the partial parenteral nutrition (PPN), early enteral nutrition (EEN), and diabetes mellitus special enteral nutritional emulsion (DEN) groups. The differences in the effects of three nutritional modes were compared.

Results (1) On postoperative day four, the total protein level in the EEN and DEN groups was significantly higher than that in the PPN group ($P < 0.05$). On postoperative day ten, body mass index, lymphocyte count, total protein level, and pre-albumin level in the DEN group were significantly higher than those in the PPN group ($P < 0.05$). (2) On postoperative day four, there was no significant difference in the fasting blood glucose level between the EEN and DEN groups ($P > 0.05$), but this level was significantly lower than that in the PPN group ($P < 0.05$). On postoperative day ten, fasting and postprandial blood glucose levels in the DEN group were significantly lower than those in the PPN group. (3) On postoperative day four, the C-reactive protein level in the DEN group was significantly lower than that in the other groups ($P < 0.05$). (4) The incidence rates of complications in the PPN, EEN, and DEN groups were 25.0%, 10.0%, and 5.0%, respectively. The incidence of complications in the PPN group was significantly higher than that in the other groups. However, there was no significant difference in perioperative indexes among the three groups ($P > 0.05$).

Conclusion Enteral nutrition is more conducive to the recovery of patients with gastric cancer and type 2 diabetes mellitus after operation; the special enteral nutrition emulsion for diabetes mellitus is more effective than the conventional nutrition solution in stabilizing blood sugar levels and reducing the degree of inflammation.

Received: 16 October 2021
Revised: 1 December 2021
Accepted: 21 December 2021

Key words: gastric cancer; type 2 diabetes mellitus; enteral nutrition; parenteral nutrition

Gastric cancer is one of the most common malignant tumors of the digestive tract, and surgery is the main treatment. Reasonable perioperative treatment and nursing are important factors affecting the rehabilitation process of patients [1, 2]. Owing to changes in lifestyle and food spectrum, the incidence rate of type 2 diabetes mellitus (T2DM) is increasing rapidly in China [3, 4]. Many elderly patients with gastric cancer have T2DM. Such patients often experience poor basic nutrition and poor treatment compliance. Inappropriate postoperative nutrition can lead to unstable blood glucose levels, slow wound healing, immune imbalance, and other complications. Therefore, it is necessary to develop more targeted nutritional interventions. This study collected 120 elderly patients as the research object to prospectively explore the differences in the effects of three nutritional pathways on the postoperative rehabilitation of elderly patients with gastric cancer complicated with T2DM, to provide a basis for clinical rational selection.

✉ Correspondence to: Yan Li. Email: 495543950@qq.com
* Supported by a grant from the General Project of Youth Science Foundation (No. 81604115).

Materials and methods

Materials

From January 2017 to April 2021, a total of 120 elderly patients with gastric cancer complicated with T2DM were selected from the Department of General Surgery of Mianyang Central Hospital. The inclusion criteria were as follows: (1) The patient's first diagnosis was primary gastric cancer with a clear pathological basis; (2) The patient should have met the diagnostic criteria for T2DM published in the 2017 edition of the American Diabetes Association [5]; (3) Gastric cancer was divided into stages I-III, and the patient should have undergone radical surgery of D2 and above; (4) Age ≥ 60 years old; (5)Informed consent was provided by the patient and the family. The exclusion criteria were as follows: (1) Presence of Roux-en-Y gastrointestinal anastomosis; (2) Presence of dysfunction of other important organs, such as cardiac insufficiency, renal insufficiency, and so on; (3) Before operation, the patient received anticancer treatment such as radiotherapy, chemotherapy, or immunotherapy. Finally, 120 patients were included in the study. There were 78 males and 42 females, with an average age of 71.7 ± 5.4 years.

Intervention methods and grouping

According to the different nutritional modes, patients were randomly divided into the partial parenteral nutrition (PPN) group, early enteral nutrition (EEN) group, or diabetes mellitus special enteral nutritional emulsion (DEN) group. The specific measures were as follows: PPN group: meeting the nitrogen demand of 0.2 g/(kg·d) and non-protein heat card of 22 kcal/(kg·d) as the standard; considering factors such as the enhancement of postoperative insulin resistance and systemic stress response, it was finally determined that 70% of energy was supplied by fat emulsion and 30% by glucose solution—vitamins, electrolytes, and trace elements were added simultaneously. Insulin was prepared as follows: 1 U: (4-8) g sugar neutralization solution. The above nutrients were mixed into a parenteral nutrition solution, which was continuously injected through the peripheral vein for 24 h. According to the actual recovery status of the patient, there was a gradual change from a liquid diet to a normal diet one week after the operation. In the EEN group, 250 mL of normal saline was injected through the nasal feeding tube 12 h after the operation, and the patient's reaction was observed. If there was no obvious discomfort, then the enteral nutrient solution was injected. In the DEN group, similar to that in the EEN group, 250 mL of normal saline was injected through the nasal feeding tube 12 h after the operation, and the patient's reaction was observed. If there is no obvious discomfort, use enteral nutrition infusion pump, the speed should be slow to fast, injection of 500 mL special nutrition emulsion (Chinese medicine approved J20140077, Fresenius Kabihuaru Pharmaceutical Co., LTD.), with a tube feeding speed of approximately 20 mL/h. After that, there was an increase of approximately 20 mL/h every day, but the maximum dropping speed should not exceed 120 mL/h, which was adjusted according to the actual situation of the patient.

Test indicators

(1) Nutritional indexes: body mass index (BMI), lymphocyte count (LYM), total protein level, pre-albumin level, and other indexes were repeatedly measured before the operation and on the first, fourth, and tenth day after the operation. BMI was not measured on the first day after the operation because of the inconvenience of lying on bed. (2) Blood glucose level and inflammatory indexes: fasting and 2 h postprandial blood glucose levels, leukocyte count, and C-reactive protein levels were repeatedly measured before the operation and on the first, fourth, and tenth day after the operation. Blood samples were collected by full-time nurses of our department. The blood sample indexes were tested in the laboratory department of our hospital. (3) Perioperative indicators: postoperative hospital stay, postoperative exhaust time, incidence of complications, and types of complications were recorded objectively.

Statistical analysis

All data were analyzed using SPSS 20.0 software package. The collected data were repeatedly entered, checked, and corrected by two people. The measurement data are expressed as $\bar{\chi} \pm s$, and the statistical inference was analyzed using one-way analysis of variance. The counting data are expressed as frequency and rate, and the chi-square test or Fisher exact probability test was used for comparison. $P < 0.05$ was considered to indicate a statistically significant difference.

Results

Comparison of nutritional indexes between the three groups

There was no significant difference in the nutritional indexes between the three groups before the operation and on the first day after the operation ($P > 0.05$). On postoperative day four, the total protein level in the EEN and DEN groups was significantly higher than that in the PPN group ($P < 0.05$), but there was no significant difference in the other indexes ($P > 0.05$). On postoperative day ten, BMI, LYM, and total protein and pre-albumin levels in the DEN group were significantly higher than those in the PPN group ($P < 0.05$; Table 1).

Comparison of fasting blood glucose and 2-h postprandial blood glucose levels among the three groups

On postoperative day four, there was no significant difference in the fasting blood glucose level between the EEN and DEN groups ($P > 0.05$), but this level was significantly lower than that in the PPN group ($P < 0.05$). On postoperative day ten, fasting and 2-h postprandial blood glucose levels in the DEN group were significantly lower than those in the PPN group, but there was no significant difference between the DEN and EEN groups ($P > 0.05$; Table 2).

Comparison of leukocyte count and C-reactive protein level among the three groups

Before and 1 day after the operation, there was no significant difference in the leukocyte count and C-reactive protein (CRP) level among the three groups ($P > 0.05$). On postoperative days four and ten, the white blood cell count and CRP level in the DEN group were significantly lower than those in the PPN and EEN groups ($P < 0.05$; Table 3).

Comparison of perioperative indexes among

Table 1 Comparison of nutritional indicators among the three groups

Index	PPN (n = 40)	ENN (n = 40)	DEN (n = 40)	F	P
Preoperative					
BMI	24.14 ± 3.76	25.91 ± 3.05	24.85 ± 3.08	1.446	0.244
LYM	1.85 ± 0.68	1.84 ± 0.79	1.80 ± 0.79	2.106	0.131
total protein	62.08 ± 8.38	64.74 ± 9.97	63.48 ± 6.45	0.502	0.607
Pre- -albumin	200.22 ± 54.97	232.61 ± 88.10	221.58 ± 70.65	1.031	0.363
The first day after surgery					
LYM	1.03 ± 0.53	1.21 ± 0.69	1.17 ± 0.81	0.379	0.686
total protein	53.26 ± 5.08	57.39 ± 6.18	55.83 ± 5.34	2.821	0.067
Pre-albumin	162.05 ± 43.81	185.01 ± 50.77	178.63 ± 41.57	1.354	0.266
The fourth day after surgery					
BMI	23.18 ± 3.43	25.15 ± 3.01	24.14 ± 3.06	1.929	0.154
LYM	0.97 ± 0.35	1.35 ± 0.44	1.71 ± 0.71	10.020	0.000
total protein	50.98 ± 5.13	54.57 ± 4.79[a]	54.89 ± 4.75[a]	3.937	0.025
Pre-albumin	127.38 ± 31.17	139.21 ± 37.71	148.34 ± 46.99	1.440	0.245
The tenth day after surgery					
BMI	22.70 ± 3.39	24.64±2.94	25.07 ± 3.07[a]	3.236	0.046
LYM	0.97 ± 0.35	1.35±0.44[a]	1.71 ± 0.71[ab]	10.020	0.000
total protein	50.23 ± 11.28	52.59±15.76	61.22 ± 15.98[ab]	3.183	0.048
Pre-albumin	113.38 ± 28.35	134.46±25.36[a]	157.00 ± 40.68[ab]	9.205	0.000

BMI, body mass index; LYM, lymphocyte count; PPN, partial parenteral nutrition; EEN, early enteral nutrition; DEN, diabetes mellitus special enteral nutritional emulsion. [a] compared with PPN group, $P < 0.05$; [b] compared with EEN group, $P < 0.05$

Table 2 Comparison of fasting and 2-hour postprandial blood glucose levels among the three groups

Index	PPN (n = 40)	ENN (n = 40)	DEN (n = 40)	F	P
Fasting blood-glucose					
Before surgery	7.3 ± 1.2	6.7 ± 1.3	7.2 ± 0.9	1.574	0.216
1d postoperatively	10.2 ± 2.8	10.6 ± 2.8	9.9 ± 3.4	0.271	0.763
4d postoperatively	10.3 ± 1.8	8.7 ± 2.5[a]	8.7 ± 2.4[a]	3.357	0.041
10d postoperatively	8.8 ± 1.3	7.8 ± 1.7[a]	6.9 ± 1.0[a]	9.713	0.000
After 2h postprandial blood glucose					
Before surgery	9.3 ± 1.3	8.5 ± 2.4	8.4 ± 1.5	1.505	0.230
1d postoperatively	10.5 ± 2.4	9.9 ± 2.8	9.5 ± 3.6	0.572	0.567
4d postoperatively	10.5 ± 2.5	9.4 ± 2.7	8.9 ± 2.1[a]	2.240	0.115
10d postoperatively	10.5 ± 2.2	9.3 ± 2.7	7.9 ± 1.4[a]	7.211	0.001

PPN, partial parenteral nutrition; EEN, early enteral nutrition; DEN, diabetes mellitus special enteral nutritional emulsion. [a] compared with PPN group, $P < 0.05$; [b] compared with EEN group, $P < 0.05$

Table 3 Comparison of leukocyte count and C-reactive protein level among the three groups

Index	PPN (n = 40)	ENN (n = 40)	DEN (n = 40)	F	P
Preoperative					
WBC	6.21 ± 1.54	5.95±1.40	5.92±1.72	0.209	0.811
CRP	8.42 ± 11.34	10.15±10.74	10.71±17.83	0.152	0.859
1d postoperatively					
WBC	12.15 ± 3.58	11.83±2.52	12.58±3.03	0.299	0.742
CRP	68.15 ± 44.37	58.94±39.01	61.51±47.31	0.236	0.790
4d postoperatively					
WBC	8.24 ± 2.44	7.66±1.99	6.76±1.79[ab]	2.544	0.087
CRP	36.27 ± 33.97	22.62±15.66[a]	18.74±12.78[ab]	3.255	0.045
10d postoperatively					
WBC	9.40 ± 5.82	7.53±2.47	6.57±1.36[ab]	2.971	0.059
CRP	29.84 ± 31.53	18.89±19.47	12.53±8.23[ab]	3.192	0.048

WBC, white blood cell; CRP, C-reactive protein; PPN, partial parenteral nutrition; EEN, early enteral nutrition; DEN, diabetes mellitus special enteral nutritional emulsion. [a] compared with PPN group, $P < 0.05$; [b] compared with EEN group, $P < 0.05$

Table 4 Comparison of perioperative indicators among the three groups

Index	PPN (n = 40)	ENN (n = 40)	DEN (n = 40)	F/χ^2	P
Postoperative hospital stay	17.64 ± 7.14	15.66 ± 4.41	14.25 ± 3.87	2.037	0.139
Post-operative exhaust time	4.03 ± 1.25	3.75 ± 0.98	3.39 ± 1.07	3.074	0.054
The incidence of complications	25.0% (10/40)	10.0% (4/40)	5.0% (2/40)	7.500	0.024
Complications type				15.000	0.059
Acute cholecystitis	3	0	0		
Anastomotic fistula	1	2	0		
Infection of incisional wound	4	2	0		
Hypostatic pneumonia	2	0	2		

PPN, partial parenteral nutrition; EEN, early enteral nutrition; DEN, diabetes mellitus special enteral nutritional emulsion

the three groups

The incidence rates of complications in the PPN, EEN, and DEN groups were 25.0% (10/40), 10.0% (4/40), and 5.0% (2/40), respectively. The incidence of complications was significantly higher in the PPN group than in the other groups. However, there was no significant difference in the perioperative indexes, including postoperative hospital stay, postoperative exhaust time, and complication type composition among the three groups ($P > 0.05$; Table 4).

Discussion

With improvements in comprehensive treatment, the survival rate of patients with gastric cancer has improved significantly. However, some patients with gastric cancer, especially those with early gastric cancer, will still have recurrence or metastasis in the short term even if they receive standard radical surgery. Some researchers believe that [6] this may be related to tumor-related malnutrition or immune deficiency. T2DM is a common endocrine disease that has an impact on the metabolism of important nutrients such as sugar, fat, and protein. The resulting high-glucose environment is a good culture medium for bacterial growth. Concomitantly, when the patient is in a state of stress, the chemotaxis of leukocytes is weakened and, consequently, opportunistic pathogenic bacteria enter the patient's body owing to being weak, inducing infection [7]. Disordered homeostasis has a significant negative impact on the postoperative rehabilitation of patients with malignant tumors, which can lead to slow recovery of intestinal peristalsis and delayed or nonunion of incision healing and can even promote recurrence [8]. Therefore, it is necessary to develop and implement more targeted postoperative interventions in patients with gastric cancer complicated with T2DM.

The concept of rapid rehabilitation surgery affirms the positive role of EEN in the surgical rehabilitation of patients with gastric cancer [9], but there are only few reports on the significance of EEN in patients with gastric cancer complicated with T2DM. In this study, we randomly divided patients into the PEN group, EEN group, and DEN group. After the intervention, on postoperative day four, the total protein levels in the EEN and DEN groups were significantly higher than that in the PPN group. On postoperative day ten, BMI,

LYM, and total protein and pre-albumin levels in the DEN group were significantly higher than those in the PPN group. This indicates that enteral nutrition can play a more supportive role than parenteral nutrition, and the effectiveness of enteral nutritional emulsion for diabetes is stronger than that of general nutrition. This may be related to the following advantages of enteral nutrition [10, 11]: (1) it has a stronger stimulatory effect on the recovery of gastrointestinal function; (2) it is more conducive to the recovery of "intestinal liver circulation" and promotes the synthesis of liver-derived protein; and (3) it maintains the function of intestinal mucosa and stabilizes the intestinal flora. There are microvascular lesions in the gastrointestinal tissue of diabetes patients, which becomes a negative factor affecting the recovery of gastrointestinal function postoperatively. Hyperglycemia is not conducive to the postoperative rehabilitation of patients with [12]. The current research also supports the fact that enteral nutrition-based interventions should be carried out as soon as possible for patients undergoing intestinal surgery without contraindications. Enteral nutrition is safer and cheaper for patients than parenteral nutrition, which requires placing and maintaining a central venous catheter. Enteral nutrition also helps maintain the integrity of the intestinal mucosal structure and function and prevent secondary complications, while long-term parenteral nutrition can lead to steatohepatitis. After starting treatment, patients with enteral nutrition do not need continuous monitoring, while patients with parenteral nutrition need regular monitoring. In this study, on postoperative day four, there was no significant difference in the fasting blood glucose level between the EEN and DEN groups, but this level was significantly lower than that in the PPN group. On postoperative day ten, fasting and 2-hour postprandial blood glucose levels in the DEN group were significantly lower than those in the PPN group, but these levels showed no significant difference between the DEN and EEN groups. This indicates that enteral nutritional emulsion may play a role in stabilizing the blood glucose level in the early postoperative stage. Blood glucose control was poor in the PPN group. For patients who must undergo a parenteral nutrition-based intervention in the clinic, the possibility of hyperglycemia should be fully considered with timely interventions. Because of the advantage of special enteral nutrition emulsion in controlling the blood glucose level, the CRP level in the DEN group was also significantly lower on the fourth and tenth day after the operation.

Alternative, this study found that enteral nutrition is more conducive than parenteral nutrition for the postoperative recovery of patients with gastric cancer complicated with T2DM, and that enteral nutritional emulsion for diabetes is more effective in stabilizing the blood glucose level and reducing the degree of inflammation than the conventional nutrition solution. However, this study has some shortcomings: (1) the samples were collected from a single center; hence, there may have been some sampling bias; (2) the sample size is limited. In the future, results from multicenter research with a larger sample size may generate more conclusive findings.

Acknowledgments

Not applicable.

Funding

Supported by a grant from the General Project of Youth Science Foundation (No. 81604115).

Conflicts of interest

The authors indicated no potential conflicts of interest.

Author contributions

Not applicable.

Data availability statement

Not applicable.

References

1. Bilgin S, Gozum S. Effect of nursing care given at home on the quality of life of patients with stomach cancer and their family caregivers' nursing care. Eur J Cancer Care (Engl). 2018;27(2):e12567.
2. Ding J, Sun B, Song P, et al. The application of enhanced recovery after surgery (ERAS)/fast-track surgery in gastrectomy for gastric cancer: a systematic review and meta-analysis. Oncotarget. 2017;8(43):75699-75711.
3. Shen YN, Zhao F, Zhou LX, et al. Evaluation of exercise-related clinical practice guidelines for type 2 diabetes mellitus patients. Chin Nurs Manage (Chinese). 2018;18(6):755-761.
4. Kong JH, Zhang J, Huang YY, et al. The application of nutritional risk screening in nutritional assessment of elderly diabetic nephropathy. Chin J Clin Healthe (Chinese). 2017;20(1):58-60.
5. Chamberlain JJ, Herman WH, Leal S, et al. Pharmacologic therapy for type 2 diabetes: synopsis of the 2017 American Diabetes Association standards of medical care in diabetes. Ann Intern Med. 2017;166(8):572-578.
6. Ida N, Nakamura K, Saijo M, et al. Prognostic nutritional index as a predictor of survival in patients with recurrent cervical cancer. Mol Clin Oncol. 2018;8(2):257-263.
7. Massara M, De Caridi G, Serra R, et al. The role of procalcitonin as a marker of diabetic foot ulcer infection. Int Wound J. 2017;14(1):31-34.
8. Zhang TH, Dai JY. The effect on blood glucose of different gastrointestinal reconstruction after radical surgery for gastric cancer patients with type-2 diabetes mellitus. Chin J Mod Operat Surg (Chinese). 2017;22(8):592-595.
9. Li YJ, Huo TT, Xing J, et al. Meta-analysis of efficacy and safety of fast-track surgery in gastrectomy for gastric cancer. World J Surg, 2014;38(12):3142-3151.
10. Gao L, Zhao Z, Zhang L, et al. Effect of early oral feeding on gastrointestinal function recovery in postoperative gastric cancer

patients: a prospective study. J BUON. 2019;24(1):194-200.
11. Song GM, Liu XL, Bian W, et al. Systematic review with network meta-analysis: comparative efficacy of different enteral immunonutrition formulas in patients underwent gastrectomy. Oncotarget. 2017;8(14):23376-23388.
12. Gregersen H, Liao D, Drewes AM, et al. Ravages of diabetes on gastrointestinal sensory-motor function: implications for pathophysiology and treatment. Curr Gastroenterol Rep. 2016;18(2):6.

DOI 10.1007/s10330-021-0529-9
Cite this article as: Li Yan, Zhou Yan, Chen Mao, et al. Effects of three nutritional pathways on postoperative rehabilitation in patients with gastric cancer and type 2 diabetes mellitus. Oncol Transl Med. 2022;8(5):226–231.

Oncology and Translational Medicine
DOI 10.1007/s10330-021-0535-5

October 2022, Vol. 8, No. 5, P232–P238

ORIGINAL ARTICLE

Bioinformatics analysis of potential hub genes associated with biological characteristics and survival in patients with gastric cancer*

Libo Feng[1], Liu Yu[2], Xiaolong Chen[1] (✉)

[1] Department of Gastrointestinal Surgery, The Affiliated Hospital of Southwest Medical University, Luzhou 646000, China
[2] Department of Electrocardiogram, The Affiliated Hospital of Southwest Medical University, Luzhou 646000, China

Abstract

Objective Gastric cancer (GC) is a serious threat to human health. In this study, we aimed to explore the differentially expressed genes (DEGs) and identify potential targets for the treatment of GC.

Methods The gene expression profile of GSE79973 which compared tissue samples from gastric cancer patients and healthy individuals, downloaded from the GEO database, was submitted to the GCBI online analysis platform to screen for DEGs. Gene ontology (GO) analysis, pathway analysis, and construction of networks, including gene signal and gene co-expression networks, were performed to identify the core DEGs. Survival analysis was performed to determine the relationship between these genes and patient survival time.

Results Nine hundred eighty-three genes were identified as DEGs ($P < 0.001$; FC > 2). GO analysis showed that DEGs were primarily involved in processes such as angiogenesis, cell metabolism, cell adhesion, redox processes, and cell migration. The metabolism of xenobiotics by cytochrome P450, ECM-receptor interaction, drug metabolism by cytochrome P450, metabolic pathways, and the PI3K-Akt signaling pathway were significantly enriched in pathway analysis. Genes such as *UGT2B15*, Hepatocyte growth factor (HGF), Nidogen-2 (NID2), Follistatin-like protein 1 (FSTL1), and Inhibin beta A chain (INHBA) were closely linked to other genes in the network. Survival analyses indicated that *HGF*, *NID2*, *FSTL1*, and *INHBA* expression levels were inversely correlated with survival time in patients with gastric cancer.

Conclusion *HGF*, *NID2*, *FSTL1*, and *INHBA* may be potential key genes associated with the biological characteristics and survival in patients with gastric cancer.

Received: 16 November 2021
Revised: 21 January 2022
Accepted: 15 March 2022

Key words: gastric cancer; differentially expressed genes; enrichment analysis; bioinformatics

Tumors are a global health problem. Gastric cancer is the third leading cause of cancer-related deaths worldwide [1]. In China, the incidence of gastric cancer is approximately 679.1/100,000, and the mortality rate is as high as 498/100,000, making gastric cancer the second most common malignant cancer in China [2]. In the United States, 26,370 new cases of gastric cancer were estimated in 2016, of which 10,370 people were estimated to have died [3]. Presently, the preferred treatment for gastric cancer is radical surgery, usually combined with systemic chemotherapy in the perioperative period [4, 5]. The lack of specific performance resulted in most patients being in the late stage of diagnosis. Although, the five-year mortality rate of early gastric cancer has reduced in recent years, it remains 30%–50% in advanced gastric cancer cases [6]. The rapid development of genomics and gene chip technology has led to the occurrence, development, and prognosis of gastric cancer being studied at the gene level. Bioinformatics technology uses multiple analytical methods (including gene ontology (GO) and pathway analyses) and biological networks (including co-expression, signal, and protein interaction networks) to identify potential core genes from thousands of differentially expressed genes (DEGs).

✉ Correspondence to: Xiaolong Chen. Email: 1870747218@qq.com
*Supported by a grant from the Project of Southwest Medical University-Three Affiliated Hospitals (No. 2017-ZRQN-028).

In this study, DEGs were screened based on the gene expression profiles of gastric cancer and normal tissues, which were downloaded from the gene expression omnibus (GEO) database. Various bioinformatics analyses and biological networks were applied to further filter out the core DEGs that may serve as molecular markers and potential therapeutic targets for gastric cancer, and this is also helpful in understanding the molecular mechanisms underlying gastric cancer development.

Materials and methods

Microarray data

The gene expression data set GSE79973 [7] was downloaded from the GEO data repository (http://www.ncbi.nlm.nih.gov/geo/). Twenty samples were included in this dataset: 10 gastric cancer and 10 normal tissues. Gene expression profiles were obtained using the GPL570 [HG-U133_Plus_2] Affymetrix Human Genome U133 Plus 2.0 Array.

Data preprocessing and screening of DEGs

Gene-Cloud of Biotechnology Information (GCBI) (https://www.gcbi.com.cn/gclib/html/index), an online genetic data analysis software based on the R language, was used to normalize and analyze the gene chip data. The cut-offs to filter out differentially expressed genes were set to $P < 0.001$ and fold change (FC) > 2.

Function and pathway enrichment of DEGs

Gene ontology analysis, which annotates and classifies genes according to biological pathways, molecular functions, and cell locations [8], is commonly used in functional studies [9]. DEGs were enriched in various biological functions, pathways, and cell localization through GO analysis and were easily dertermined by GO analysis. Gene expression data of gastric cancer were submitted to GCBI for functional enrichment analysis to uncover biological processes. DEGs with a false discovery rate (FDR) < 0.05 and $P < 0.05$ were considered significant. The Kyoto Encyclopedia of Genes and Genomes (KEGG) (http://www.genome.jp/kegg/), established by the Bioinformatics Center at Kyoto University, Japan, is a useful database resource for genome sequencing and other high-throughput experimental techniques generated from molecular-level information, especially large molecular data sets. KEGG combines genomic information with high-level functional information and systematically analyzes the function of genes by computerizing known biological processes within the cell and standardizing existing gene function interpretations [10, 11]. Pathway analysis was used to identify the pathway entries in which DEGs were enriched and to determine the related changes in cellular pathways. Statistical significance was set at $P < 0.05$.

Signal network and co-expression network analysis

Biological networks reflect the interrelationship between genes or genes and other functions or pathways. Signal network analysis conducts interaction analysis through relational or predictive relationships in the GCBI database and identifies important nodes from the network diagram parameters. A co-expression network was constructed based on gene expression similarity. This network displayed the similarities between genes in a clear and hierarchical manner and helped identify key regulatory genes and interactions.

Survival analysis

Gene expression profiling interactive analysis (GEPIA) (http://gepia.cancer-pku.cn/) is an online analytical tool based on TCGA database. This included various modules, including differential expression analysis, profile mapping, correlation analysis, and patient survival analysis. Survival analysis was used to compare different genes based on gene expression levels. A survival curve was plotted based on the survival time of patients with respect to different gene expression levels, to determine the relationship between the gene and patient survival time.

Results

Differential gene expression between gastric cancer and normal tissues

A total of 983 DEGs were identified between normal and gastric cancer samples according to the following criteria: $P < 0.001$ and FC > 2. This included 547 upregulated and 436 downregulated genes (Fig. 1).

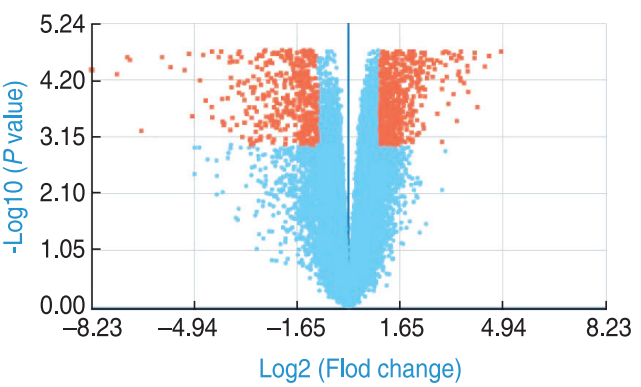

Fig. 1 Volcano plot of DEGs

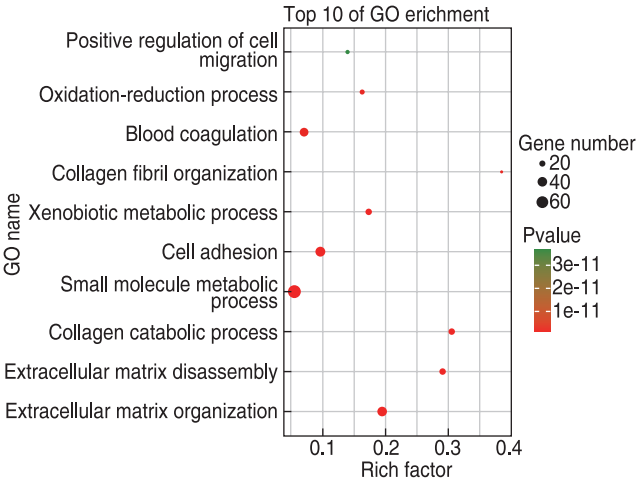

Fig. 2 The top 10 most enriched GO analysis categories

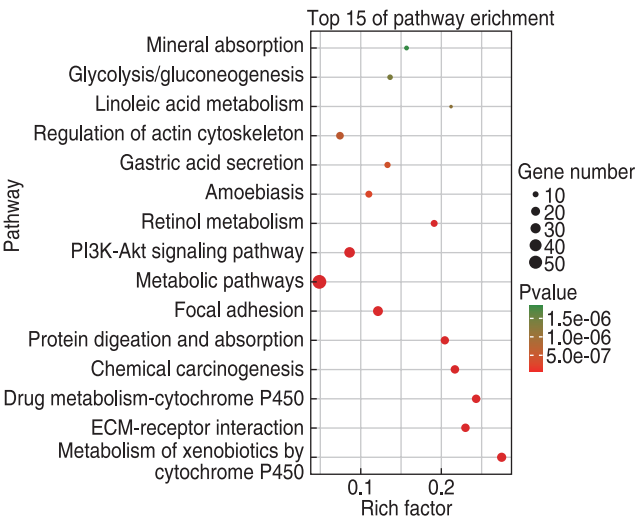

Fig. 3 The top 15 most enriched Kyoto Encyclopedia of Genes and Genomes (KEGG) pathways

Function and pathway enrichment analysis

Gastric cancer gene expression was investigated at a functional level. A total of 983 DEGs (FDR < 0.05) were classified into 232 GO terms. Based on the decreasing FDR values the top categories were (Fig. 2) extracellular matrix organization, extracellular matrix disassembly, collagen catabolic process, small molecule metabolic process, cell adhesion, xenobiotic metabolic process, collagen fibril organization, blood coagulation, oxidation-reduction process, and positive regulation of cell migration. Pathway enrichment analysis was used to identify significant biological pathways related to the DEGs. A total of 50 enriched pathways were identified with an FDR < 0.05. The results revealed that biological processes such as metabolism of xenobiotics by cytochrome P450s (FDR = 2.5×10^{-19}), ECM-receptor interaction (FDR = 4.65 $\times 10^{-18}$), drug metabolism by cytochrome P450s (FDR = 7.81×10^{-17}), metabolic pathways (FDR = 3.2×10^{-13}), and the PI3K-Akt signaling pathway (FDR = 9.75×10^{-13}) were significantly enriched (Fig. 3).

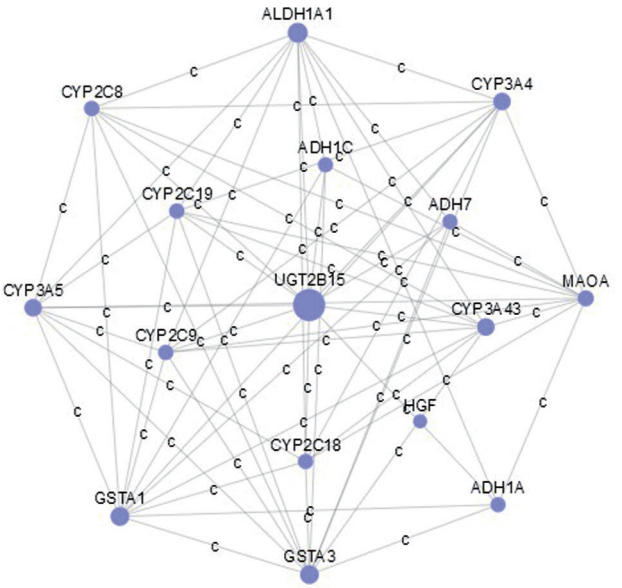

Fig. 4 Signal network of DEGs

Construction of signal and co-expression networks

Genes interact with and regulate one another. Networks visualize the relationships of DEGs to determine the upstream and downstream regulatory relationships between genes, which enables the identification of core genes. The signal and co-expression networks of DEGs are shown in Fig. 4 and Fig. 5, respectively. The cytochrome P450 family genes (such as *CYP2C8*, *CYP2C9*, *CYP2C18*, *CYP2C19*, *CYP3A4*, *CYP3A5*, and *CYP3A43*) and several members of the alcohol dehydrogenase family (such as *ADH1A*, *ADH1C*, and *ADH7*), are related to gastric cancer (Fig. 4). Furthermore, the UDP glucuronosyl transferase 2 family polypeptide B15 (*UGT2B15*) was most closely linked with other genes in the network. The relationships between the top 49 significant DEGs, including 39 upregulated and 10 downregulated genes, is shown in Fig. 5.

Survival analysis

Survival analyses were performed to determine the association between gene expression levels and patient survival time. Patients with gastric cancer and high expression of genes such as *HGF*, *NID2*, *FSTL1*, and *INHBA* had shorter survival times than those with lower expression of these genes (Fig. 6–9). The *P* value of each of the four genes was less than 0.05 (*P* = 0.0041, 0.0013, 0.023, and 0.028, respectively).

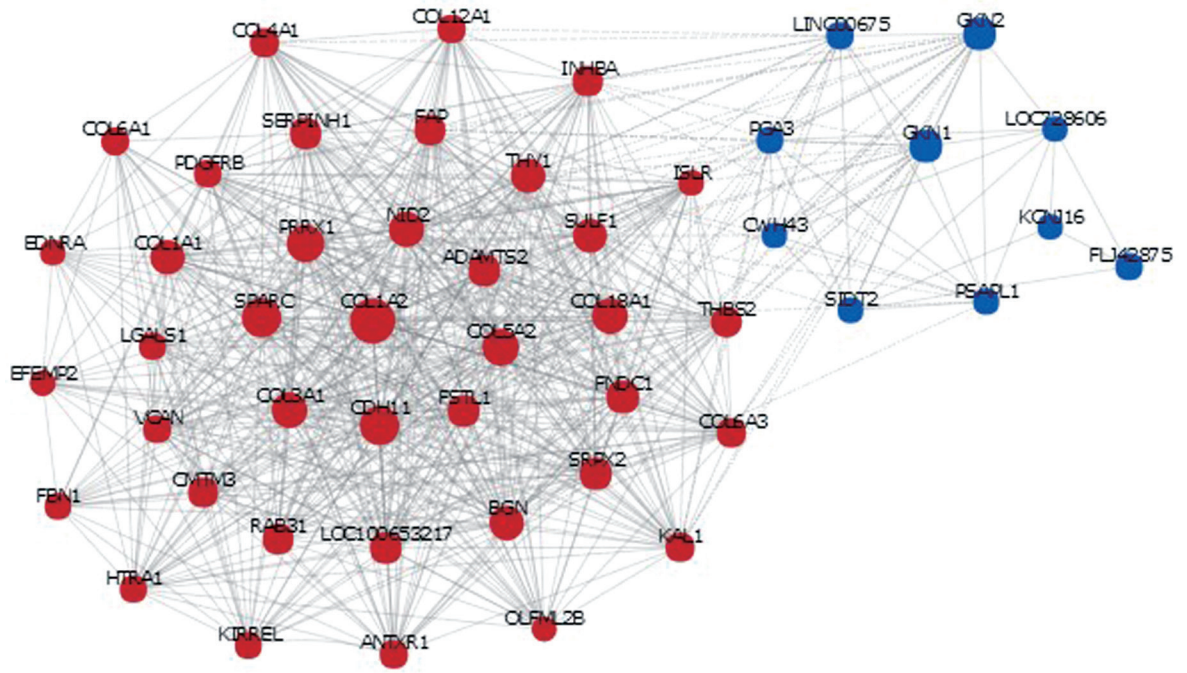

Fig. 5 Co-expression network of DEGs. The red nodes represent upregulated genes, and the blue nodes represent downregulated genes

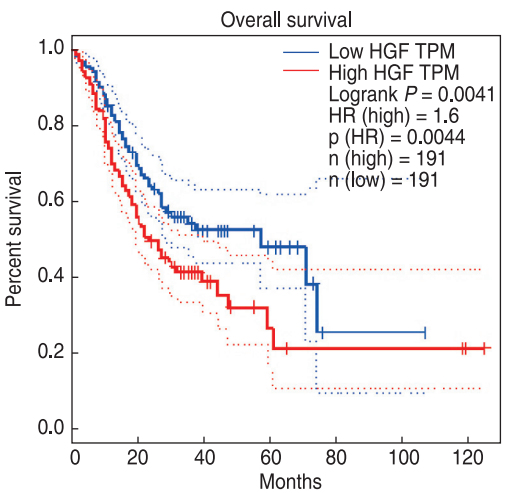

Fig. 6 Survival curve of HGF

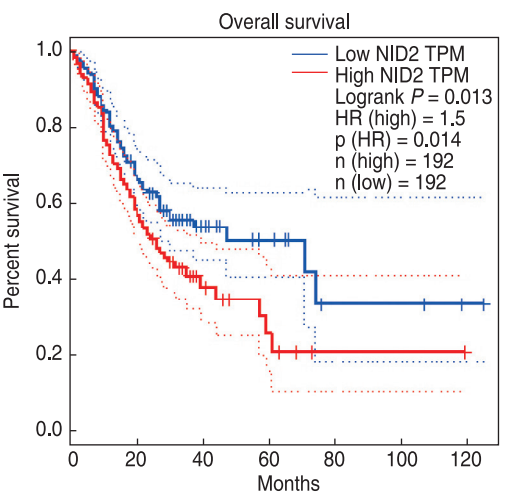

Fig. 7 Survival curve of NID2

Discussion

Gastric cancer is the fourth most common malignancy and the third largest cause of cancer-related deaths worldwide. Although radical surgery combined with systemic chemotherapy has improved the survival rate in patients with gastric cancer, most patients are diagnosed at an advanced stage. Radical resection has a high recurrence rate and results in poor response to treatment [12, 13]. To improve the survival rate in patients with gastric cancer, medical scientists have been committed to understanding gastric cancer based on molecular mechanisms and seeking new therapeutic targets [14]. Genomics, epigenetics, and proteomics have been used to elucidate the molecular mechanisms underlying gastric cancer and identify biomarkers that are associated with poor prognosis and possess curative effects [15, 16]. These biomarkers may serve as therapeutic targets in patients with advanced gastric cancer. Therefore, based on bioinformatics analyses, core DEGs were identified and gastric cancer was better understood at the genetic level, which may provide a new direction for the future

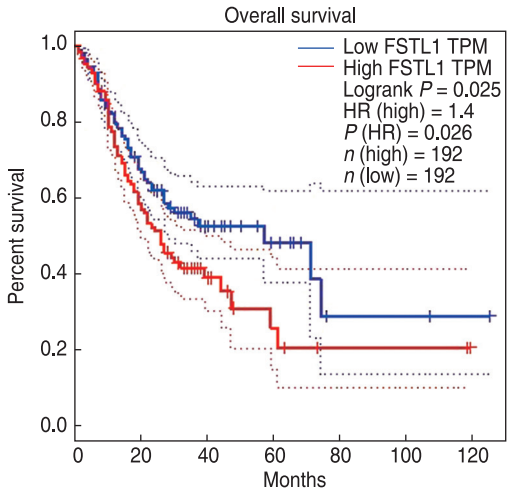

Fig. 8 Survival curve of FSTL1

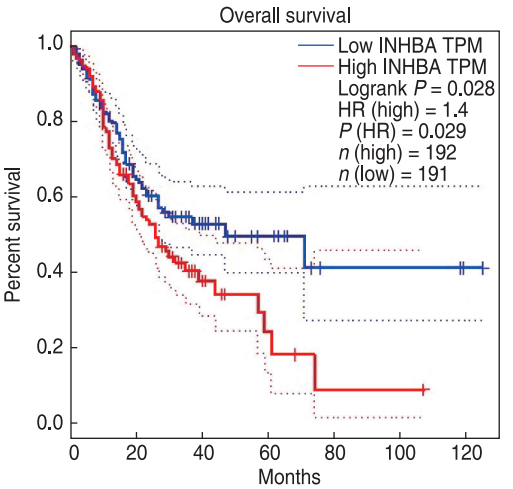

Fig. 9 Survival curve of INGBA

treatment of gastric cancer.

In this study, 983 DEGs were screened by comparing tissue samples from patients with gastric cancer and healthy individuals. Among them, 547 genes were upregulated and 436 were downregulated. The most significant genes were primarily involved in signal transduction, cell proliferation, apoptosis, biosynthesis, gene expression, hormone secretion, and biological metabolism. GO enrichment analysis classifies genes according to their functions and identifies significantly different biological functions by counting the degree of enrichment of genes involved with different functions. The most significant functions were in processes such as cell metabolism, substance metabolism, cell adhesion, coagulation reactions, redox processes, cell migration, and angiogenesis. Additionally, 76, 44, and 20 genes were enriched in the metabolic pathway of small molecules, cell adhesion, and angiogenesis, respectively. Recent evidence has indicated that neovascularization is a necessary condition for tumor growth and metastasis [17]. Cell adhesion, molecular metabolism, and cell migration are all associated with tumor development and progression [18]. Pathway enrichment analysis and pathway relation network construction of DEGs indicated biological processes such as pathways in cancer, adherens junction, focal adhesion, the WNT signaling pathway, and the pentose phosphate pathway to be significant.

The signal networks suggest that *UGT2B15*, *ALDH1A1*, and cytochrome P450 family genes (such as *CYP2C8*, *CYP2C9*, *CYP2C18*, *CYP2C19*, *CYP3A4*, *CYP3A5*, and *CYP3A43*), and hepatocyte growth factor (*HGF*) are closely related to gastric cancer. *HGF* is a ubiquitous cytokine that is involved in multiple biological processes. *HGF* stimulates tumor cells by activating the homologous receptor c-Met [19, 20]. *HGF/c-MET* signaling strongly participates in angiogenesis, proliferation, progression, and metastasis in many human cancers, including head and neck, non-small cell lung carcinoma, pancreatic, cervical, and prostate cancers [21–25]. *HGF/Met* expression levels are inversely correlated with survival time in patients with late-stage nasopharyngeal carcinoma [26]. Recently, research has shown that *HGF* expression was enhanced in gastric cancer tissues, and the overexpression of *HGF* stimulated an increase in vascular endothelial growth factor (VEGF) expression, which could significantly promote proliferation and increase cell migration [27]. It has been reported that cells overexpressing *HGF* are less sensitive to the suppression of biological processes such as cell growth, cell migration, cell invasion, colony formation, and cell cycle regulation by the *C-Met* inhibitor [28]. Therefore, *HGF*, which acts as a cancer promoter, plays a vital role in gastric cancer and may be a promising therapeutic target [27]. After co-expression analysis of the DEGs, we found that genes, including *COL1A2*, *CDH11*, *SPARC*, *COL18A1*, *COL3A1*, *NID2*, *BGN*, *THY1*, and *FSTL1* were closely related to the rest of the genes. These genes are primarily involved in various signaling pathways, such as angiogenesis, cell adhesion, and cell proliferation, and play important roles in tumorigenesis and metastasis.

Potential genes, such as *HGF*, *NID2*, *FSTL1*, and *INHBA*, were further confirmed to be related to gastric cancer by drawing their survival curves. The results indicated that the expression levels of these genes were negatively correlated with the overall survival in patients with gastric cancer. This correlation may be due to these genes playing an substantial role in promoting metastasis and the development of gastric cancer. Therefore, these genes may be potential targets for the treatment of gastric cancer, and interventions to inhibit their expression may help improve the survival rate in patients with gastric cancer.

Conclusions

Bioinformatics analyses have been increasingly applied in research on various clinical diseases. In this study, we identified the core DEGs, including *HGF*, *NID2*, *FSTL1*, and *INHBA*, which may be involved in proliferation, progression, metastasis of gastric cancer and survivial of patients with gastric cancer.. This finding verifies the reliability of DEGs and provides a theoretical basis for further related research. These genes may provide new insights into the diagnosis, treatment, prognosis, and prevention of gastric cancer. However, as this study was based on minimal bioinformatics analyses of gene chip data, further experiments are needed to validate the potential of these genes.

Acknowledgments

Not applicable.

Funding

Supported by a grant from the Project of Southwest Medical University-Three Affiliated Hospitals (No. 2017-ZRQN-028).

Conflicts of interest

The authors indicated no potential conflicts of interest.

Author contributions

Not applicable.

Data availability statement

Not applicable.

Ethical approval

Not applicable.

References

1. Bray F, Ferlay J, Soerjomataram I, et al. Global cancer statistics 2018: GLOBOCAN estimates of incidence and mortality worldwide for 36 cancers in 185 countries. CA Cancer J Clin. 2018;68(6):394-424.
2. Chen W, Zheng R, Baade PD, et al. Cancer statistics in China, 2015. CA Cancer J Clin. 2016;66(2):115-132.
3. Siegel RL, Miller KD, Jemal A. Cancer statistics, 2019. CA Cancer J Clin. 2019;69(1):7-34.
4. Cunningham D, Allum WH, Stenning SP, et al. Perioperative chemotherapy versus surgery alone for resectable gastroesophageal cancer. N Engl J Med. 2006;355(1):11-20.
5. Ychou M, Boige V, Pignon JP, et al. Perioperative chemotherapy compared with surgery alone for resectable gastroesophageal adenocarcinoma: an FNCLCC and FFCD multicenter phase III trial. J Clin Oncol. 2011;29(13):1715-1721.
6. Hamashima C, Shabana M, Okada K, et al. Mortality reduction from gastric cancer by endoscopic and radiographic screening. Cancer Sci. 2015;106(12):1744-1749.
7. He J, Jin Y, Chen Y, et al. Downregulation of ALDOB is associated with poor prognosis of patients with gastric cancer. Oncol Targets Ther. 2016;9:6099-6109.
8. Ashburner M, Ball CA, Blake JA, et al. Gene ontology: tool for the unification of biology. The Gene Ontology Consortium. Nat Genet. 2000;25(1):25-29.
9. Hulsegge I, Kommadath A, Smits MA. Globaltest and GOEAST: two different approaches for Gene Ontology analysis. Bmc Proceedings. 2009;3(S4):S10.
10. Kanehisa M, Araki M, Goto S, et al. KEGG for linking genomes to life and the environment. Nucleic Acids Res. 2008;36(Database issue): D480-484.
11. Kanehisa M, Furumichi M, Tanabe M, et al. KEGG: new perspectives on genomes, pathways, diseases and drugs. Nucleic Acids Res. 2017;5(D1):D353-D361.
12. Fujii M, Kochi M, Takayama T. Recent advances in chemotherapy for advanced gastric cancer in Japan. Surg Today. 2010;40(4):295-300.
13. Kang H, Kauh JS. Chemotherapy in the treatment of metastatic gastric cancer: is there a global standard? Curr Treat Options Oncol. 2011;12(1):96-106.
14. Bang YJ, Kim YW, Yang HK, et al. CLASSIC trial investigators. Adjuvant capecitabine and oxaliplatin for gastric cancer after D2 gastrectomy (CLASSIC): a phase 3 open-label, randomised controlled trial. Lancet. 2012;379(9813):315-321.
15. Lin LL, Huang HC, Juan HF. Discovery of biomarkers for gastric cancer: a proteomics approach. J Proteomics. 2012;75(11):3081.
16. Yamashita K, Sakuramoto S, Watanabe M. Genomic and epigenetic profiles of gastric cancer: Potential diagnostic and therapeutic applications. Surg Today. 2011;41(1):24.
17. Rak J, Mitsuhashi Y, Bayko L, et al. Mutant ras oncogenes upregulate VEGF/VPF expression: implications for induction and inhibition of tumor angiogenesis. Cancer Res. 1995;55(20):4575-4580.
18. Berger H, Marques MS, Zietlow R, et al. Gastric cancer pathogenesis. Helicobacter. 2016;21 Suppl 1:34-38.
19. Owusu BY, Galemmo R, Janetka J, et al. Hepatocyte growth factor, a key tumor-promoting factor in the tumor microenvironment. Cancers (Basel). 2017;9(4):35.
20. Spina A, De PV, Cerulo G, et al. HGF/c-MET axis in tumor microenvironment and metastasis formation. Biomedicines. 2015;3(1):71-88.
21. Arnold L, Enders J, Thomas SM. Activated HGF-c-met axis in head and neck cancer. Cancers (Basel). 2017;9(12).
22. Boromand N, Hasanzadeh M, Shahidsales S, et al. Clinical and prognostic value of the C-Met/HGF signaling pathway in cervical cancer. J Cell Physiol. 2018;233(6):4490-4496.
23. Martin TA, Mason MD, Jiang WG. HGF and the regulation of tight junctions in human prostate cancer cells. Oncol Rep. 2014;32(1): 213-224.
24. Pothula SP, Xu Z, Goldstein D, et al. Targeting the HGF/c-MET pathway: stromal remodelling in pancreatic cancer. Oncotarget, 2017;8(44):76722-76739.
25. Tsuta K, Kozu Y, Mimae T, et al. C-MET/Phospho-MET protein expression and MET gene copy number in non-small cell lung carcinomas. J Thorac Oncol. 2012 Feb;7(2):331-339.
26. Qian CN, Guo X, Cao B, et al. Met protein expression level correlates with survival in patients with late-stage nasopharyngeal carcinoma. Cancer Res. 2002;62(2):589.
27. Si Y, Zhang H, Ning T, et al. miR-26a/b inhibit tumor growth and angiogenesis by targeting the HGF-VEGF Axis in gastric carcinoma. Cell Physiol Biochem. 2017;42(4):1670-1683.
28. Ahn SY, Kim J, Kim MA, et al. Increased HGF expression induces resistance to c-MET Tyrosine Kinase inhibitors in gastric cancer.

Anticancer Res. 2017;37(3):1127-1138.

DOI 10.1007/s10330-021-0535-5
Cite this article as: Feng LB, Yu L, Chen XL. Bioinformatics analysis of potential hub genes associated with biological characteristics and survival in patients with gastric cancer. Oncol Transl Med. 2021;8(5):232–238.

Oncology and Translational Medicine
DOI 10.1007/s10330-022-0586-6

October 2022, Vol. 8, No. 5, P239–P246

ORIGINAL ARTICLE

Allosteric probe-modified liposome loading bufalin-fluorouracil complex for targeted colorectal cancer therapy*

Fajiang Mao[1, 2], Xingli Wu[1], Chenyue Yuan[1], Haiyan Huang[1], Yanyan Qiu[1], Jianlin Ren[1] (✉), PeihaoYin[2] (✉)

[1] Department of Oncology, Shanghai Municipal Hospital of Traditional Chinese Medicine, Shanghai University of Traditional Chinese Medicine, Shanghai 200071, China
[2] Interventional Cancer Institute of Chinese Integrative Medicine, Putuo Hospital, Shanghai University of Traditional Chinese Medicine, Shanghai 200062, China

Abstract

Objective Bufalin, the main active anti-tumor monomer of toad venom, is crucial in cancer treatment. However, intrinsic issues, such as poor solubility and systematic toxicity, have considerably mitigated its anticancer functions and caused unwanted side effects. It is essential to develop innovative targeting systems to precisely and efficiently deliver anticancer drugs to achieve satisfying therapeutic efficiency.

Methods This work established a novel and more efficient system for simultaneously detecting and killing colorectal cancer cells. The proposed method designed two allosteric probes, a report probe and a recognize probe. The method exhibited high sensitivity towards cell detection via the recognizing probe identifying target cancer cells and the report probe's signal report. Combining bufalin and fluorouracil endowed better tumor cell inhibition.

Results We observed significantly enhanced fluorescence dots surrounding the HCT-116 cell membranes. No fluorescence increments in the other three cells were identified, indicating that the established liposome complex could specifically bind with target cells. In addition, the best ratio of bufalin to fluorouracil was 0.15 and 0.5, respectively. This improved the anti-tumor effects and achieved more than 60% tumor cell inhibition.

Conclusion This method will provide new opportunities for intracellular biomolecule detection and targeted cancer cell therapy.

Received: 30 June 2022
Revised: 21 July 2022
Accepted: 26 August 2022

Key words: bufalin; fluorouracil; colorectal cancer; imaging; therapy

Globally, colorectal cancer (CRC) is one of the most threatening malignant tumors, the second most common cancer, and the second leading cause of death. It seriously affects patients' life quality and brings heavy economic burden to the society [1-3]. In recent years, CRC incidence and mortality have increased due to gradually deteriorating factors, such as environment, occupation, living habits, and inheritance [4, 5]. CRC incidence has been rapidly rising in those under the age of 50 over the last 20 years [6]. Therefore, it is vital to establish complete novel nanomaterials with high tumor accumulation to deliver therapeutic units that augment therapeutic efficiency.

Bufalin is the main active anti-tumor monomer of toad venom, a kind of traditional Chinese medicine secreted from the glands behind the ears of *Bufo gargarizans* [7-9]. Bufalin has therapeutic effects on various solid tumors, including gastric cancer, liver cancer, esophageal cancer, lung cancer, and leukemia, due to its characteristics, such as inducing tumor cell apoptosis, inhibiting tumor cell proliferation, inhibiting tumor blood vessel formation,

✉ Correspondence to: Peihao Yin. Email: yinpeihao@shutcm.edu.cn
Jianlin Ren. Email: renjianlin666@126.com
* Supported by grants from the Medical Guidance Project of Shanghai Science and Technology Commission (No. 19401935200) and the Budget Internal Medicine Research Project of Shanghai University of Traditional Chinese Medicine (No. 2020LK065).

reversing tumor cell multidrug resistance, and promoting or enhancing tumor cell differentiation [10, 11]. Even though numerous studies have proven bufalin's potential anti-tumor influence, it is also criticized for cardiac side effects, such as arrhythmia and conduction block, limiting its clinical application [10, 12]. Additionally, the characteristics of bufalin, such as its insolubility in water, fast metabolism, and short half-life in the body, greatly limit its application in cancer treatment [13, 14]. Scientists have strived to deal with these deficiencies and promote applying bufalin in tumor therapy. Currently, there are two main methods for improving the performance of bufalin: chemically modifying the bufalin structure to create bufalin derivatives or circumventing its shortcomings through nanotechnology. For example, Zou *et al.* [15] embedded bufalin in the cavity of β-cyclodextrin (β-CD) to obtain higher stability and anti-tumor effects. They demonstrated that the water solubility of the complex was 24 or 34 times greater in water and phosphate-buffered saline (PBS) buffer, respectively. In recent years, various liposome-based methods to enhance the water solubility of bufalin have been proposed [16-18]. Li *et al.* [19] suggested a composed method that could realize the synergetic therapeutic efficacy of bufalin against melanomas by utilizing immune-liposome bufalin and anti-cluster of differentiation 40 (CD40) antibody adjuvant co-delivery. Although these methods have ameliorated the development of highly efficient bufalin-based strategies with better biocompatibility, their inability to simultaneously report tumor cells and therapeutic progress does not meet the requirements of accurate cancer therapies.

Herein, we proposed a novel and more efficient system for simultaneously detecting and killing CRC cells. We designed two allosteric probes: a report probe and a recognize probe. The recognize probe specially binds with the surface proteins of target cancer cells and release a blocker probe to initiate an attached rolling circle amplification (RCA) process. The recognize probe facilitates liposome and target cancer cell fusion, resulting in the transport of the report probe to the surface of the liposome and target cancer cells. Bufalin goes into cancer cells for anti-tumor treatment. In addition, RCA products induced by the released blocker probe unfold the report probes and generate fluorescence to flag the occurrence of the anti-tumor treatment.

Materials and methods

Materials

Liposome3000 (Lipofectamine® 3000 Transfection Reagent), the liposome extruder, and the filter membrane were provided by Invitrogen (Carlsbad, California, USA), Mercer (Shanghai, China), and Beyotime Biotechnology Co., Ltd. (Shanghai, China), respectively. Bufalin and 5-fluorouracil were purchased from Shanghai Ronghe Pharmaceutical Technology Development Co., Ltd. (Shanghai, China) and Beijing Soulebao Technology Co., Ltd. (Beijing, China), respectively.

We obtained HCT116 colon cancer cells, A549 lung cancer cells, HeLa cervical cancer cells, and FHC normal colon epithelial cell lines from the Shanghai Institute of Life Sciences, Chinese Academy of Sciences cell bank. All cells were cultured in Roswell Park Memorial Institute (RPMI)-1640 medium containing penicillin (100 U/mL) and streptomycin (100 g/mL) in 10% fetal bovine serum and placed in a 37 °C constant temperature and humidity incubator with 5% CO_2. Cells were sub-cultured every three days.

Table 1 details the oligonucleotide nucleic acids used in the experiment. The oligonucleotide nucleic acids used in this study were bought and purified from Shanghai Sangon Biological Engineering Technology and Services Co., Ltd. (Shanghai, China). The obtained oligonucleotide nucleic acids were diluted to 10 μM by high-performance liquid chromatography (HPLC) water and stored for the following experiments. The buffer-related regents and enzymes, such as bovine serum albumin (BSA), phi29 DNA polymerase, and T4 DNA ligase enzymes, were purchased from New England BioLabs (MA, USA). Fluorescence spectra were detected by a Hitachi F-4700 Fluorescence Spectrophotometer (Beijing, China). All solutions were prepared with ultrapure water, obtained using a water purification system (Milli-Q, Germany).

Methods

Investigating the designed allosteric probe for target cell recognition

We labeled the fluorescent probe and the corresponding quenching group on both ends of the allosteric probe. The purified and diluted allosteric probe was heated to 95 °C for 5 min and then slowly cooled to room temperature within 20 min. Afterward, 5 μL allosteric probe was mixed with the cells for 30 min. The fluorescence signals were detected using a Hitachi F-4700 Fluorescence Spectrophotometer (Beijing, China).

Table 1 Synthesized oligonucleotide sequence details

Title	Sequence (5'–3')
H1 probe	GAC GAC TAA TAA GAT TAA TCC TGT CCT CAA CAT CAG TCT GA TAA GCT AAT GTT CCT CAG CTG CTC TAG CTT ATC AGA CTG
H2 probe	TGT CCT AAT TAG AAT AAT CTC GAG TTC TAA GCT AGA GCA TC CAA TCA ACA TTA GCT TAT CAG ACT GAT GTT GAT TGG ATG CTC
S strand	AAC AGG ATT AAT CTT ATT AGT CGT CCT CGA GAT TAT TCT AAT TA GGA CAG CAG TTG AGG TAA TAG TCA CG

Detection performance evaluation

Obtained cells were diluted to different concentrations with RNase-free ddH_2O to investigate the detection sensitivity of the method. Different concentrations of cells (15 μL), 15 μL T4 DNA ligase enzyme, and 10 μL of established sensing scaffold were mixed in 4 μL 10× NE Buffer and incubated for 50 min at 37 °C. Afterward, the fluorescence spectra from 500 nm to 700 nm were collected in a 100 μL quartz cuvette with 490 nm excitation. We evaluated the method's selectivity by detecting different synthesized microRNAs (miRNAs) using the above procedures.

Establishing a subcutaneous transplanted tumor model in BALB/C nude mice

SPF grade BALB/C nude mice (20, four-week-old, male mice weighing 20 ± 2 g) were provided by the Shanghai SHREK company (License Number scxk 2017-0005) (Shanghai, China). They were raised and managed in the SPF-grade animal room of the Municipal Hospital of Traditional Chinese Medicine affiliated with the Shanghai University of Traditional Chinese Medicine. A 1-mL sterile syringe was used to aspirate cells with a density of 1×10^7/mL. The HCT116 cell suspension (100 μL) was injected when the needle reached the inoculation site. Then the nude mice were put back into the cage, and their general states were recorded. When the tumor body of nude mice grew to more than 62.5 cm^3, bufalin and 5-fluorouracil were encapsulated in liposomes modified with allosteric probes (the ratio of the two drugs was 0.15 μM bufalin to 12.5 μM 5-fluorouracil). We intraperitoneally injected 4.2 mg/kg of drug-loaded liposomes every two days, and the cumulative administration intervention lasted 30 days.

Live imaging observations of small animals

We injected 5 μL (10 μM) of allosteric probe-modified drug-loaded liposomes into the tumor site of the mice and observed the reaction for 30 min. The RCA product (5 μL) was injected into the tumor site. After 1 h, the nude mice were imaged. The fluorescence signal of the tumor body was detected by a small animal imager, and the excitation and emission lights were 530–550 and 560–600 nm, respectively (the fluorescent dye of the probe was Cy3. Its best excitation wavelength is 540 nm, and the emission wavelength is 570 nm).

Hematoxylin and eosin (HE) pathological staining

The nude mice were killed, subcutaneous tumor bodies were stripped, weighed, and measured, and the liver tissue and subcutaneous tumor of the nude mice were taken out for paraffin embedding. The specimens were clamped into the embedding box and put into the paraffin embedding machine for embedding. The wax blocks were put into the microtome for slicing 4 μM thick tissue paraffin sections. The wax block was put into a 60 °C oven and preheated for 10 min. Xylene, absolute ethanol, 95% ethanol, 80% ethanol, and 70% ethanol were dewaxed for 2 min. The following HE staining steps were executed:

i) Hematoxylin staining solution for 10 min.
ii) Differentiation solution for 30 s.
iii) Eosin staining solution for 2 min.
iv) Tap water washing and soaking for 5 min.
v) 95% ethanol and absolute ethanol dehydration for 2 min.
vi) Xylene permeabilization for 2 min.

The specimens were sealed with neutral gum and observed under an optical microscope (magnification: × 4 and × 40). According to the results of the pathological sections of liver tissues of nude mice in each group, all the groups showed liver damage except for the control group and group C, but no serious systemic adverse reactions occurred.

Data analysis

Each test underwent at least three independent replicates, displayed as the mean ± standard deviation (SD). Data were visualized using GraphPad Prism 8.0 software (CA, USA). A Student's *t*-test was used to analyze the comparisons between two groups. Multiple groups were compared with a one-way ANOVA and the least-significant difference (LDS) method. Differences were considered significant when $P < 0.05$.

Results

Working principle of the proposed strategy

Fig. 1 illustrates the working mechanism of the method. The proposed method for simultaneously detecting and treating CRC was mainly composed of two parts: i) fluorescence generation after the target CRC cells were recognized to report the occurrence of tumor cells and aptamer facilitated fusion of target colorectal cells with liposome, resulting in bufalin transport from liposomes to target cells to kill tumor cells. We designed two allosteric probes, the report and recognize probes (Fig. 1a), for the detection process. The recognize probe contained two DNA sequences: an aptamer sequence that could recognize the surface proteins of target cells and a blocker probe for initiating RCA. The report probe was designed with a hairpin structure and a cholesterol on its terminal to anchor it on the surface of liposomes and colorectal cells. We utilized liposomes to deliver bufalin and simultaneously improve water solubility for the anti-tumor process (Fig. 1b). The target cell protein aptamer in the designed recognize probe could provide targeted CRC cell recognition and accelerate liposome and colorectal cell fusion. The anti-tumor liposome complex was established by packaging bufalin with liposomes and loading the two designed allosteric probes onto the surface. In practice, the recognize probe on the surface of the liposome complex could bind with surface proteins

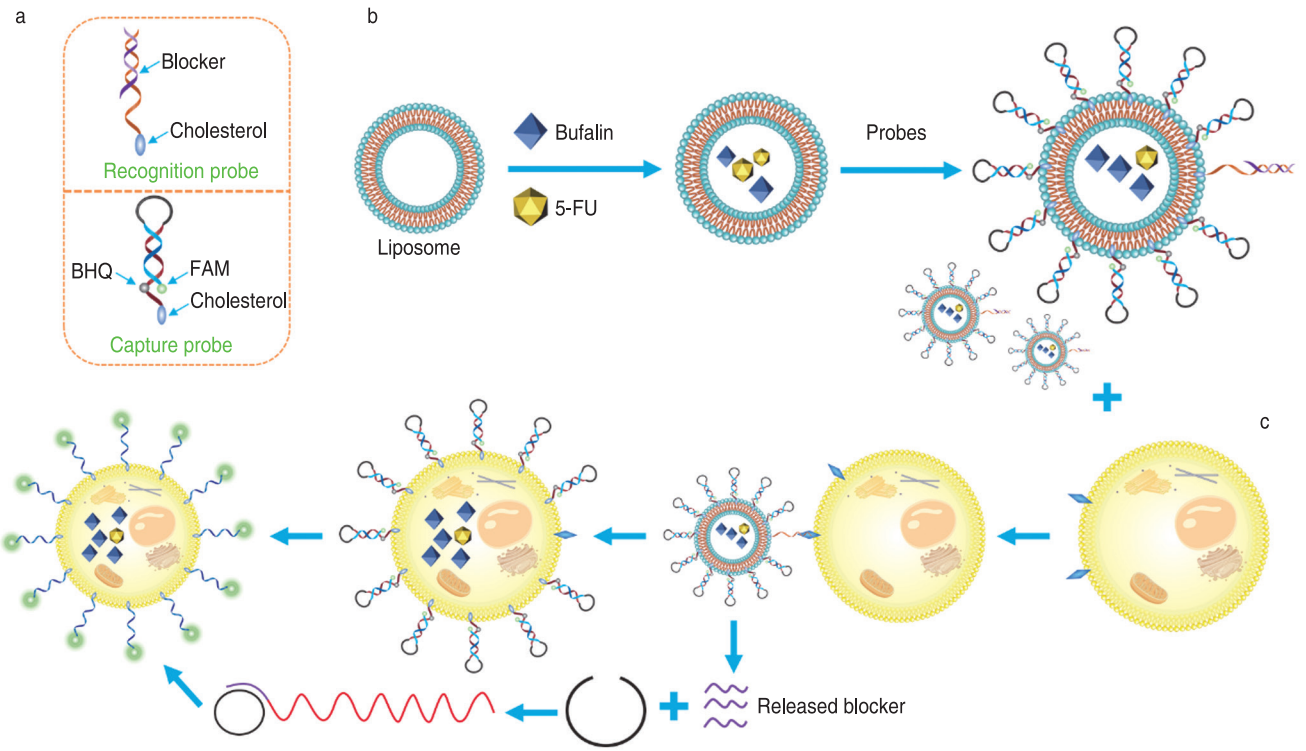

Fig. 1 The working principle of the proposed method for simultaneously detecting and therapizing CRC. (a) Details on how to design report and recognize probes; (b) Assembling bufalin into liposomes and the anchor designed allosteric probes on the liposome surface; (c) The working process of the method

by interacting with the aptamer and then draw them up when identifying the target CRC cells. Moreover, the aptamer-based recognition between the liposome complex and target CRC cells could facilitate liposomes fusing with cells and release blockers in the recognize probe. Meanwhile, the released blocker could further initiate the RCA process to produce single-strand DNA (ssDNA) sequences. As a result, the report probes on the surface of liposomes may be transported to the surface of target colorectal cells, importing bufalin into cancer cells to exert anti-tumor effects. Simultaneously, the obtained RCA products could recognize and specifically unfold report probes to generate fluorescence and flag tumor cells.

Investigating the designed probes and bufalin and 5-fluorouracil anti-tumor effects

The two probes were designed with different secondary structures with distinctive functional requirements. The recognition probe was composed of two parts, an aptamer of the cancer cell surface protein and a complementary blocker sequence. The report probe was designed with a stem-loop structure, which the RCA product could unfold to produce fluorescence. It is worth noting that the 3'-ends of these two probes were linked with cholesterol to anchor them in the phospholipid bilayer. First, we verified whether the designed recognition probe could specifically recognize target cancer cells and release the blocker sequences through a fluorescence assay (Fig. 2a). As shown in Fig. 2b, the obtained fluorescence intensity of the probes, when incubated with target CRC cells, was significantly higher than that in the control group. Furthermore, there were no obvious fluorescence enhancements in the non-specific group to incubate the probe with NCM 356 cells, which has no corresponding proteins on its surface, indicating that the designed recognize probe could specially bind with target cells and release blocker probes. We studied the RCA process through polyacrylamide gel electrophoresis (PAGE) analysis with a synthesized blocker as the initiator. We observed an approximately 20 bp band in lane 1 in the PAGE results. When the blocker was mixed with a padlock in lane 2, a higher band appeared (approximately 50 bp) – the complemented blocker and padlock complex. In lane 3, a light band was stuck in the well, indicating a long product that could not flow down (Fig. 2c). Therefore, the released blocker could hybridize with the two terminals of the padlock and subsequently initiate the RCA process. We then investigated whether the obtained RCA products could unfold the report probe through a fluorescence assay. As shown in Fig. 2d, we obtained an enhanced fluorescence when the RCA products were

mixed with the report probe. Furthermore, no significant fluorescence was observed when the report probe was incubated with other DNA sequences, demonstrating that the RCA products could specifically recognize and unfold the report probe to generate fluorescence signals.

We studied the anti-tumor effect of bufalin and 5-fluorouracil by detecting HCT116 cell viability after treating them with bufalin for different time periods. We concluded that bufalin and 5-fluorouracil could inhibit and kill HCT116 cells (Fig. 2c). 5-fluorouracil showed a relatively more stable inhibitory effect on cells. The inhibitory effect of both drugs was lower than 0.4, which is relatively low and needs further improvements (Fig. 2e). We decided to use bufalin in combination with 5-fluorouracil to increase the anti-tumor effect and optimize the ratio of bufalin to 5-fluorouracil. The results confirmed that the best ratio of bufalin to fluorouracil was 0.15 μM (bufalin) and 12.5 μM (fluorouracil), which could achieve more than a 60% tumor cell inhibition effect. Hence, combining the drugs showed better tumor cell inhibition (Fig. 2f).

Optimizing liposome complex assembly and the RCA process

The anti-tumor effect of the liposome complex loading bufalin and 5-fluorouracil may be closely associated with liposome size. Therefore, we investigated the anti-tumor effect of the liposomes with different sizes by detecting

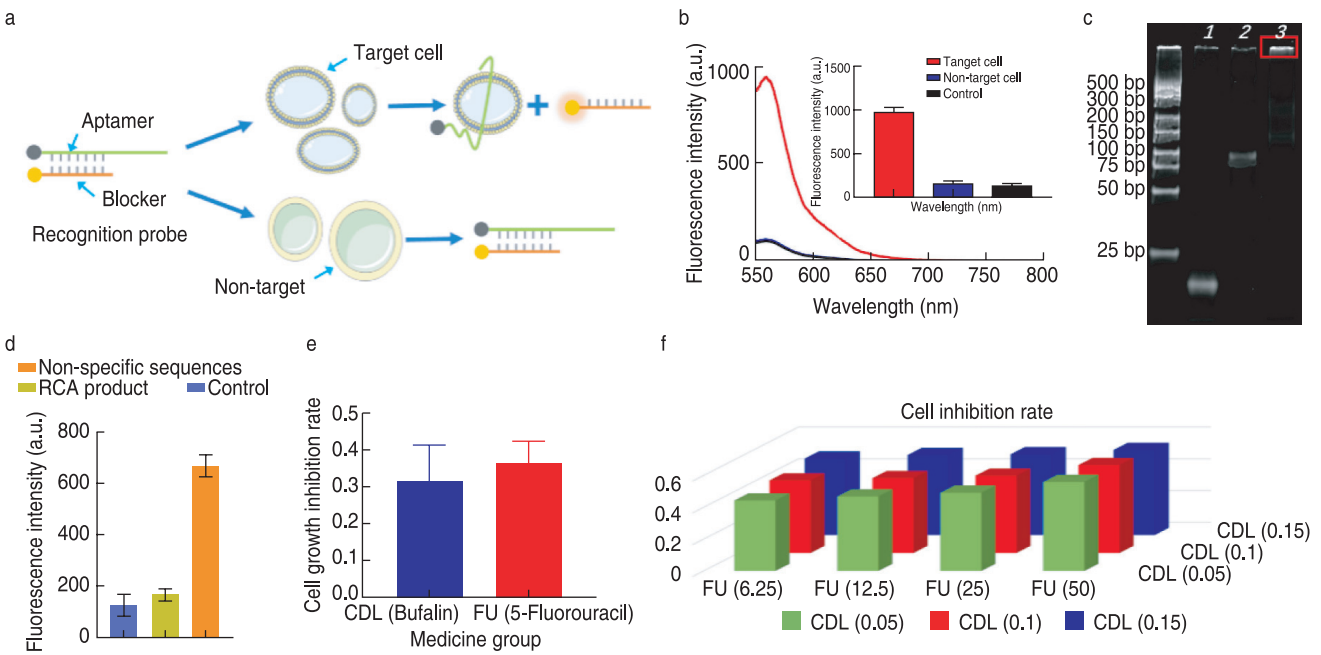

Fig. 2 Investigating the designed probes and bufalin and 5-fluorouracil anti-tumor effects. (a) Illustration of the fluorescence assay for investigating the recognition probe; (b) Fluorescence spectrum of the recognition probe when incubated with the target cell, non-specific cell, and control (1× PBS buffer); (c) PAGE analysis of the RCA process with a synthesized blocker as an initiator; (d) Fluorescence intensity report probes when incubated with RCA products or not; (e) HCT116 cell viability after liposome complex treatments; (f) Cell inhibition rate when treated with bufalin in combination with 5-fluorouracil at different ratios

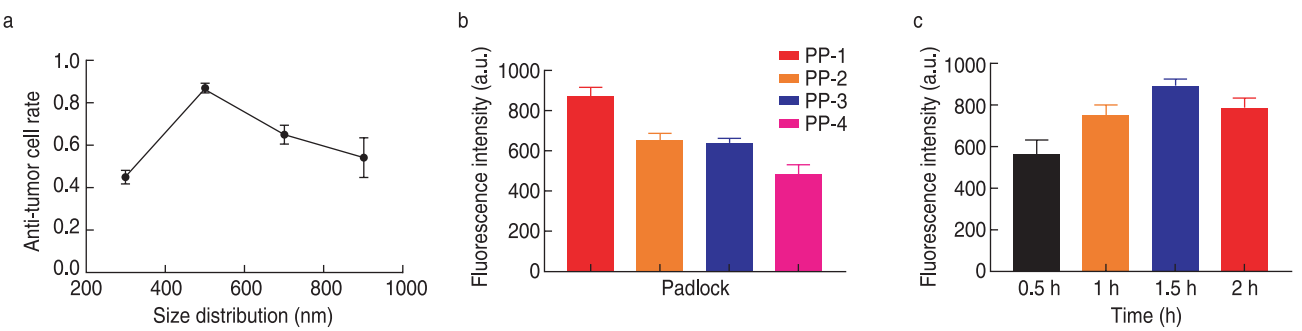

Fig. 3 Optimizing liposome complex assembly and the RCA process. (a) Anti-tumor cell rate of the liposome complex with different size distributions; (b) Fluorescence intensity of the RCA process with the four designed padlocks; (c) Fluorescence intensity of the RCA process at different times

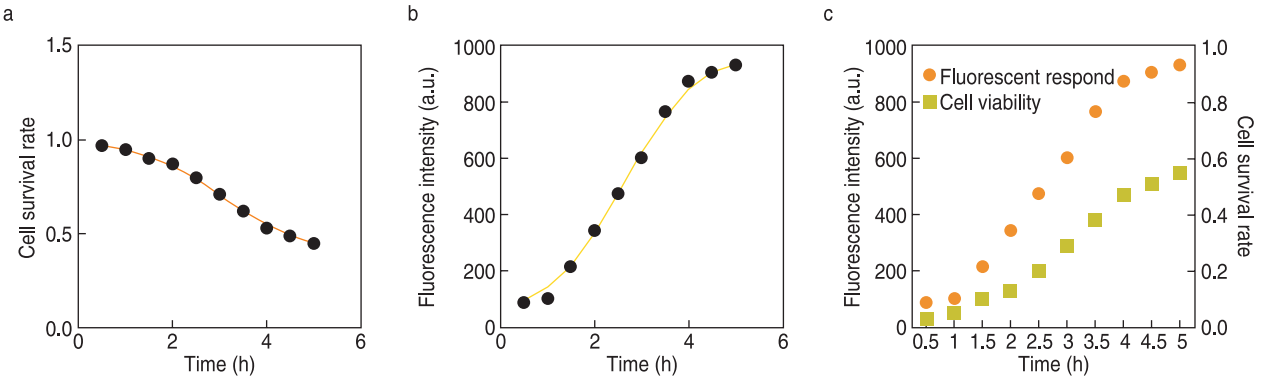

Fig. 4 The proposed method inhibits CRC *in vitro*. (a) HCT116 cell viability was obtained at different incubation times; (b) HCT116 cell fluorescence intensities were obtained at different incubation times; (c) Comparison of tumor inhibition rate and fluorescence intensity over time

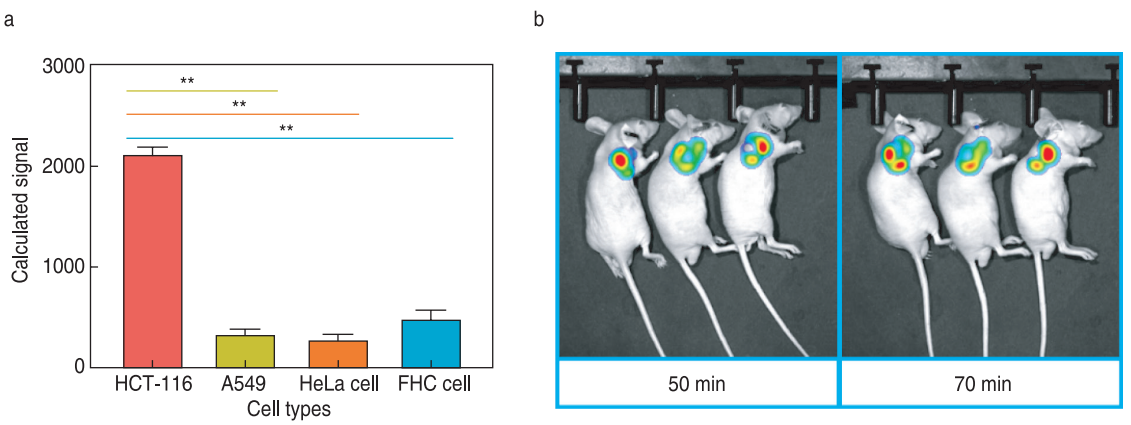

Fig. 5 Analytical performance of the proposed method. (a) Fluorescence signal of the cell when incubated with the established biosensor; (b) Animal imaging of the constructed CRCs after 50 min and 70 min of incubation

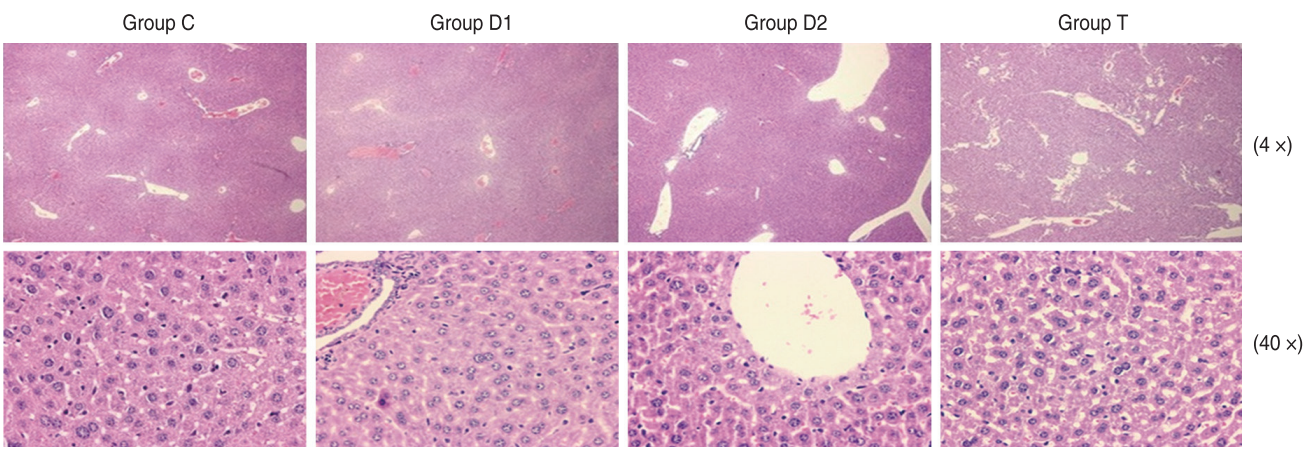

Fig. 6 Comparison of HE staining in the livers of nude mice in each group

cell viability after incubating them with HCT116 cells. The anti-HCT116 cell rate increased with liposome size, ranging from 300 nm to 500 nm (Fig. 3a). No further enhancements were observed with sizes greater than 500 nm, suggesting that liposomes with a 500 nm diameter could provide an optimized anti-tumor effect. Hence, we designed a desired padlock that could not be cyclized by undesired DNA sequences (PP1, PP2, PP3, and PP4)

with varied complementary lengths and blocker and secondary structures to meet such a requirement (Table S1). The fluorescence assay showed that all four padlocks initiated the RCA reaction in the presence of the blocker (Fig. 3b). PP1 had a length of 42 nucleotides, no inner hairpin structure, and yielded the highest fluorescence intensity. We investigated the time of the RCA process and observed the most RCA products at 1.5 h (Fig. 3c), indicating that the time for RCA is also enough for liposomes and cancer cells to fuse.

Feasibility of the proposed method for CRC treatments in vitro

We tested the cell viability of HCT116 cells treated with the complex at various intervals to confirm the anti-tumor efficacy of the liposome complex loading bufalin and 5-fluorouracil in CRC cells. We found that the anti-tumor effect of this complex was time-dependent (Fig. 4a). In addition, we showed that the fluorescence intensity increased over time and was positively correlated with impaired tumor growth (Fig. 4b, c). In summary, these data revealed the anti-tumor effects of the complex in vitro and its time and dose dependence.

Feasibility of the proposed method for CRC treatments in vivo

With the HCT116 cells as the target, we tested the fluorescence response of the system after recognizing the target CRC cells under the optimized experimental conditions. As illustrated in Fig. 5a, we applied the whole sensing system to detect HCT116 cells and three other cells that did not express the corresponding proteins on their membrane surfaces. We eventually noticed significantly enhanced fluorescence dots surrounding HCT116 cell membranes and no fluorescence increments in the other three cells, indicating that the established liposome complex could specifically bind with target cells. Having demonstrated the *in vitro* sensing capability of the established liposome complex, we sought to test its performance in *in situ* imaging and targeted therapy in a xenograft mouse model. A CRC model was utilized to investigate targeted identification and therapy. The fluorescence signal of the cancer models was monitored with different incubation times to uncover whether target protein recognition could specifically induce the following *in situ* imaging process and facilitate cell fusion. The fluorescence signal of liposome-treated cancer models dramatically increased when incubated for 60 min, while the control groups (without adding the liposome complex) displayed minimal tumor fluorescence enhancement (Fig. 5b).

In addition, we found that this liposome complex had no severe systemic side effects in the HE-stained liver and spleen tissues of mice treated with this complex or the corresponding control. We then evaluated therapeutic safety by analyzing the collected main viscera. We also collected normal organs of control mice (no tumor inoculation) under the same condition to reasonably evaluate possible side effects and other significant differences. Firstly, we investigated possible hepatic toxicity. According to the HE pathological sections of liver tissues of nude mice in each group, except for the control group, all groups showed slight liver damage, but no serious systemic adverse reactions occurred (Fig. 6).

Conclusion

This study established novel nuclear-shell biopolymers by loading bufalin and 5-fluorouracil into liposomes and anchoring the designed recognition and report probes. After recognizing the target CRC cell, the released blocker initiated the RCA process and unfolded the report probes. This strategy will aid in specific cancer cell recognition and reduce the undesired death of healthy cells that commonly occurs in conventional chemotherapy. This method will provide new opportunities for intracellular biomolecule detection and targeted cancer therapy.

Acknowledgments

Not applicable.

Funding

Supported by grants from the Medical Guidance Project of Shanghai Science and Technology Commission (No. 19401935200) and the Budget Internal Medicine Research Project of Shanghai University of Traditional Chinese Medicine (No. 2020LK065).

Conflicts of interest

The authors indicated no potential conflicts of interest.

Author contributions

All authors contributed to the data acquisition and interpretation and reviewed and approved the final version of this manuscript.

Data availability statement

Not applicable.

Ethical approval

This study was approved by the Experimental Animal Ethics Committee of Shanghai Municipal Hospital of Traditional Chinese Medicine, Shanghai University of Traditional Chinese Medicine.

References

1. Kishore C, Bhadra P. Current advancements and future perspectives of immunotherapy in colorectal cancer research. Eur J Pharmacol.

2021 Feb 15;893:173819.
2. Rajendran S, Barbon S, Pucciarelli S. Spotlight on circadian genes and colorectal cancer crosstalk. Endocr Metab Immune Disord Drug Targets. 2021;21(1):4-11.
3. Harlé A. Cell-free DNA in the management of colorectal cancer. Recent Results Cancer Res. 2020;215:253-261.
4. Perrod G, Rahmi G, Cellier C. Colorectal cancer screening in Lynch syndrome: Indication, techniques and future perspectives. Dig Endosc. 2021;33(4):520-528.
5. Patel SG, Murphy CC, Lieu CH, et al. Early age onset colorectal cancer. Adv Cancer Res. 2021;151:1-37.
6. Patel SG, Ahnen DJ. Colorectal cancer in the Young. Curr Gastroenterol Rep. 2018;20(4):15.
7. Cho YJ, Lee JE, Park MJ, et al. Bufalin suppresses endometriosis progression by inducing pyroptosis and apoptosis. J Endocrinol. 2018;237(3):255-269.
8. Lan YL, Wang X, Lou JC, et al. Bufalin inhibits glioblastoma growth by promoting proteasomal degradation of the Na+/K+-ATPase α1 subunit. Biomed Pharmacother. 2018;103:204-215.
9. LingHu HR, Luo H, Gang L. Bufalin induces glioma cell death by apoptosis or necroptosis. Onco Targets Ther. 2020;13:4767-4778.
10. Lan YL, Lou JC, Jiang XW, et al. A research update on the anticancer effects of bufalin and its derivatives. Oncol Lett. 2019;17(4):3635-3640.
11. Xie Y, Yan X, Sun L. The mechanism of bufalin-induced apoptosis of K562/A02. Med Sci Monit. 2019;25:2542-2552.
12. Li M, Wang XJ, Zhao Q, et al. Bufalin-induced cardiotoxicity: new findings into mechanisms. Chin J Nat Med. 2020;18(7):550-560.
13. Cheng CS, Wang J, Chen J, et al. New therapeutic aspects of steroidal cardiac glycosides: the anticancer properties of Huachansu and its main active constituent Bufalin. Cancer Cell Int. 2019;19:92.
14. Emam H, Refaat A, Jawaid P, et al. Hyperthermia and radiation reduce the toxic side-effects of bufadienolides for cancer therapy. Oncol Lett. 2017;14(1):1035-1040.
15. Zou A, Zhao X, Handge UA, et al. Folate receptor targeted bufalin/β-cyclodextrin supramolecular inclusion complex for enhanced solubility and anti-tumor efficiency of bufalin. Mater Sci Eng C Mater Biol Appl. 2017 Sep 1;78:609-618.
16. Yuan J, Zeng C, Cao W, et al. Bufalin-loaded PEGylated liposomes: antitumor efficacy, acute toxicity, and tissue distribution. Nanoscale Res Lett. 2019;14(1):223.
17. Yuan J, Zhou X, Cao W, et al. Improved antitumor efficacy and pharmacokinetics of Bufalin via PEGylated liposomes. Nanoscale Res Lett. 2017;12(1):585.
18. Gao L, Zhang L, He F, et al. Surfactant assisted rapid-release liposomal strategies enhance the antitumor efficiency of bufalin derivative and reduce cardiotoxicity. Int J Nanomedicine. 2021;16:3581-3598.
19. Li Y, Yuan J, Yang Q, et al. Immunoliposome co-delivery of bufalin and anti-CD40 antibody adjuvant induces synergetic therapeutic efficacy against melanoma. Int J Nanomedicine. 2014;9:5683-5700.

DOI 10.1007/s10330-022-0586-6
Cite this article as: Mao FJ, Wu XL, Yuan CY, et al. Allosteric probe-modified liposome loading bufalin-fluorouracil complex for targeted colorectal cancer therapy. Oncol Transl Med. 2022;8(5):239–246.

Oncology and Translational Medicine
DOI 10.1007/s10330-022-0595-5

October 2022, Vol. 8, No. 5, P247–P258

ORIGINAL ARTICLE

Mechanism of lncRNA SNHG19 miR-299-5p MAPK6 signaling axis promoting metastasis of non-small cell lung cancer cells

Qian Zhong , Rong Qiu (✉)

Department of Respiratory Medicine, Suining Central Hospital, Suining 629000, China

Abstract

Objective The aim of this study was to explore the mechanism behind lncRNA small nucleolar RNA host gene 19 (lncRNA SNHG19)/microrNA-299-5P (miR-299-5p)/mitogen-activated protein kinase 6 (MAPK6) signaling axis promoting metastasis of non-small cell lung cancer (NSCLC).

Methods To analyze the abnormal expression of lncRNAs in NSCLC, 50 surgically resected NSCLC and adjacent tissue samples were collected from August 2021 to August 2022. The mRNA expression levels of lncRNA SNHG19, Mir-299-5p, and MAPK6 were detected by qRT-PCR. The functions of lncRNA SNHG19, Mir-299-5p and MAPK6 were investigated by CCK-8, clone formation, EdU, scratch, Transwell western blotting (WB)and *in vivo* xenograft assay. RNA fluorescence *in-situ* hybridization (FISH), RNA pull-down, dual luciferase reporter, and RNA co-immunoprecipitation assays were used to explore the mechanism of action between lncRNA SNHG19, miR-299-5p, and MAPK6.

Results High expression of lncRNA SNHG19 was correlated with poor prognosis, tumor size, lymph node metastasis, and TNM stage in NSCLC patients ($P < 0.05$). Cell function experiments showed that lncRNA SNHG19 could improve the proliferation, clone formation, migration, and invasion ability of A549 cells both *in vitro* and *in vivo* (all $P < 0.05$) and increased the relative expression levels of vimentin and MAPK6 ($P < 0.05$). The relative expression level of E-cadherin was decreased ($P < 0.05$). lncRNA SNHG19 can interact with Mir-299-5p and regulate the expression level of MAPK6.

Conclusion lncRNA SNHG19 is upregulated in NSCLC tissues and cells, and its high expression is associated with tumor progression and poor survival. Moreover, it can act as a molecular sponge for Mir-299-5p to regulate MAPK6 expression and promote the proliferation and metastasis of A549 cells.

Received: 5 September 2022
Revised: 21 September 2022
Accepted: 13 October 2022

Key words: long noncoding RNA small nucleolar RNA host gene 19; MicroRNA-299-5p; non-small cell lung cancer (NSCLC); metastasis

The mortality and incidence of lung cancer rank among the top malignant tumors, and non-small cell lung cancer (NSCLC) patients have the worst prognosis [1]. At present, most treatment regimens are selected according to the stage of NSCLC as determined by the tumor, node and metastasis (TNM) classification of malignant tumors. However, due to the strong heterogeneity of NSCLC, there are great individual differences in treatment efficacy. It is difficult to meet the needs of clinical treatment when using only TNM classification as the basis for the selection of NSCLC treatment regimens. Therefore, it is necessary to further study the underlying molecular mechanisms related to the occurrence and development of NSCLC, to improve the early diagnosis and treatment of NSCLC. Long non-coding RNA (lncRNA) is a class of transcripts with a length of more than 200 nucleotides. Several studies have shown that [2, 3], lncRNA is involved in various physiological and pathological processes such as cell differentiation, apoptosis, and migration. lncRNA small nucleolar RNA host gene 19 (SNHG19) is a recently discovered lncRNA, which has been confirmed to be abnormally expressed in the brain of pancreatic cancer [4], triple-negative breast cancer [5], other tumors, and Alzheimer's disease [6] patients. MicroRNA (miRNA) is a small non-coding RNA consisting of 19-25 nucleotides, which can affect the occurrence and development of tumors. Recent reports have shown that Mir-299-5p plays a cancer suppressor role in a variety of cancers [7]. The

✉ Correspondence to: Rong Qiu. Email: shendou64196@163.com

results of a bioinformatics prediction using the ENCORI database showed that lncRNA SNHG19 had a target binding site for Mir-299-5p. Mitogen-activated protein kinase 6 (MAPK6) has a highly conserved gene sequence, which can activate cancer cell proliferation, survival, migration, and metastasis, and participate in angiogenesis and chemotherapy resistance through multiple signaling pathways, thus playing a cancer-promoting function [8]. In this study, the expression of lncRNA SNHG19, Mir-299-5p, and MAPK6 in NSCLC tissues and cell lines was detected, the changes in cell proliferation, migration, and invasion were observed, and the regulatory relationship between lncRNA SNHG19, Mir-299-5p and MAPK6 was analyzed. To explore the specific regulatory mechanisms of lncRNA SNHG19, Mir-299-5p, and MAPK6 in NSCLC, the following report is presented.

Materials and methods

Samples and participants

Samples from 50 patients having undergone surgical resection of NSCLC, from August 2021 to August 2022, were collected and confirmed as NSCLC by postoperative pathological diagnosis. All patients had complete clinical data and had not received radiotherapy or chemotherapy before operation. There were 26 males and 24 females, aged 55–73 (61.86 ± 5.14) years. At the same time, 50 cases of adjacent lung tissues were collected, which were pathologically diagnosed as normal lung tissues and frozen in liquid nitrogen. This study was approved by the ethics committee of our hospital (ethical approval number: 102467), and all patients gave informed consent and voluntarily provided tissue samples.

Reagents and instruments

Human bronchial epithelial cell line 16HBE and NSCLC cell lines A549, NCI-H292, NCI-H460, and NCI-H1703 were purchased from the Shanghai Cell Resource Center, Chinese Academy of Sciences. Dulbecco's modified eagle medium (DMEM) medium, fetal bovine serum, Streptomycin/penicillin, TRIzol reagent, High-capacity cDNA Reverse Transcription Kit, mirVana miRNA isolation Kit, Lipofectamine™ 2000 kit Streptomycin affinity coupled magnetic beads, and SuperSignal West Pico PLUS chemiluminescence substrate were purchased from Thermo Fisher (USA); construction, identification, packaging, and titer determination of lentiviral expression vectors were completed by Guangzhou Yuanjing Biotechnology Co., LTD, People's Republic of China. SYBR Premix Ex TAQii Kit was purchased from Dalian Baosheng Biotechnology Co., LTD, People's Republic of China. All-in-one miRNA qRT-PCR kit was purchased from Asia Pacific Hengxin Biotechnology (Beijing) Co., LTD, People's Republic of China. Polymerase chain reaction (PCR) primers and internal reference were purchased from Shanghai Shenggong Bioengineering Co., LTD, People's Republic of China. RNA fluorescence *in situ* hybridization (FISH) kit was purchased from Guangzhou Ruibo Biotechnology Co., LTD, People's Republic of China. Cck-8 kit, hematoxylin eosin (HE) staining and bicinchoninic acid (BCA) protein concentration assay kits were purchased from Shanghai Biyuntian Biotechnology Co., LTD, People's Republic of China. Matrigel matrix glue was purchased from Shanghai Yanhui Biotechnology Co., LTD, People's Republic of China. Rabbit Argonaute2 antibody, MAPK6, E-cadherin, vimentin, and Ki-67 were purchased from Abcam, Cambridge, UK. SP method rabbit antibody immunohistochemistry kit was purchased from Fuzhou Feijing Biotechnology Co., LTD, People's Republic of China. All other reagents were commercially available as analytically pure.

Cell culture, grouping and transfection

A549, NCI-H292, NCI-H460, NCI-H1703, and 16HBE cells were resuscitated and cultured with DMEM containing 10% fetal bovine serum and 100 mg/mL streptomycin/penicillin in an electric thermostatic incubator at 37°C, 5% CO_2, and saturated humidity. A549 was divided into the control group (without transfection), si-SNHG19 group (transfected si-SNHG19), SNHG19 group (transfected SNHG19), SNHG19-Mt group (transfected mutant SNHG19), miR-299-5p mimic group (transfected with miR-299-5p mimic), SNHG19+ miR-299-5p mimic group (transfected with SNHG19+ miR-299-5p mimic), si-SNHG19 + miR-299-5p inhibitor group (transfected with Si-SNHG19 + miR-299-5p inhibitor), si-MAPK6 group (transfected with SI-MAPK6), and SNHG19 + si-MAPK6 group (transfected with SNHG19+ si-MAPK6) and were transiently transfected according to the groups. The cells were collected 48 h post-transfection for subsequent experiments. A549 was divided into control group (without transfection), si-SNHG19 group (transfected si-SNHG19) and SNHG19 group (transfected SNHG19). Lentivirus transfection was performed according to the groups, and stable expression cell lines were constructed.

QRT-PCR of lncRNA SNHG19, miR-299-5p, and MAPK6 in tissues and cells

TRIzol reagent and mirVana miRNA isolation kit were used to extract total RNA and miRNAs from cancer tissues and cells of each group. Total RNA was transcribed into cDNA using a reverse transcription kit. A 20 μL PCR reaction mix was prepared using 1 μg cDNA template, 0.5 μg each of forward and reverse primers and SYBR Premix Ex TaQii kit. miRNAs were detected by all-in-one miRNA qRT-PCR kit. Reaction conditions: 94°C pre-denaturation for 2 min, 94°C for 30 s, 55°C for 30 s, 72°C

for 2 min for 35 cycles. qRT-PCR was performed using ABI 7500 real-time PCR instrument, and the relative expression levels of lncRNA SNHG19, miR-299-5p, and MAPK6 were calculated by the $2^{-\Delta\Delta CT}$ method.

FISH detection

FISH kit was used to detect the localization of lncRNA SNHG19 in A549 cells. Cells were routinely seeded on slides in 24-well plates, cultured for 24 h and then fixed with 4% paraformaldehyde for 10 min. We added 0.5% Triton X-100 and let it permeate for 5 min. The pre-hybridization solution and hybridization solution were preheated at 37°C for 30 min, then added to the slide and placed at 37°C for 20 min. The lncRNA SNHG19 probe was diluted at a ratio of 1:50 with hybridization solution, added to the slide, and kept away from light overnight at 37°C. The unbound probe was eluted, and 4', 6-diamidino-2-phenylindole (DAPI) was added to avoid light reaction for 8 min. The anti-fluorescence quench was dropped, and the slices were sealed, observed, and photographed under the BX51 fluorescence microscope (Olympus Company of Japan) was used.

RNA pull-down test

A549 cells were taken and transfected with biotin-labeled Mir-299-5p. After 48 h of normal culture, appropriate lysates were added to fully lysate the cells. The lysates were collected, streptomycin affinity coupled magnetic beads were added, fully mixed, and incubated at 4°C for 3 h. lncRNA SNHG19 levels were detected by qRT-PCR.

Dual luciferase reporter assay

The wild-type psicheck2-SnHG19-Luc and mutant PsichecK2-SnHG19-Mut-Luc fluorescent plasmids were constructed and co-transfected into A549 cells with Mir-299-5p mimics. The wild-type PsichecK2-MAPK6-Luc fluorescent plasmid was constructed. The cells were transfected into the control group, Si-SNHG19 group, SI-SNHG19 + Mir-299-5p inhibitor group, SNHG19 group, SNHG19-MT group, and SNHG19+ Mir-299-5p mimic group, and the luciferase activity in each group was detected by Varioskan LUX enzyme labeling instrument (Thermo Fisher Company of USA).

RNA immunoprecipitation

A549 cells were harvested and lysed with an appropriate amount of lysate. AGO2 antibody and immunoglobulin G (IgG) were added to the magnetic beads, incubated at room temperature (20–25°C) for 30 min, then cell lysates were added, incubated overnight at 4°C, and purified immunoprecipitated RNA was detected by qRT-PCR.

CCK-8 assay

Cells in the logarithmic growth phase were inoculated in 96-well plates after trypsin digestion and cultured for 5 d. Cck-8 was detected once a day. Cck-8 solution was added to each well and the culture was continued for 2 h.

Determination of cell proliferation ability

Clone formation experiment: after trypsin digestion, the cells in each group were seeded in a 6-well plate at an inoculation density of 1000 cells/well. The cells were cultured in a 5% CO_2 incubator at 37°C for 10 d. The medium was discarded, washed with 1 × PBS, fixed with methanol for 30 min, and stained with 1% crystal violet for 20 min. Then we observed, photographed, and clone counted.

BrdU incorporation experiment: Cells were seeded in 24-well plates with 3×10^5 cells per well, fixed with 4% paraformaldehyde for 20 min, washed 3 times with PBS, underwent DNA proteolysis for 30 min, incubated in 0.2% Triton X-100 for 8 min, washed 3 times with PBS, and blocked with 10% fetal bovine serum for 1 h. The cells were incubated with primary antibody against BrdU (1:1000), washed with PBS, and incubated with secondary antibody against light for 1 h. BrdU positive cells were observed and counted under a fluorescence microscope.

Scratch test

The cells in the logarithmic growth phase of each group were seeded in 6-well plates at a cell density of 1×10^6 cells/well, and the cell confluency was observed to reach 90%. Scratches were made with a 200 μL pipette tip to remove the shed cells, and serum-free medium was added and cultured for 24 h. Photos were taken immediately after the scratch and then again after 24 h of culturing, and the scratch width was measured using Image J software (National Institutes of Health.). The cell migration rate was calculated as: (initial scratch width – scratch width after 24 h)/initial scratch width ×100%.

Transwell experiment

Serum-free DMEM medium was diluted with Matrigel glue at a ratio of 1:3, and evenly spread on the bottom of the upper chamber membrane after mixing. The medium was placed overnight in a 37°C incubator with 5% CO_2 and exposed to ultraviolet light for 30 min the next day. Cells passing through the upper chamber were fixed with 4% paraformaldehyde for 30 min, stained with crystal violet, observed, and photographed under a light microscope, and the cell invasion rate was calculated as the number of invaded cells in each group/the number of invaded cells in the control group × 100%.

Western blotting

Samples of NSCLC and adjacent tissues were homogenized, and an appropriate amount of pre-cooled radio immunoprecipitation assay (RIPA) was added, and the mixture was fully mixed and incubated for 1.5 h on ice. After centrifugation at 20,000 *g* at 4°C for 10 min, the supernatant was removed, and the sample was prepared after BCA quantification. The protein of the sample was separated by gel electrophoresis, the membrane was turned, and the target band was intercepted and immersed in the blocking solution made of 5% skim milk powder, and then blocked on a shaker for 1 h at room temperature. The blocking solution was diluted to make the incubation solution, with a dilution ratio of 1:500, and the solution was fully shaken and left to incubate overnight at 4°C. After washing the film, the corresponding secondary antibody incubation solution with a dilution ratio of 1:5000 was added and incubated at room temperature for 2 h. Electrochemiluminescence solution (ECL) chemiluminescence solution was added and the reaction was kept away from light for 5 min. The results were collected using quantitative imager.

In vivo xenograft experiments

Nude mice were randomly divided into 16 groups according to the cell name of each group. Eight cells were randomly divided into each group and injected into both sides of the axilla with a density of 5×10^6 cells / ml. The volume of subcutaneous tumors was measured every 4 d with a digital caliper, and the formula was: volume =1/2 (length × width^2). After 23 d, the nude mice were euthanized, and the tumors were completely removed. The tumors were measured and photographed, fixed in 10% formaldehyde solution, and then embedded in paraffin and sectioned. The remaining 8 mice were injected with cell suspension at a density of 3×10^6 cells /mL through the tail vein. After 60 d, the nude mice were euthanized, and the lung tissues were completely removed and photographed as paraffin sections.

HE staining was used to observe metastatic lung nodules of NSCLC

Paraffin sections were stained according to the instructions of the HE staining kit, observed and photographed under a light microscope, and the number of lung nodules was calculated.

Immunohistochemical analyses

Immunohistochemical streptavidin-perosidase (SP) method was used to detect the expression of MAPK6 in NSCLC and adjacent tissues and Ki-67, E-cadherin, and vimentin in nude mouse tumors. The paraffin sections were processed and stained according to the kit requirements, and the experimental results were photographed under the light microscope. Five different fields were randomly selected for each section, and Image J software was used for image analysis. The average value was taken as the relative expression levels of Ki-67, E-cadherin, and vimentin.

Statistical analysis

SPSS 24.0 (Chicago, IL, USA) statistical software was used to analyze and process the data. Measurement data were expressed as mean ± standard deviation ($\chi \pm s$). Independent sample *t*-test was used for the comparison between two groups, and one-way analysis of variance was used for the comparison between multiple groups. Enumeration data were expressed in the form of rate (%), and comparison between groups was performed by chi-square test. $P < 0.05$ indicates statistical significance.

Results

The relationship between lncRNA SNHG19 expression and clinicopathological features in NSCLC

Among the multiple aberrantly expressed lncRNAs in NSCLC, lncRNA SNHG19 is one of the significantly upregulated lncRNAs with high relative abundance (Fig. 1a). The results of qRT-PCR detection showed (Fig. 1b) that the relative expression of lncRNA SNHG19 was increased in NSCLC cell lines ($P < 0.05$). The relative expression of lncRNA SNHG19 was the highest in A549 cells, therefore A549 cells were selected for subsequent experiments. The results of survival analysis showed (Fig. 1c) that high expression of lncRNA SNHG19 was significantly associated with overall survival ($P < 0.05$). The expression of lncRNA SNHG19 was correlated with tumor size, lymph node metastasis, and TNM classification in patients with NSCLC ($P < 0.05$) (Table 1).

lncRNA SNHG19 promotes the growth of NSCLC cells in vitro

The results of CCK-8 (Fig. 2a), colony formation (Fig. 2b), scratch (Fig. 2c), and Transwell experiments (Fig. 2d) showed that compared with the control group, the si-SNHG19 group had better proliferation, colony formation, migration, and invasion abilities. These abilities of the SNHG19 group were significantly improved, and the difference with the control group was statistically significant ($P < 0.05$). The results of WB detection showed that (Fig. 2e), compared with the expression levels of E-cadherin and vimentin in the control group, the relative expression level of E-cadherin increased and the relative expression level of vimentin decreased in the

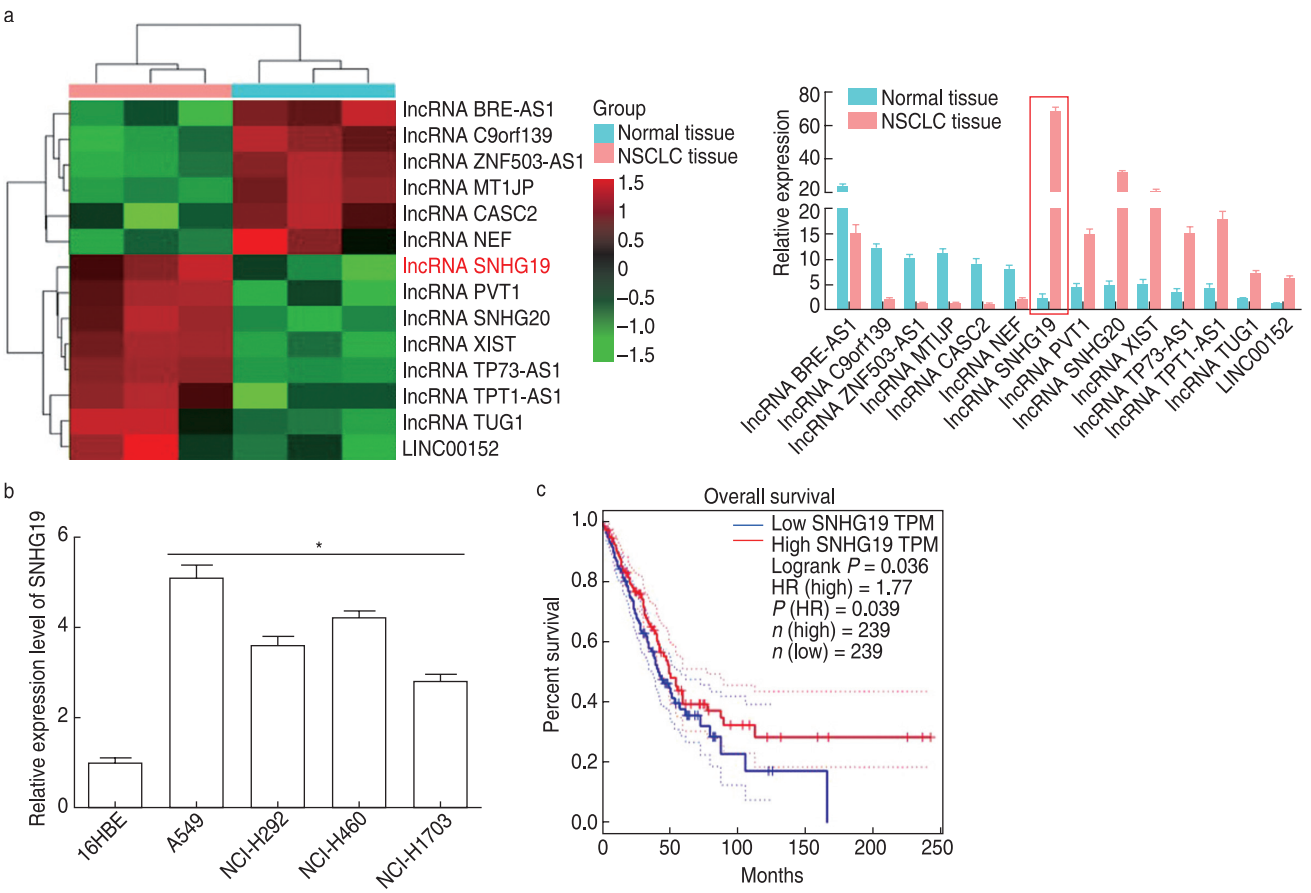

Fig. 1 Expression of lncRNA SNHG19 in NSCLC. (a) Hierarchical clustering heatmap of aberrantly expressed lncRNAs in NSCLC; (b) Tissue qRT-PCR test results; (c) qRT-PCR detection results of NSCLC cell lines; (d) Survival analysis results

si-SNHG19 group, while the relative expression level of E-cadherin decreased and the relative expression level of vimentin increased in the SNHG19 group. The difference was statistically significant ($P < 0.05$).

lncRNA SNHG19 promotes proliferation and metastasis of NSCLC cells in vivo

The results of the *in vivo* xenograft experiments showed that the tumor volume for the si-SNHG19 group was smaller than that for control group, and the tumor volume for the SNHG19 group was bigger than that for control group ($P < 0.05$, Fig. 3a). The results of qRT-PCR detection (Fig. 3b) showed that compared with the expression of lncRNA SNHG19 in the control group, the expression of lncRNA SNHG19 in the si-SNHG19 group decreased, while the expression of lncRNA SNHG19 in the SNHG19 group increased ($P < 0.05$), suggesting that the recombinant vectors were stably expressed in each group. The results of lung tissue HE staining (Fig. 3c) showed that compared with the nodules in the control group, the number of metastatic lung nodules in the si-SNHG19 group decreased, and the number of metastatic lung nodules in the SNHG19 group increased ($P < 0.05$). The results of immunohistochemistry showed (Fig. 3d) that compared with the control group, the relative expression levels of Ki-67 and vimentin in the si-SNHG19 group decreased, while those of E-cadherin increased, and the relative expression levels of Ki-67 and vimentin in the SNHG19 group increased while those of E-cadherin decreased ($P < 0.05$).

lncRNA SNHG19 regulates the expression of miR-299-5p in NSCLC

qRT-PCR detection results showed (Fig. 4a) that miR-299-5p was lowly expressed in NSCLC tissues and cell lines ($P < 0.05$). After fluorescent staining, lncRNA SNHG19 was red, the nucleus was blue, and lncRNA SNHG19 was mainly expressed in the cytoplasm (Fig. 4b). RNA pull-down assay and dual-luciferase reporter gene assay showed (Fig. 4c) that miR-299-5p could be pulled down by lncRNA SNHG19, and miR-299-5p mimic could reduce lncRNA SNHG19 luciferase of wild-type 3'UTR. The lncRNA SNHG19 luciferase activity had no effect on the mutant 3'UTR lncRNA SNHG19, indicating that lncRNA SNHG19 can directly target miR-299-5p. The results of co-immunoprecipitation assay (Fig. 4d) showed

Table 1 Relationship between lncRNA SNHG19 expression and clinicopathological features of NSCLC patients [*n* (%)]

Pathological features	*n*	lncRNA SNHG19		χ^2 value	*P value*
		High expression	Low expression		
Age (years)				0.321	0.571
≤ 49	26	12 (48.00)	14 (56.00)		
> 49	24	13 (52.00)	11 (44.00)		
Sex				1.282	0.258
Male	26	11 (44.00)	15 (60.00)		
Female	24	14 (56.00)	10 (40.00)		
Smoking history				1.282	0.258
No	24	10 (40.00)	14 (56.00)		
Yes	26	15 (60.00)	11 (44.00)		
Histological type				1.064	0.786
Adenocarcinoma	26	14 (56.00)	12 (48.00)		
Squamous cell carcinoma	13	6 (24.00)	7 (28.00)		
Adenosquamous carcinoma	8	3 (12.00)	5 (20.00)		
Large-cell carcinoma	3	2 (8.00)	1 (4.00)		
Tumor size (cm)				12.500	< 0.001
≤ 3	18	15 (60.00)	3 (12.00)		
> 3	32	10 (40.00)	22 (88.00)		
Tumor differentiation				0.347	0.556
High-middle grade	32	15 (60.00)	17 (68.00)		
Low grade	18	10 (40.00)	8 (32.00)		
Lymph node metastasis				5.195	0.023
No	28	18 (72.00)	10 (40.00)		
Yes	22	7 (28.00)	15 (60.00)		
TNM classification (stage)				4.160	0.041
I–II		19 (76.00)	12 (48.00)		
III		6 (24.00)	13 (52.00)		

that both lncRNA SNHG19 and miR-299-5p were significantly enriched in the microriboprotein complex of AGO2, indicating that AGO2 protein directly binds to lncRNA SNHG19 and miR-299-5p in NSCLC cells. The results of CCK-8 (Fig. 4e), EdU (Fig. 4f), and Transwell experiments (Fig. 4g) showed that compared with the proliferation and migration abilities of the control group, those of the SNHG19+miR-299-5p mimic group had no significant difference ($P > 0.05$), those of the SNHG19 group were significantly improved, while those of the miR-299-5p mimic group were significantly decreased ($P < 0.05$).

lncRNA SNHG19 affects the expression of MAPK6 in NSCLC by regulating miR-299-5p

The results of qRT-PCR showed (Fig. 5a) that the expression of MAPK6 was significantly upregulated in NSCLC tissues and cell lines ($P < 0.05$). The results of WB detection showed (Fig. 5b) that compared with MAPK6 expression level of the control group, the relative expression level of MAPK6 was significantly decreased, and increased in the si-SNHG19 and SNHG19 groups, respectively ($P < 0.05$). The relative expression level of MAPK6 was significantly increased and decreased in the +miR-299-5p inhibitor SNHG19+miR-299-5p mimic groups, respectively ($P < 0.05$). The results of dual-luciferase reporter gene detection showed (Fig. 5c) that the fluorescence of Luc-MAPK6 in the SNHG19-Mt group, si-SNHG19+miR-299-5p inhibitor group, and SNHG19+miR-299-5p mimic group was significantly higher than that in the control group. There was no significant difference in luciferase activity ($P > 0.05$). The activity of Luc-MAPK6 luciferase was significantly decreased and increased in the si-SNHG19 SNHG19 groups, respectively ($P < 0.05$). The results of the co-immunoprecipitation assay showed (Fig. 5d) that the enrichment of AGO2 on SNHG19 decreased and the enrichment on MAPK6 increased after silencing lncRNA SNHG19, while the enrichment of AGO2 on SNHG19 in cells overexpressing lncRNA SNHG19 increased, and the enrichment on MAPK6 decreased ($P < 0.05$).

The cancer-promoting effect of lncRNA SNHG19 is associated with MAPK6

The results of CCK-8 (Fig. 6a), EdU (Fig. 6b), and Transwell experiments (Fig. 6c) showed that compared with the proliferation and migration abilities of cells control group, those in the SNHG19 group were

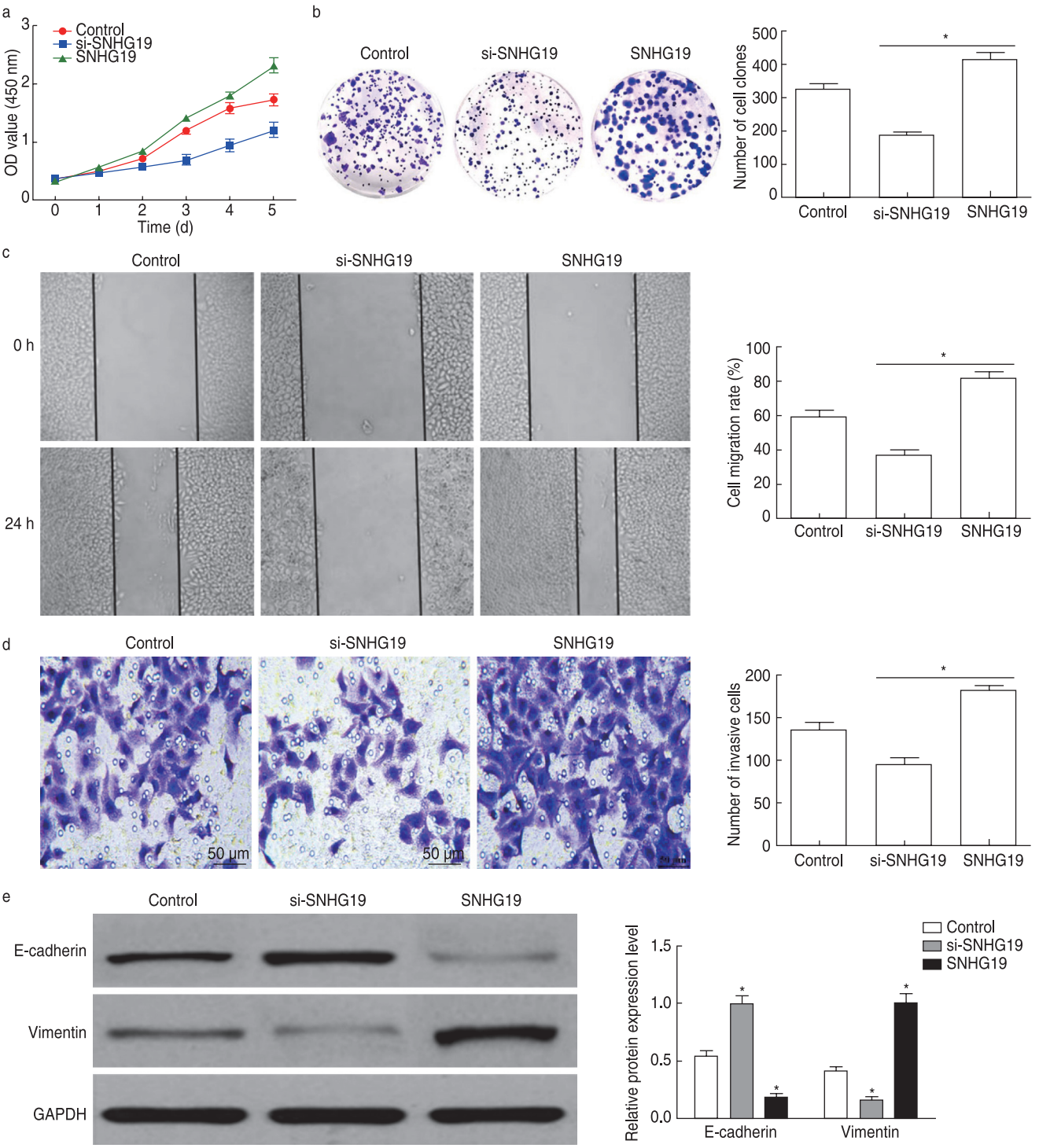

Fig. 2 lncRNA SNHG19 promotes NSCLC cell growth *in vitro*. (a) CCK-8 test results; (b) Experimental results of clone formation; (c) Scratch test results; (d) Transwell experimental results; (e) Western blotting test results. Compared with the control group, * $P < 0.05$

significantly improved, while those of the cells in the si-MAPK6 group were significantly reduced ($P < 0.05$). The results of WB detection showed (Fig. 6d) that compared with the control group, the relative expression levels of E-cadherin in the si-SNHG19 group and si-MAPK6 group were significantly increased, and the relative expression levels of vimentin and MAPK6 were significantly decreased. The relative expression levels of E-cadherin in the SNHG19 group were significantly decreased, while the relative expression levels of vimentin and MAPK6

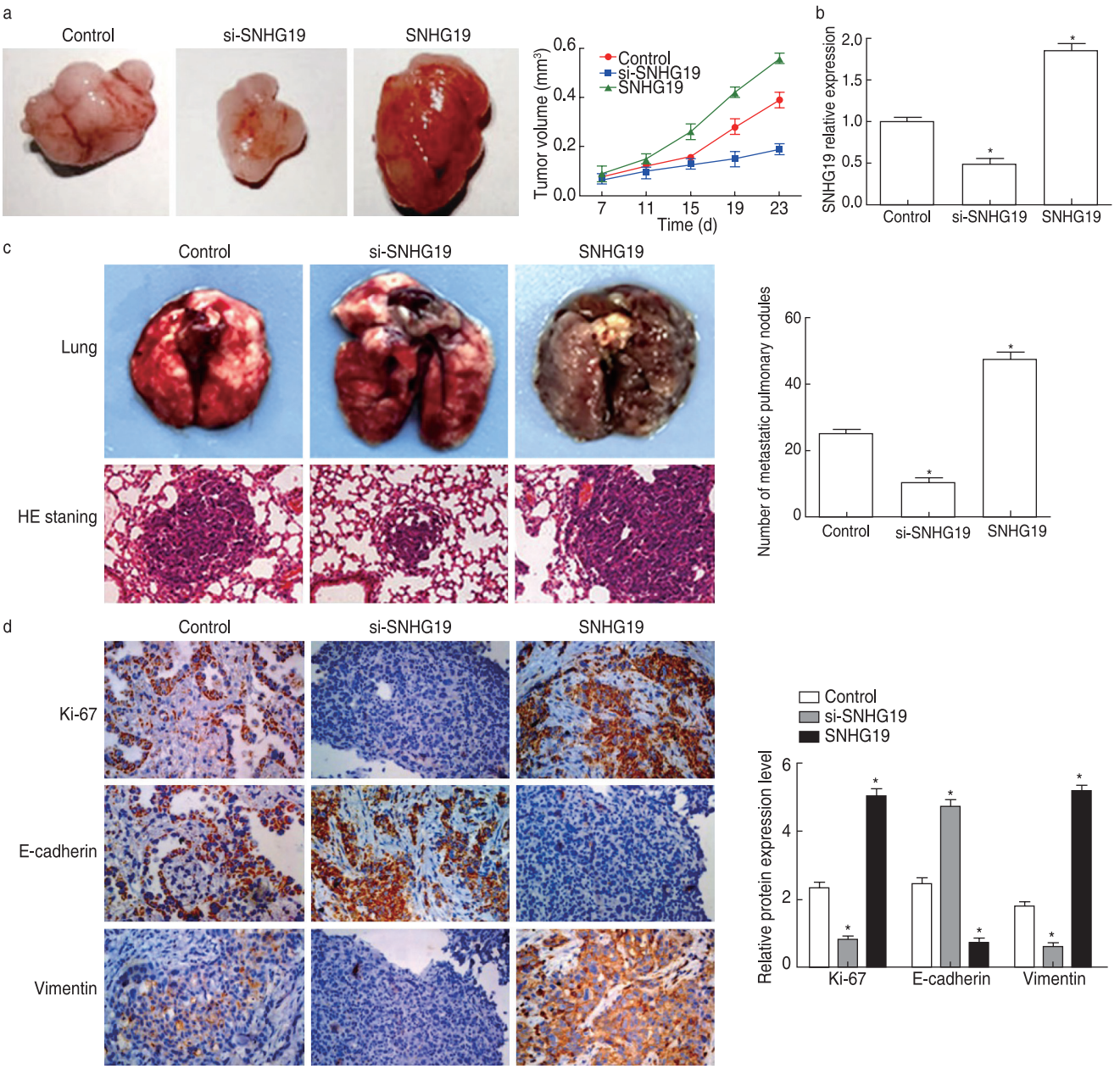

Fig. 3 lncRNA SNHG19 promotes proliferation and metastasis of NSCLC cells *in vivo*. (a) Results of *in vivo* xenograft experiments; (b) qRT-PCR test results; (c) HE staining results and quantitative observation of metastatic pulmonary nodules; (d) Immunohistochemical test results (× 400). Compared with the control group, * $P < 0.05$

were significantly increased ($P < 0.05$).

The mechanism of lncRNA SNHG19 affecting NSCLC by regulating MAPK6 through miR-299-5p

The results of this study showed that lncRNA SNHG19 and MAPK6 were upregulated in NSCLC and played a tumor-promoting role, while miR-299-5p was down-regulated and played a tumor suppressor role. There is a targeted inhibitory relationship between MAPK6, and it is speculated that lncRNA SNHG19 regulates MAPK6 through miR-299-5p, and its possible mechanism is shown in Fig. 7.

Discussion

In the human genome, in addition to miRNAs with powerful regulatory and epigenetic modification functions, there are many other noncoding RNAs. lncRNAs were initially considered to be by-products

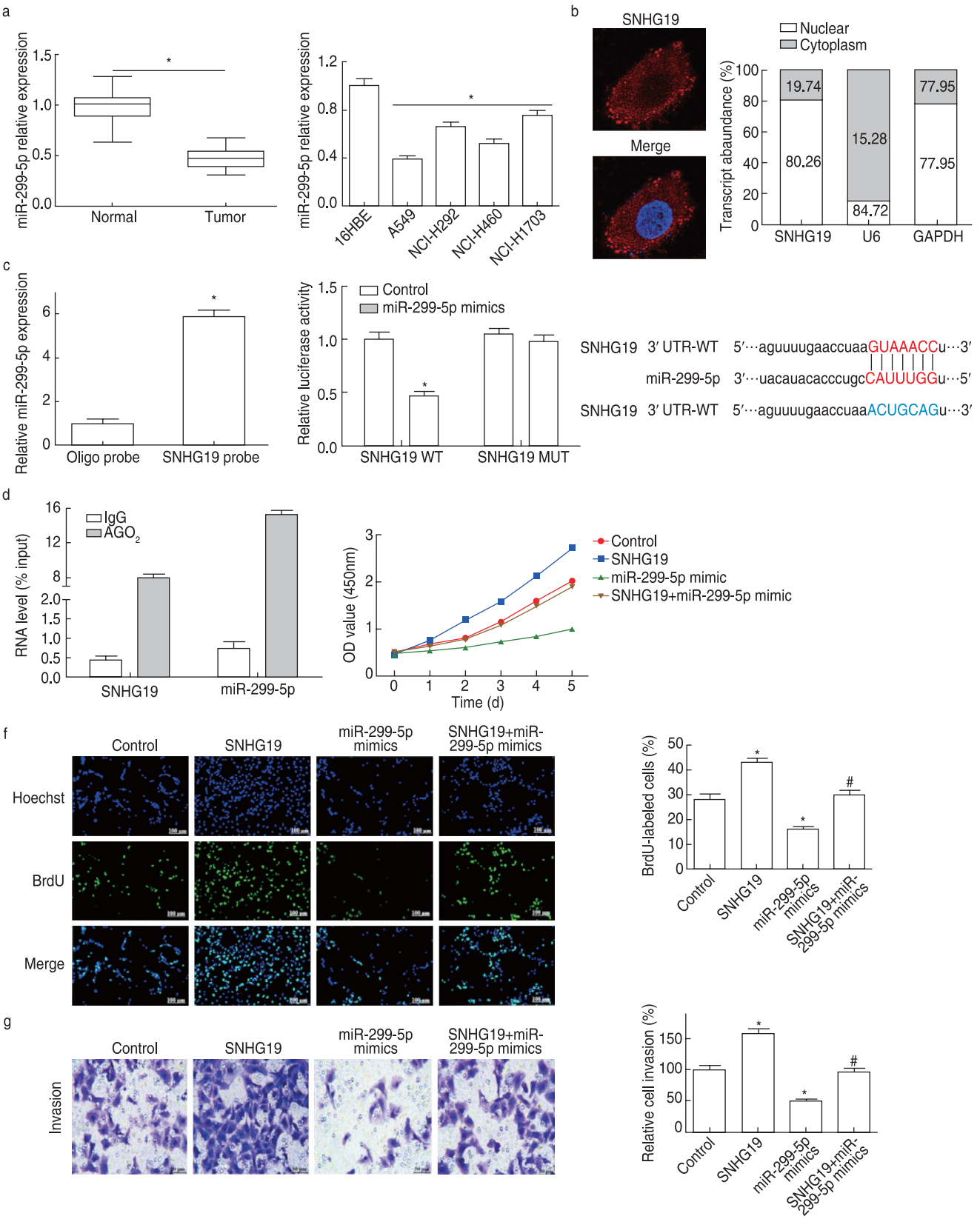

Fig. 4 lncRNA SNHG19 regulates the expression of miR-299-5p in NSCLC. (a) qRT-PCR test results; (b) FISH test results; (c) RNA pull-down assay and dual-luciferase reporter gene assay results; (d) Co-immunoprecipitation test results; (e) CCK-8 test results; (f) EdU test results; (g) Transwell test results. Compared with the control group, $^{*}P < 0.05$; compared with the SNHG19 group, $^{\#}P < 0.05$

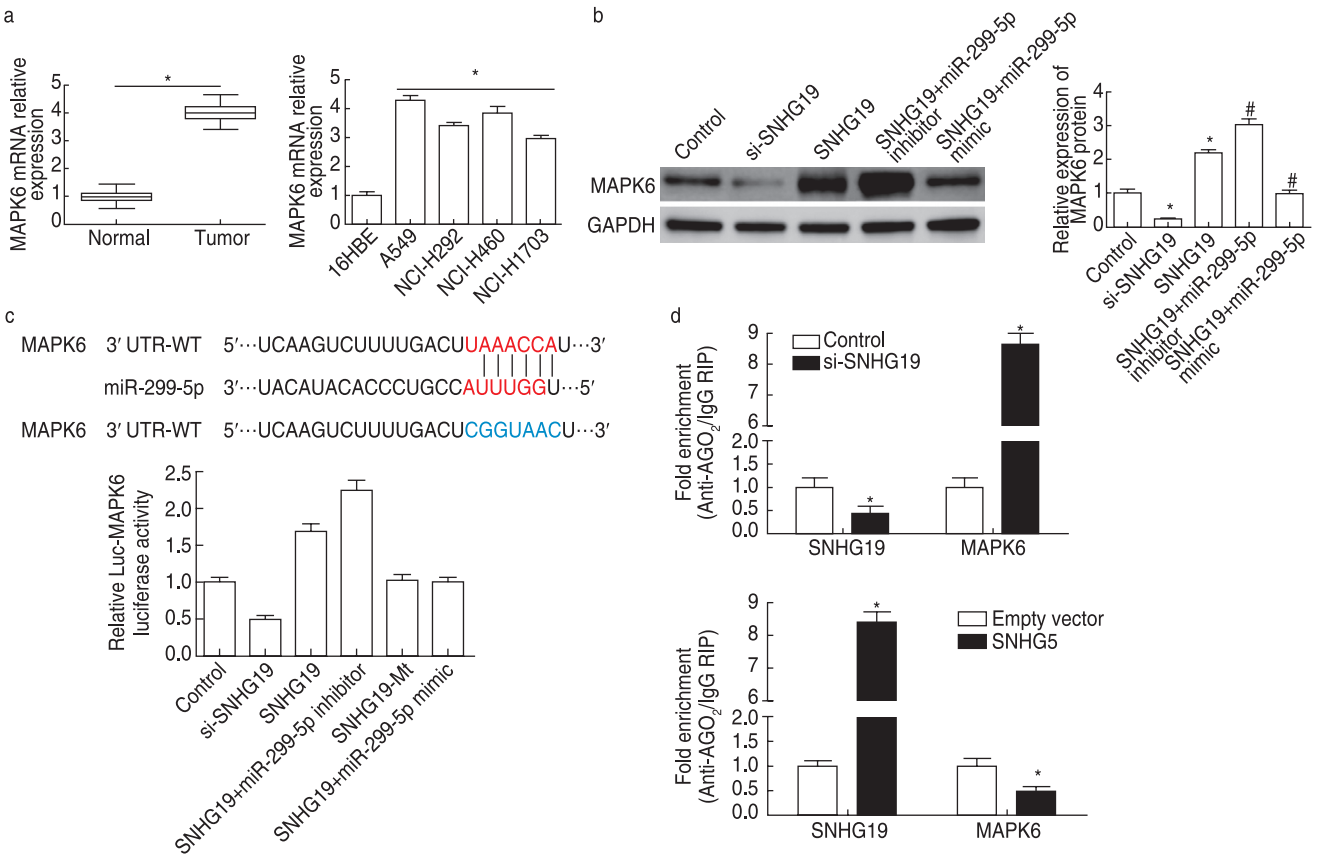

Fig. 5 lncRNA SNHG19 affects the expression of MAPK6 in NSCLC by regulating miR-299-5p. (a) qRT-PCR test results; (b) Western blotting test results; (c) Dual-luciferase reporter gene assay results; (d) Co-immunoprecipitation test results. Compared with the control group, * $P < 0.05$; compared with the SNHG19 group, # $P < 0.05$

of RNA polymerase II transcription and genomic noise, however, increasing evidence suggests that they can participate in many biological processes and play an important role in the occurrence and development of diseases [9, 10]. Wu [11] found that lncRNA DUXAP8 can promote the proliferation, epithelial-mesenchymal transition (EMT) and aerobic glycolysis of NSCLC cells, and its high expression is related to the poor prognosis of NSCLC patients. The study of Zeng [12] showed that lncRNA PVT1 is upregulated in NSCLC tissues and cell lines, which can promote the proliferation, migration, and invasion of NSCLC cells. The study of Wang [13] confirmed that the expression of lncRNA HNF1A-AS1 is upregulated in NSCLC tissues and cells, which can promote cell proliferation and inhibit cell apoptosis, and is closely related to the clinicopathological stage of patients. Knockout of lncRNA HNF1A-AS1 can significantly enhance the radiosensitivity of NSCLC cells. These studies prove that in-depth understanding of the role of lncRNA in NSCLC is beneficial for improved diagnosis and treatment efficiency of NSCLC.

lncRNA SNHG19 was first discovered in Alzheimer's disease brain tissue [6]. Subsequent studies have shown [5] that it is highly expressed in breast cancer tissues. The results of Zhao [14] showed that lncRNA SNHG19 was upregulated in NSCLC cancer tissues, cell lines, and patient plasma, and could promote the proliferation, migration, and invasion of NSCLC cells. However, a few studies have reported on the relationship between the expression of lncRNA SNHG19 and the occurrence and development of NSCLC, and its energy supply in NSCLC has not been fully elucidated. In this study, lncRNA SNHG19 was abnormally expressed in NSCLC tissues and cell lines, and its high expression indicated that the patient's NSCLC was in the advanced stage and had a poor prognosis. Cell function experiments in this study showed that lncRNA SNHG19 could significantly promote the proliferation and metastasis of NSCLC both *in vitro* and *in vivo*. The results from a bioinformatics prediction using ENCOPI database showed that lncRNA SNHG19 has a binding site with miR-299-5p, but no studies have confirmed the targeting effect of the two. In order to explore the mechanism of lncRNA SNHG19 in NSCLC, this study confirmed that lncRNA SNHG19 can act as a molecular sponge for miR-299-5p in the cytoplasm and exert its cancer-promoting effect by regulating the level of MAPK6. We used RNA

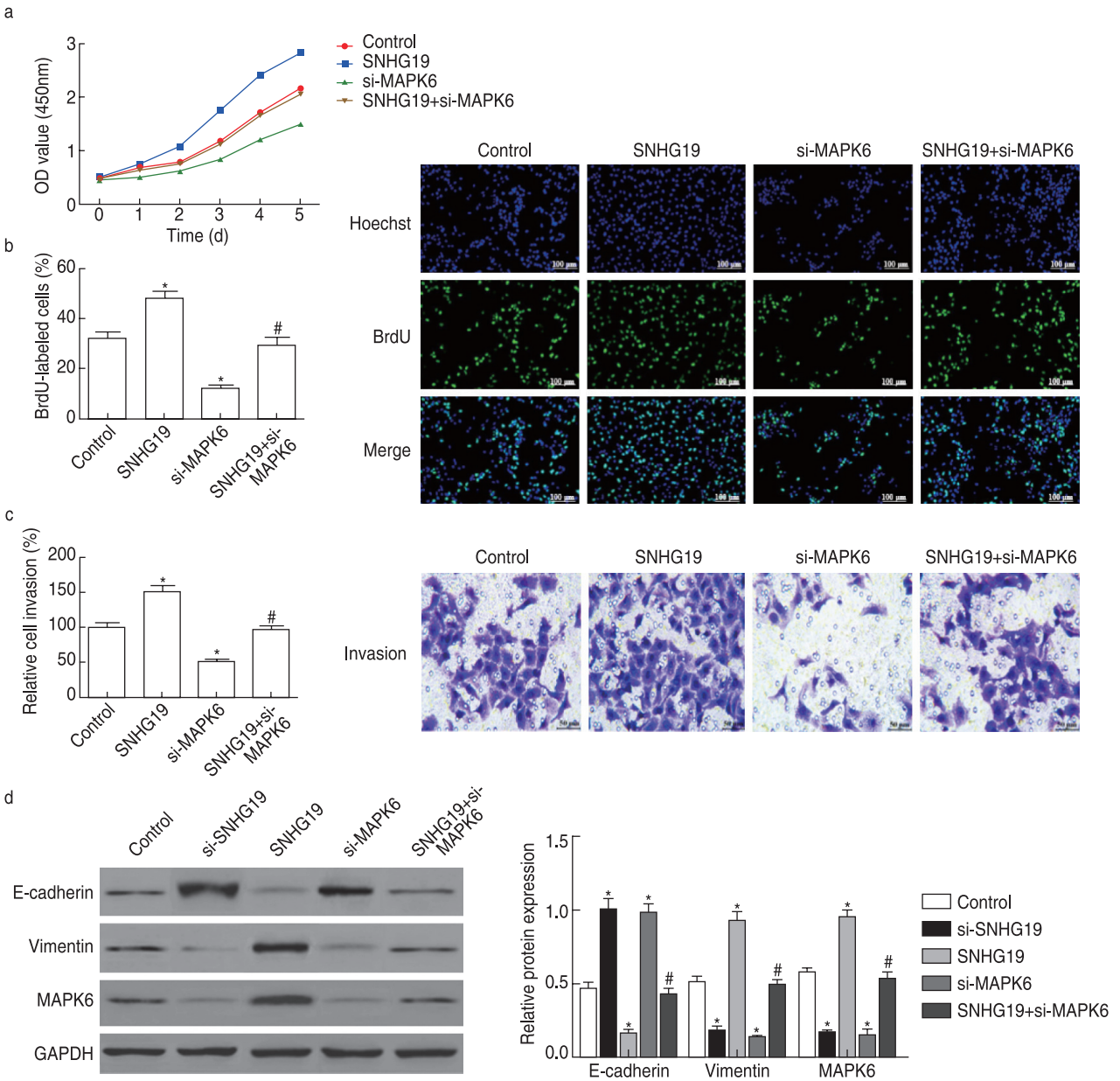

Fig. 6 The cancer-promoting effect of lncRNA SNHG19 is associated with MAPK6. (a) CCK-8 test results; (b) EdU test results; (c) Transwell experimental results; (d) Western blotting test results. Compared with the control group, * $P < 0.05$; compared with the SNHG19 group, # $P < 0.05$

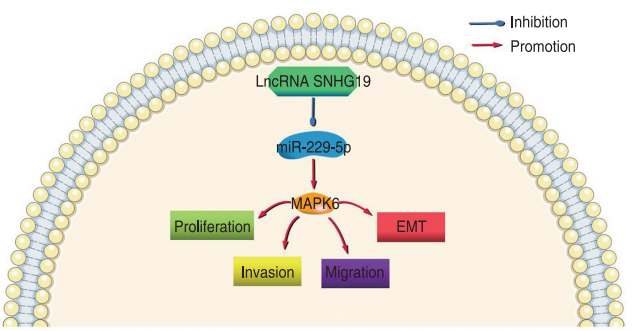

Fig. 7 Illustration of the mechanism of lncRNA SNHG19 affecting NSCLC by regulating MAPK6 through miR-299-5p

pull-down assay, dual-luciferase reporter gene detection, and RNA co-immunoprecipitation detection to reach these results. A potential site for miR-299-5p binding in the MAPK6 3'UTR was also shown in the Target Scan Human database. However, a few studies report on the specific mechanism of lncRNA SNHG19/miR-299-5p/MAPK6 signaling axis in NSCLC.

MAPK6, also known as ERK3, is an atypical member of the MAPK family, which is associated with the metastasis of breast and gastric cancers and is an important molecule in the occurrence and development of cancer in general [15, 16]. The results of Wu [17] showed that MAPK6 is upregulated

in NSCLC cells and is involved in the occurrence and development of NSCLC under the regulation of hsa-miR-98-5p and lncRNA NEAT1. Epithelial-mesenchymal transition is a key process in cancer cell metastasis, during which epithelial cells lose their ability to adhere to cells and acquire a variety of mesenchymal properties including invasion and migration. The upregulated and downregulated levels of the mesenchymal cell marker vimentin and epithelial marker E-cadherin, respectively, are characteristic of EMT. MAPK6 levels are closely related to EMT [18]. The research report of Lv [19] showed that MAPK6 can activate the EMT process, thereby promoting the proliferation, migration and invasion of breast cancer cells, which is closely related to the prognosis of breast cancer patients. In this study, silencing lncRNA SNHG19 down-regulated the expression level of MAPK6 and suppressed the expression of EMT-related proteins, suggesting that MAPK6 is involved in the carcinogenesis of lncRNA SNHG19 in NSCLC.

In conclusion, lncRNA SNHG19 is upregulated in NSCLC tissues and cells, and its high expression is associated with tumor progression and poor survival. lncRNA SNHG19 acts as a molecular sponge for miR-299-5p to regulate MAPK6 expression and promote the proliferation and metastasis of A549 cells, which may become a new biomarker and therapeutic target for NSCLC.

Acknowledgments
Not applicable.

Funding
Not applicable.

Conflicts of interest
The authors indicated no potential conflicts of interest.

Author contributions
Not applicable.

Data availability statement
Not applicable.

Ethical approval
Not applicable.

References

1. Luo Y, Ma S, Sun Y, et al. MUC3A induces PD-L1 and reduces tyrosine kinase inhibitors effects in EGFR-mutant non-small cell lung cancer. Int J Biol Sci. 2021;17(7):1671-1681.
2. Rakhshan A, Esmaeili MH, Kahaei MS, et al. A Single Nucleotide Polymorphism in GAS5 lncRNA is Associated with Risk of Bladder Cancer in Iranian Population. Pathol Oncol Res. 2020;26(2):1251-1254.
3. Wu D, Li H, Wang J, et al. LncRNA NEAT1 promotes gastric cancer progression via miR-1294/AKT1 axis. Open Med (Wars). 2020; 15(1):1028-1038.
4. Chang YW, Hsu CL, Tang CW, et al. Multiomics reveals ectopic ATP synthase blockade induces cancer cell death via a lncRNA-mediated Phospho-signaling network. Mol Cell Proteomics. 2020;19(11):1805-1825.
5. Li XX, Wang LJ, Hou J, et al. Identification of long noncoding RNAs as predictors of survival in triple-negative breast cancer based on network analysis. Biomed Res Int. 2020;2020:8970340.
6. Cao M, Li H, Zhao J, et al. Identification of age- and gender-associated long noncoding RNAs in the human brain with Alzheimer's disease. Neurobiol Aging. 2019;81:116-126.
7. Fateh A, Feizi MAH, Safaralizadeh R, et al. Importance of miR-299-5p in colorectal cancer. Ann Gastroenterol. 2017;30(3):322-326.
8. Elkhadragy L, Alsaran H, Long W. The C-Terminus Tail regulates ERK3 kinase activity and its ability in promoting cancer cell migration and invasion. Int J Mol Sci. 2020;21(11):4044.
9. Chen X, Yang Y, Sun J, et al. LncRNA HCG11 represses ovarian cancer cell growth via AKT signaling pathway. J Obstet Gynaecol Res. 2022;48(3):796-805.
10. Xu G, Yang H, Liu M, et al. lncRNA TINCR facilities bladder cancer progression via regulating miR 7 and mTOR. Mol Med Rep. 2020; 22(5):4243-4253.
11. Wu C, Song W, Wang Z, et al. Functions of lncRNA DUXAP8 in non-small cell lung cancer. Mol Biol Rep. 2022;49(3):2531-2542.
12. Zeng SHG, Xie JH, Zeng QY, et al. lncRNA PVT1 promotes metastasis of non-small cell lung cancer through EZH2-mediated activation of Hippo/NOTCH1 signaling pathways. Cell J. 2021;23(1):21-31.
13. Wang Z, Liu L, Du Y, et al. The HNF1A-AS1/miR-92a-3p axis affects the radiosensitivity of non-small cell lung cancer by competitively regulating the JNK pathway. Cell Biol Toxicol. 2021;37(5):715-729.
14. Zhao GY, Ning ZF, Wang R. LncRNA SNHG19 promotes the development of non-small cell lung cancer via mediating miR-137/E2F7 Axis. Front Oncol. 2021;11:630241.
15. Cai Q, Zhou W, Wang W, et al. MAPK6-AKT signaling promotes tumor growth and resistance to mTOR kinase blockade. Sci Adv, 2021;7(46):eabi6439.
16. Bogucka K, Pompaiah M, Marini F, et al. ERK3/MAPK6 controls IL-8 production and chemotaxis. Elife. 2020;9:e52511.
17. Wu F, Mo Q, Wan X, et al. NEAT1/hsa-mir-98-5p/MAPK6 axis is involved in non-small-cell lung cancer development. J Cell Biochem. 2019;120(3):2836-2846.
18. Hu C, Huang S, Wu F, et al. miR-98 inhibits cell proliferation and induces cell apoptosis by targeting MAPK6 in HUVECs. Exp Ther Med. 2018;15(3):2755-2760.
19. Lv P, Qiu X, Gu Y, et al. Long non-coding RNA SNHG6 enhances cell proliferation, migration and invasion by regulating miR-26a-5p/MAPK6 in breast cancer. Biomed Pharmacother. 2019;110:294-301.

DOI 10.1007/s10330-022-0595-5
Cite this article as: Zhong Q, Qiu R. Mechanism of lncRNA SNHG19 miR-299-5p MAPK6 signaling axis promoting metastasis of non-small cell lung cancer cells. Oncol Transl Med. 2022;8(5):247–258.

Oncology and Translational Medicine
DOI 10.1007/s10330-021-0546-6
October 2022, Vol. 8, No. 5, P259–P263

ORIGINAL ARTICLE

Effects of sorafenib and regorafenib on the expression of hypoxia-inducible factors in hepatocellular carcinoma-transplanted nude mice

Ganxin Wang[1, 2], Bai Wei[1], Qian Ma[1], Shu Huang[3] (✉), Qi Wu[1]

[1] Division of Oncology, Liyuan Hospital, Tongji Medical College, Huazhong University of Science and Technology, Wuhan 430077, China
[2] Cancer Center, Union Hospital, Tongji Medical College, Huazhong University of Science and Technology, Wuhan 430022, China
[3] Department of Hepatology of Integrated Traditional Chinese and Western Medicine, The Third People's Hospital of Hubei Province Affiliated to Jianghan University, Wuhan 430056, China

Abstract

Objective The objective of this study was to investigate the inhibitory effects of sorafenib and regorafenib on the growth of hepatocellular carcinoma (HCC) using a subcutaneous transplantation tumor model in nude mice and exploring the effects of sorafenib and regorafenib on the expression of hypoxia-inducible factor (HIF)-1α, HIF-2α, and HIF-1β in HCC tissues collected from HCC-transplanted nude mice.

Methods HepG2 cells were inoculated intradermally into nude mice. The mice were randomly assigned to either sorafenib treatment (100 mg/kg), regorafenib treatment (20 mg/kg), or solvent control group (dimethylsulfoxide) (n = 8 per group) and received once-daily treatment for 14 days. The tumor volumes were recorded every 3 days after the initiation of treatment. The expression levels of HIF-1α, HIF-1β, HIF-2α, and SART1 in the HCC tissues were examined via quantitative real-time PCR (qRT-PCR) analysis and Western blotting.

Results The tumors in the sorafenib and regorafenib treatment groups grew slower and smaller than did the tumors in the solvent control group. qPCR analysis and western blotting demonstrated that the mRNA and protein expressions of HIF-1α and HIF-1β were down-regulated. The expression of HIF-2α and SART1 was up-regulated in the sorafenib treatment group (P < 0.05); meanwhile, the expression of HIF-1α and HIF-1β was up-regulated, and that of HIF-2α and SART1 was down-regulated in the regorafenib treatment group (P < 0.05).

Conclusion The expression of hypoxia-associated factor is up-regulated by sorafenib and down-regulated by regorafenib, which may induce the different effects of sorafenib on the expression of HIFs.

Received: 25 December 2021
Revised: 25 August 2022
Accepted: 20 September 2022

Key words: sorafenib; regorafenib; liver cancer; hypoxia-inducible factor; hypoxia-associated factor

In 2018, liver cancer became the sixth most common cancer and the fourth leading cause of cancer-related deaths worldwide [1]. Hepatocellular carcinoma (HCC) is one of the most common cancers, accounting for more than 90% of primary liver cancers, with approximately 850,000 new cases per year globally [2, 3]. The main curative treatment is surgical resection and liver transplantation. Most patients with HCC show intrahepatic or extrahepatic metastasis at the time of diagnosis. Therefore, the recurrence and mortality rates of HCC are high, and the prognosis remains poor [4]. In recent years, new biotargeted drugs have become available [5], providing new hope for the treatment of advanced HCC.

Studies have shown that sorafenib (BAY 43-9006), a novel multi-target drug, has broad anti-tumor and anti-angiogenic effects [6] and is a standard first-line therapeutic drug for HCC. Clinical studies have confirmed that in patients with advanced HCC and Child–Pugh A liver function, sorafenib is the only therapeutic drug that has been shown to improve overall survival in randomized

✉ Correspondence to: Shu Huang. Email: huangshu_2020@163.com

studies [7]. Regorafenib (BAY 73-4506) is a diphenylurea multikinase inhibitor that is clinically effective and well tolerated according to phase I–III clinical trials [8, 9]. On April 27, 2017, the US Food and Drug Administration approved regorafenib treatment for patients with HCC with disease progression after sorafenib treatment. Thus, regorafenib has started to be used as a second-line therapeutic drug in patients with HCC.

The rapid growth of HCC cells results in insufficient blood and oxygen supply to certain tumor tissues. The hypoxic environment accelerates tumor angiogenesis and metastasis, contributing to the development of multidrug resistance [10]. Hypoxia-inducible factor (HIF)-1 and HIF-2 are important transcription factors associated with hypoxic conditions and closely involved in the development of solid tumors [11]. Their structural domains and regulatory mechanisms are shown in Fig. 1. HIF-1 comprises a functional subunit (HIF-1α) and a constitutive subunit (HIF-1β) [12]. Our previous studies have found that an increased HIF-1α expression is a beneficial predictive factor for a poor prognosis in patients with HCC. HIF-2α may exert an anti-tumor activity by inducing apoptosis in HCC cells [13], suggesting that HIF-1α and HIF-2α may play different roles in HCC.

To date, the effects of sorafenib and regorafenib on HIF expression have not yet been studied. In the present study, we utilized a nude mouse model inoculated with human HCC cells to investigate the effects of sorafenib and regorafenib on tumor growth and HIF-1α, HIF-2α, and HIF-1β expression in HCC tumors.

Materials and methods

Reagents

Sorafenib tosylate and regorafenib tablets were purchased from Bayer AG (Leverkusen, Germany) and dissolved in dimethylsulfoxide (DMSO; MP Biomedicals, Santa Ana, CA, USA) stored at –20°C. The stock solution was diluted to a working concentration using a cell culture medium (Dulbecco's modified eagle medium [DMEM]; Gibco BRL, Grand Island, NJ, USA), and the final DMSO concentration was < 0.1%.

Cell lines and culture conditions

Human hepatoma HepG2 cells were purchased from the China Center for Type Culture Collection (Wuhan University, Wuhan, China). The cells were cultured in DMEM (Gibco BRL) containing 10% fetal bovine serum (Logan, UT, USA) and 1% penicillin–streptomycin (Mediatech, Inc., Herndon, VA, USA). The medium was changed every 2 days.

Animals and xenotransplantation

The BALB/c nude mice included in this study were half male and half female, were 4–6 weeks old, and weighed 14–20 g. Xenografts were transplanted according to the method published by Yang *et al.* [13]. The tumor diameters were measured every 3 days after the initiation of dosing until Day 15. The largest (a) and smallest (b) diameters were measured, and the tumor volume was calculated using the following formula: V (mm^3) = $ab^2/2$. The

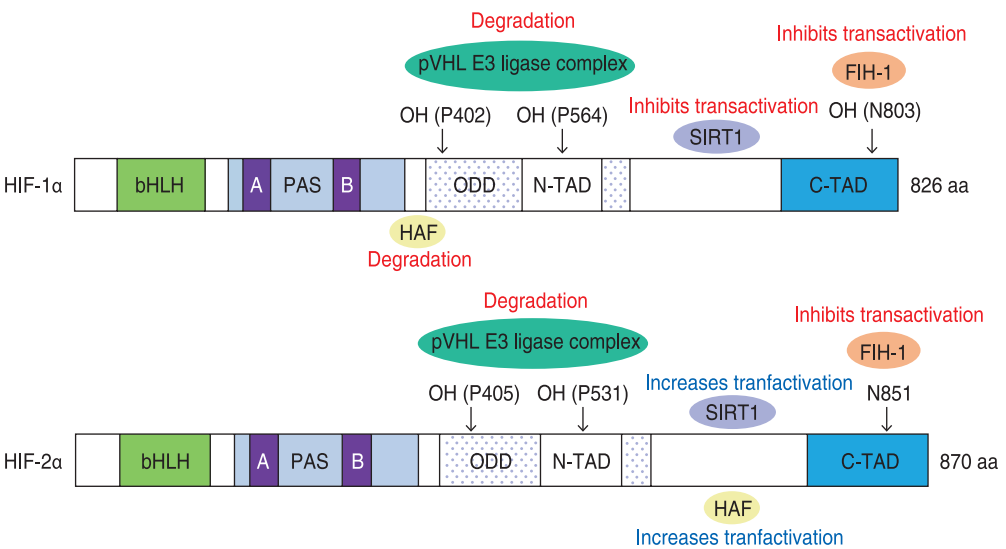

Fig. 1 Structural domains of hypoxia-inducible factor (HIF)-1/2α and their post-translational protein modifications. The von Hippel–Lindau protein (pVHL) E3 ligase complex regulates the oxygen-dependent degradation of HIF-1α and HIF-2α. Hypoxia-associated factor (HAF) causes HIF-1α ubiquitylation and degradation but promotes HIF-2α transactivation under prolonged hypoxia. Sirtuin 1 (SIRT1) selectively binds to HIF-1α and HIF-2α, mediating degradation and transactivation, respectively

xenografted mice were randomly assigned to either of the following three groups (n = 8 per group): sorafenib treatment (100 mg/kg/day), regorafenib treatment (20 mg/kg/day), and solvent control groups (DMSO). The animals were dosed via oral gavage once daily for 14 days (the first day of treatment was considered as Day 1). The tumor growth rates in the sorafenib and regorafenib treatment groups were compared with that in the solvent control group over time. The mice were sacrificed 24 h after the last administration, and their tumors were separated. Representative tumor tissues were frozen immediately in liquid nitrogen for quantitative real-time PCR (qPCR) analysis and western blotting.

qPCR analysis and western blotting

qPCR analysis and western blotting were performed as previously described [14]. The following PCR primers synthesized by Google Biotechnology Co., Ltd. (Wuhan, China) were used in this study: HIF-1α forward: 5'-ACTTCTGGATGCTGGTGATTTG-3', reverse: 5'-GCTTCGCTGTGTGTTTTGTTCT-3'; HIF-2α forward: 5'-TCATGCGACTGGCAATCAGC-3', reverse: 5'-GTCACCACGGCAATGAAACC-3'; HIF-1β forward: 5'-TCGCGTCCTTCTTCATCCGTTAGC-3', reverse: 5'-TTTCGAGCCAGGGCACTACAGG-3'; SART1 forward: 5'-AAGTACAGCCGGAGGGAGGAATAC-3', reverse: 5'-TTCATCTTGCCTGAGCCCTTG-3'; and GAPDH forward: 5'-TCGACAGTCAGCCGCATCTTCTTT-3', reverse: 5'-GCCCAATACGACCAAATCCGTTGA-3'. GAPDH was used as an internal control for both qPCR analysis and Western blotting. Anti-HIF-1α, anti-HIF-2α, anti-HIF-1β, and anti-SART1 antibodies were purchased from Proteintech Group, Inc. (Chicago, IL, USA).

Statistical analysis

SPSS version 22.0 (SPSS Inc., Chicago, IL, USA) was used for the statistical analysis. Data were expressed as means ± standard deviations ($\chi \pm s$). Two-group comparisons were performed using an independent-samples t-test and multiple-group comparisons using the least significant difference test. P values of < 0.05 were considered statistically significant.

Results

Growth of transplanted HCC in the nude mice

All nude mice (n = 24) across the treatment groups survived during the dosing period, with a tumor formation rate of 100%. The tumor growth curve (Fig. 2a) revealed that the tumor growth rates of the sorafenib and regorafenib treatment groups were significantly lower than those of the solvent control group. After the last dose administration on Day 15, the HCC tumors were separated. As shown in Fig. 2b, the tumors of the sorafenib and regorafenib treatment groups were markedly smaller than those of the solvent control group.

Expression of HIF-1α, HIF-2α, HIF-1β, and SART1 in the HCC cells

At the mRNA level, there were significant decreases in the HIF-1α and HIF-1β expression and significant increases in the HIF-2α and SART1 expression following treatment in the sorafenib treatment group compared with those in the solvent control group (P < 0.05) (Fig. 3a). In contrast, the HIF-1α and HIF-1β expression was up-regulated, and the HIF-2α and SART1 expression was down-regulated in the regorafenib treatment group (P < 0.05). These changes in expression at the mRNA level were confirmed at the protein level by western blotting (Fig. 3b).

Discussion

HCC is a malignancy with high morbidity and mortality rates. Hepatitis B virus (HBV) infection is one of the leading causes of HCC. Globally, approximately 54.4% of HCC cases are attributed to chronic infection with HBV, and the proportion can reach as high as 80% in Chinese and Black African populations [15]. HIFs are the master regulators of gene expression in hypoxic conditions and play a central role in the regulation of human metabolism. The expression of hepatitis B virus X protein (HBx)

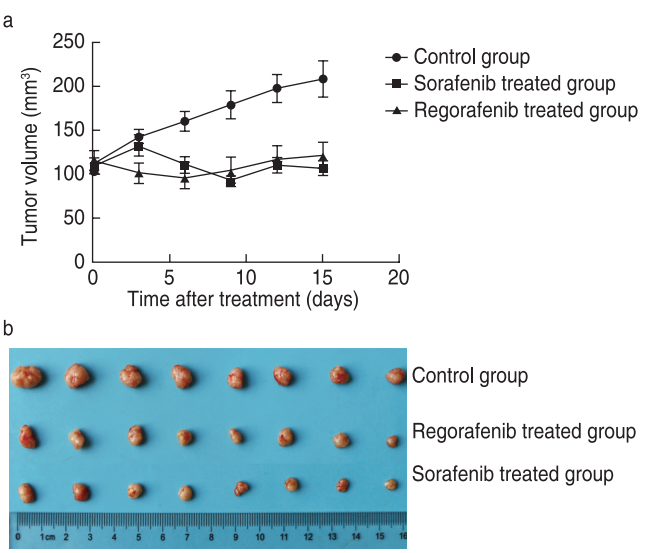

Fig. 2 (a) Tumor growth curves of BALB/c nude mice in the sorafenib treatment (square symbol), regorafenib treatment (triangle symbol), and solvent control groups (circle symbol). The tumor growth in the sorafenib and regorafenib treatment groups significantly slowed down; (b) Sizes of stripped tumor tissues from the sorafenib treatment, regorafenib treatment, and solvent control groups after 15 days of treatment. At the end of drug administration, the tumors in the sorafenib and regorafenib treatment groups were smaller than those in the solvent control group

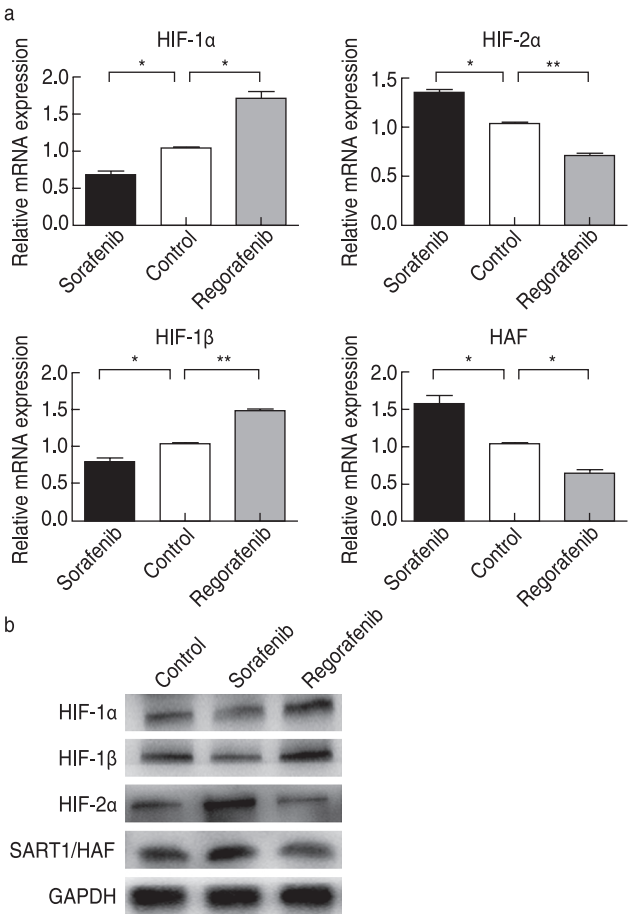

Fig. 3 (a) mRNA expression levels of hypoxia-inducible factor (HIF)-1α, HIF-2α, HIF-1β, and SART1 analyzed via quantitative real-time PCR testing. The mRNA expression levels of HIF-1α and HIF-1β significantly decreased, while those of HIF-2α and SART1 significantly increased in the sorafenib treatment group compared with those in the solvent control group. In contrast, the mRNA expression of HIF-1α and HIF-1β was up-regulated, while that of HIF-2α and SART1 was down-regulated in the regorafenib treatment group. *P < 0.01, **P < 0.001; (b) Protein expression of HIF-1α, HIF-2α, HIF-1β, and HAF examined via western blotting. The expression of these genes at the protein level coincided with their expression at the mRNA level. GAPDH was used as a loading control

has been reported to be positively correlated with the expression of HIF-α in patients with HBV-related HCC [16]. HBx can modulate chemoresistance by activating HIF-1α and increasing the HIF-2α expression level via inhibition of HIF-2α degradation [17]. The novel anticancer drugs sorafenib and regorafenib have been widely used in the systemic treatment of patients with HCC; however, it is unclear whether these two drugs affect the expression of HIF-1 and HIF-2.

In this study, we confirmed the inhibitory effects of sorafenib and regorafenib on the growth of HCC tumors using a nude mouse model, which is consistent with previous reports. Through qPCR analysis and western blotting, we found that sorafenib down-regulated the

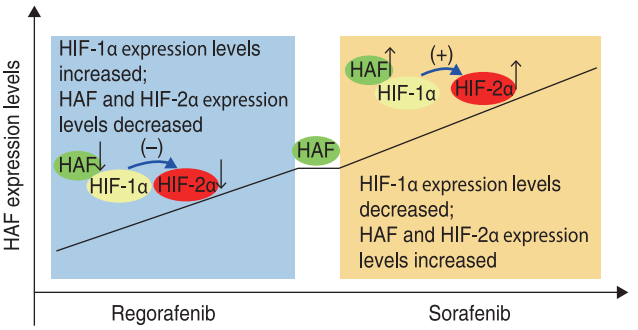

Fig. 4 Different effects between sorafenib and regorafenib on the expression of HIFs. The HAF and HIF-2α expression levels decreased, while the HIF-1α expression level increased after regorafenib treatment. Meanwhile, the HAF expression level increased after sorafenib treatment, providing a mechanism for the switch from HIF-1α to HIF-2α. This is a possible reason for the decrease in the HIF-1α expression level and increase in the HIF-2α expression level after sorafenib administration

expression of HIF-1α and HIF-1β and up-regulated that of HIF-2α. In contrast, regorafenib up-regulated the expression of HIF-1α and HIF-1β and down-regulated that of HIF-2α. These results demonstrate the opposite effects of these two drugs on the expression of HIF-1 and HIF-2. In addition, qPCR analysis and western blotting showed that the expression of SART1 was significantly up-regulated by sorafenib but down-regulated by regorafenib.

Hypoxia-associated factor (HAF, encoded by SART1) is expressed in both normal and malignant tissues [18]. It triggers HIF-1α ubiquitylation and degradation and promotes HIF-2α transactivation under prolonged hypoxia. Studies have shown that overexpression of HAF decreases the HIF-1α expression level, whereas knockdown of HAF increases the HIF-1α expression level independent of the presence of oxygen [19, 20]. These findings have also been demonstrated in other mouse HCC models [21]. In addition, a study on bladder cancer found that HIF-1α can switch to HIF-2α owing to HAF-mediated activation of the NF-κB pathway [22]. The present study showed that the expression of HAF was up-regulated by sorafenib and down-regulated by regorafenib, which may explain the opposing effects of sorafenib and regorafenib on the expression of HIFs (Fig. 4).

We have previously demonstrated that a higher expression of HIF-1α is correlated with a poor prognosis in patients with HCC. Although the role of HIF-2α remains controversial, most studies have shown that patients with HCC with a high expression of HIF-2α had a better prognosis. In this study, we found that sorafenib inhibited the expression of HIF-1α and activated the expression of HIF-2α via up-regulation of the expression of HAF, which may provide an explanation for the clinical effectiveness of sorafenib. In the future, we will

further investigate how HAF regulates HIFs and explore the option of combination therapy for HCC.

Acknowledgments
Not applicable.

Funding
Not applicable.

Conflicts of interest
All authors have completed the ICMJE uniform disclosure form. The authors have no conflicts of interest to declare.

Author contributions
All authors collected and interpreted the data and reviewed and approved the final version of the manuscript.

Data availability statement
All data generated or analyzed during this study are included in this published article (and the accompanying supplementary information files).

Ethical approval
Not applicable.

References

1. Bray F, Ferlay J, Soerjomataram I, et al. Global cancer statistics 2018: GLOBOCAN estimates of incidence and mortality worldwide for 36 cancers in 185 countries. CA Cancer J Clin. 2018;68(6):394-424.
2. Molina-Sánchez P, Lujambio A. Strategies for HCC target discovery. Aging (Albany NY). 2017;9(4):1088-1089.
3. Ding XX, Zhu QG, Zhang SM, et al. Precision medicine for hepatocellular carcinoma: driver mutations and targeted therapy. Oncotarget. 2017;8(33):55715-55730.
4. Gosalia AJ, Martin P, Jones PD. Advances and future directions in the treatment of hepatocellular carcinoma. Gastroenterol Hepatol (N Y). 2017;13(7):398-410.
5. Chen C, Wang G. Mechanisms of hepatocellular carcinoma and challenges and opportunities for molecular targeted therapy. World J Hepatol. 2015;7(15):1964-1970.
6. Xia S, Pan Y, Liang Y, et al. The microenvironmental and metabolic aspects of sorafenib resistance in hepatocellular carcinoma. EBioMedicine. 2020;51:102610.
7. Finn RS, Zhu AX, Farah W, et al. Therapies for advanced stage hepatocellular carcinoma with macrovascular invasion or metastatic disease: A systematic review and meta-analysis. Hepatology. 2018;67(1):422-435.
8. Bruix J, Qin S, Merle P, et al. Regorafenib for patients with hepatocellular carcinoma who progressed on sorafenib treatment (RESORCE): a randomised, double-blind, placebo-controlled, phase 3 trial. Lancet. 2017;389(10064):56-66.
9. Juengpanich S, Topatana W, Lu C, et al. Role of cellular, molecular and tumor microenvironment in hepatocellular carcinoma: Possible targets and future directions in the regorafenib era. Int J Cancer. 2020;147(7):1778-1792.
10. Jing X, Yang F, Shao C, et al. Role of hypoxia in cancer therapy by regulating the tumor microenvironment. Mol Cancer. 2019;18(1):157.
11. Cao S, Yang S, Wu C, et al. Protein expression of hypoxia-inducible factor-1 alpha and hepatocellular carcinoma: a systematic review with meta-analysis. Clin Res Hepatol Gastroenterol. 2014;38(5):598-603.
12. Lee SH, Golinska M, Griffiths JR. HIF-1-independent mechanisms regulating metabolic adaptation in hypoxic cancer cells. Cells. 2021;10(9):2371.
13. Yang SL, Liu LP, Niu L, et al. Downregulation and pro-apoptotic effect of hypoxia-inducible factor 2 alpha in hepatocellular carcinoma. Oncotarget. 2016;7(23):34571-34581.
14. Yu C, Yang SL, Fang X, et al. Hypoxia disrupts the expression levels of circadian rhythm genes in hepatocellular carcinoma. Mol Med Rep. 2015;11(5):4002-4008.
15. Xia BW, Zhang YC, Wang J, et al. Efficacy of antiviral therapy with nucleotide/nucleoside analogs after curative treatment for patients with hepatitis B virus-related hepatocellular carcinoma: A systematic review and meta-analysis. Clin Res Hepatol Gastroenterol. 2015;39(4):458-468.
16. Xie H, Song J, Liu K, et al. The expression of hypoxia-inducible factor-1alpha in hepatitis B virus-related hepatocellular carcinoma: correlation with patients' prognosis and hepatitis B virus X protein. Dig Dis Sci. 2008;53(12):3225-3233.
17. Hu JL, Liu LP, Yang SL, et al. Hepatitis B virus induces hypoxia-inducible factor-2α expression through hepatitis B virus X protein. Oncol Rep. 2016;35(3):1443-1448.
18. Sasatomi T, Yamana H, Shichijo S, et al. Expression of the SART1 tumor-rejection antigens in colorectal cancers. Dis Colon Rectum. 2000;43(12):1754-1758.
19. Koh MY, Darnay BG, Powis G. Hypoxia-associated factor, a novel E3-ubiquitin ligase, binds and ubiquitinates hypoxia-inducible factor 1alpha, leading to its oxygen-independent degradation. Mol Cell Biol. 2008;28(23):7081-7095.
20. Koh MY, Powis G. HAF : the new player in oxygen-independent HIF-1alpha degradation. Cell Cycle. 2009;8(9):1359-1366.
21. Koh MY, Gagea M, Sargis T, et al. A new HIF-1α/RANTES-driven pathway to hepatocellular carcinoma mediated by germline haploinsufficiency of SART1/HAF in mice. Hepatology. 2016;63(5):1576-1591.
22. Guan Z, Ding C, Du Y, et al. HAF drives the switch of HIF-1α to HIF-2α by activating the NF-κB pathway, leading to malignant behavior of T24 bladder cancer cells. Int J Oncol. 2014;44(2):393-402.

DOI 10.1007/s10330-021-0546-6
Cite this article as: Wang GX, Wei B, Ma Q, et al. Effects of sorafenib and regorafenib on the expression of hypoxia-inducible factors in hepatocellular carcinoma-transplanted nude mice. Oncol Transl Med. 2022;8(5):259–263.

Oncology and Translational Medicine
DOI 10.1007/s10330-022-0592-2

October 2022, Vol. 8, No. 5, P264–P266

CASE REPORT

Gastric signet-ring cell carcinoma with paraneoplastic eosinophilia: A case report and literature review

Shuguo Wang[1] , Haixia Wang[2] , Ping Sui[3] , Bo Han[2] (✉)

[1] Clinical Laboratory, Qingdao Municipal Hospital (Group), Qingdao 266011, China
[2] Department of Hematology, Qingdao Hospital of Traditional Chinese Medicine (Qingdao Hiser Hospital), Qingdao 266033, China
[3] Department of Medical Oncology, The Affiliated Yuhuangding Hospital of Qingdao University, Qingdao 264099, China

Abstract

We report the case of a 40-year-old female Chinese patient with gastric signet-ring cell carcinoma that was first diagnosed because of paraneoplastic eosinophilia. The patient's eosinophil count reduced markedly to normal levels within 24 h after radical gastrectomy and Billroth II anastomosis. The patient recovered well after the surgery and no abnormalities were found during the regular follow-ups. Paraneoplastic eosinophilia is an unusual manifestation that usually remains asymptomatic; moreover, cases of solid malignant tumors with eosinophilia are uncommon. To our knowledge, this is the first reported case of paraneoplastic eosinophilia in a patient with gastric carcinoma. We considered eosinophilia as a manifestation of a paraneoplastic syndrome, which can be the first clinical manifestation of a malignancy.

Received: 4 Augustl 2022
Revised: 12 September 2022
Accepted: 8 October 2022

Key words: eosinophilia; paraneoplastic syndrome; gastric signet-ring cell carcinoma

A 40-year-old Chinese female patient with two week history of epigastric discomfort was admitted to our hospital on September 1, 2016. Physical examination findings were unimpressive, and there was no significant decrease in performance status according to the patient's history. She was a life-long non-smoker without a history of allergic or parasitic diseases. An abdominal computed tomography (CT) scan only revealed a lightly thickened gastric wall and a small amount of pelvic effusion. The peripheral blood leukocyte count was normal at 5,110/μL. However, 24.5% of the leukocytes were mature eosinophils (absolute eosinophil count, 1,250/μL); this eosinophil ratio is significantly higher than normal (reference range, 0–4.5%). Immunological tests showed no remarkable findings. Serum tumor markers were as follows: CEA: 0.541 ng/mL, CA 19-9: 3.90 U/mL, and CA72-4: 0.863 U/mL. The patient declined a bone marrow biopsy. Gastroscopy and biopsy findings were suggestive of a malignant gastric carcinoma, and a part of the pathological type demonstrated gastric signet-ring-cell carcinoma. Contrast-enhanced chest CT was performed, and no cancerous lesions were observed. Radical gastrectomy for gastric cancer and Billroth II anastomosis were performed on September 5, after excluding all contraindications. Histological and pathological examinations confirmed the diagnosis of a (stomach) signet-ring-cell adenocarcinoma, located in the lamina propria, and the cutting edge was negative for malignant cells. Immunohistochemical results revealed the following: CK8/18 (+); CEA (+); HER2 (0); positive rate of Ki-67, approximately 20%; TNM stage, T1N0M0; and AJCC stage, IA. Her white blood cell count was 6500/μL, of which 360/μL were eosinophils 1 day postoperatively. At 5 and 20 days postoperatively, the percentages of peripheral eosinophils were both less than 5%, and the absolute counts were 602/μL and 462/μL, respectively. According to the National Comprehensive Cancer Network guidelines, postoperative adjuvant chemotherapy is not recommended for stage IA gastric carcinoma. The patient recovered appropriately after surgery, and no abnormalities were found during her regular follow-ups.

✉ Correspondence to: Bo Han. Email: hbdoctor@126.com

Discussion

Eosinophilia (absolute eosinophil counts in peripheral blood exceeding 450–550 cells/μL, depending on laboratory standards) is a hallmark of or a related finding in many allergic, infectious, autoimmune, idiopathic, malignant, and miscellaneous clinical scenarios [1, 2]. Eosinophils typically make up approximately 1–5% of all peripheral blood leukocytes[3, 4]. The patient in this case was a middle-aged woman who was admitted to our hospital with a complaint of only upper abdominal discomfort. There was no significant decrease in performance status according to the patient's history. Physical examination did not find any mass in the abdominal region. Routine blood examination revealed that her peripheral blood leukocyte count was 5110/μL (reference range: 4000–9500/μL), and 24.5% (reference range: 0–4.5%) of the leukocytes were mature eosinophils. No other abnormal laboratory findings were observed. The abdominal CT scan revealed only slight thickening in the gastric wall. The patient had no history of smoking, specific drug use, food allergies, parasitic infections, or exposure to tuberculosis. Parasites and their ova were not found in the patient's stool.

Eosinophilia is considered one of the manifestations of a paraneoplastic syndrome. Paraneoplastic eosinophilia is an unusual manifestation that usually remains asymptomatic [5, 7]. The clinical significance of paraneoplastic eosinophilia is undefined8. Paraneoplastic eosinophilia is uncommon in solid tumors, but it has been reported in several malignancies, including colorectal, lung, renal, cervical, head, and neck squamous cell carcinomas, Hodgkin's lymphoma, and prostate cancer [8–12]. In Table 1, we have listed important and relatively interesting clinical case reports of solid malignant tumors with paraneoplastic eosinophilia.

The pathogenesis of hypereosinophilia in solid malignant tumors is controversial and dubious. Scientists have postulated numerous explanations. Bone marrow stimulation via circulatory factors secreted by tumors is the most acknowledged and accepted theory [12, 13]. Interleukin-5, GM-CSF, and G-CSF are the most commonly implicated factors; however, the involvement of other factors remains possible. Moreover, the ectopic endocrine function of tumors which stimulates the proliferation of the bone marrow is another widely accepted theory [14, 15].

Whether an increase in eosinophils leads to a favorable or an unfavorable prognosis remains controversial [7, 16]. Most studies suggest that paraneoplastic eosinophilia reflects a more advanced disease and poor prognosis8. The patient in our report had hypereosinophilia on admission, but her eosinophil count dropped sharply to normal levels within 24 h of malignant tumor surgery. This indirectly supports the suggestion that eosinophilia in the context of a malignancy generally reflects the aggressiveness and poor prognosis of the malignancy. Our case has unique features that are worth reporting. Paraneoplastic eosinophilia in solid malignant tumors is very rare. To our knowledge, this is the first reported case of paraneoplastic eosinophilia occurring concurrently with gastric carcinoma. The patient was diagnosed with gastric signet-ring cell carcinoma, which is a pathological type with a relatively severe malignant degree. However, the tumor was still in a very early stage and could be completely surgically removed, because of early diagnosis prompted by her extremely elevated eosinophil count. Furthermore, as a paraneoplastic syndrome, eosinophilia may be considered as a predictor of early malignant tumors in the future. Do we consider the possibility of a tumor only after excluding all underlying diseases that could lead to eosinophilia, or is it possible to use eosinophil levels as a predictive factor or antitumor biomarker? We hope that our case report provides scientists with some

Table 1 Demographic and clinical characteristics of patients with malignant tumor and eosinophilia

Literature	Age (years)	Sex	Pathologic type	pTNM stage	Therapeutic strategy	Absolute eosinophil count (/μL)		Year
						Before the treatment	After the treatment	
Renu Pandit	72	Male	Non-small cell lung cancer	IIIA	Surgery	90,000	0	2006 [12]
Weiwei Zhou	75	Male	Clear cell renal cell carcinoma	pT3aN1M0, G4	Surgery	3,660–4,200	Normal level	2015 [8]
Axel Balian	60	Male	Hepatocellular carcinoma	No data	Surgery	1,500	Normal level	2008 [9]
El-Osta H	53	Male	Large cell lung carcinoma	IV stage	Palliative chemotherapy	14,560	53,760	2008 [10]
Walter R	66	Male	Head and neck squamous carcinoma	IV stage T4N2cM0	Radiotherapy and chemotherapy	9,700	Patient died	2002 [11]
Hiroki Kato	72	Female	Colon adenocarcinoma	IV stage	Prednisolone and hydroxyurea	141,580	Patient died	2010 [17]

insights on further explorations.

Acknowledgments

Not applicable.

Funding

Not applicable.

Conflicts of interest

The authors declared that they have no conflicts of interest.

Author contributions

Shuguo Wang and Ping Sui collected data and wrote the original draft. Haixia Wang re-collected the data and revised the manuscript. Bo Han conceived the manuscript and revised it. All authors read and approved the final manuscript.

Data availability statement

The data that support the findings of this study are available from the corresponding author upon reasonable request.

Ethical approval

Not applicable.

References

1. Andriamanantena D, Boye T, Gervaise A, et al. An unusual paraneoplastic manifestation in lung cancer: eosinophilic erythroderma. Rev Pneumol Clin. 2009;65(1):32-35.
2. Klion AD. Eosinophilia: a pragmatic approach to diagnosis and treatment. Hematol-Am Soc Hematol Educ Program. 2015:92-97.
3. Kovalszki A, Weller PF. Eosinophilia. Prim Care. 2016:43(4):607-617.
4. Haddad H, Sundaram S, Magro C, et al. Eosinophilic fasciitis as a paraneoplastic syndrome, a case report and review of the literature. Hematol Oncol Stem Cell Ther. 2014;7(2):90-92.
5. Samiullah, Bhurgri H, Sohail U. Eosinophilic disorders of the gastrointestinal tract. Prim Care. 2016;43(3):495-504.
6. Davis BP, Rothenberg ME. Eosinophils and cancer. Cancer Immunol Res. 2014;2(1):1-8.
7. Sakkal S, Miller S, Apostolopoulos V, et al. Eosinophils in cancer: favourable or unfavourable? Curr Med Chem. 2016;23(7):650-666.
8. Zhou WW, Guan YY, Liu XM. Paraneoplastic eosinophilia in clear cell renal cell carcinoma. Chin Med J. 2015;128(16):2271-2272.
9. Balian A, Bonte E, Naveau S, et al. Intratumoral production of interleukin-5 leading to paraneoplastic peripheral eosinophilia in hepatocellular carcinoma. J Hepatol. 2001;34(2):355-356.
10. El-Osta H, El-Haddad P, Nabbout N. Lung carcinoma associated with excessive eosinophilia. J Clin Oncol. 2008;26(20):3456-3457.
11. Walter R, Joller-Jemelka HI, Salomon F. Metastatic squamous cell carcinoma with marked blood eosinophilia and elevated serum interleukin-5 levels. Exp Hematol. 2002;30(1):1-2.
12. Pandit R, Scholnik A, Wulfekuhler L, et al. Non-small-cell lung cancer associated with excessive eosinophilia and secretion of interleukin-5 as a paraneoplastic syndrome. Am J Hematol. 2007;82(3):234-237.
13. Holroyd DJ, Banerjee S, Chaudhary KS, et al. Transmural eosinophilic gastritis with gastric outlet obstruction: case report and review of the literature. Ann R Coll Surg Engl. 2010;92(4):W18-20.
14. Gotlib J. World Health Organization-defined eosinophilic disorders: 2014 update on diagnosis, risk stratification, and management. Am J Hematol. 2014;89(3):325-337.
15. Kim TH, Song MJ, Lee JH, et al. Bleeding from a gastric subepithelial tumor associated with eosinophilia. Gastrointest Endosc. 2015;81(5):1284-1285.
16. Rothenberg ME. Humanized Anti-IL-5 antibody therapy. Cell 2016;165(3):509.
17. Kato H, Kohata K, Yamamoto J, et al. Extreme eosinophilia caused by interleukin-5-producing disseminated colon cancer. Int J Hematol. 2010;91(2):328-330.

DOI 10.1007/s10330-022-0592-2
Cite this article as: Wang SG, Wang HX, Sui P, et al. Gastric signet-ring cell carcinoma with paraneoplastic eosinophilia: A case report and literature review. Oncol Transl Med. 2022;8(5):264–266.

Call For Papers
Oncology and Translational Medicine

(CN 42-1865/R, ISSN 2095-9621)

Dear Authors,

Oncology and Translational Medicine (OTM), a peer-reviewed open-access journal, is very interested in your study. If you have unpublished papers in hand and have the idea of making our journal a vehicle for your research interests, please feel free to submit your manuscripts to us via the Paper Submission System.

Aims & Scope

- Lung Cancer
- Liver Cancer
- Pancreatic Cancer
- Gastrointestinal Tumors
- Breast Cancer
- Thyroid Cancer
- Bone Tumors
- Genitourinary Tumors
- Brain Tumor
- Blood Diseases
- Gynecologic Oncology
- ENT Tumors
- Skin Cancer
- Cancer Translational Medicine
- Cancer Imageology
- Cancer Chemotherapy
- Radiotherapy
- Tumors Psychology
- Other Tumor-related Contents

Contact Us
Editorial office of Oncology and Translational Medicine
Tongji Hospital
Tongji Medical College
Huazhong University of Science and Technology
Jie Fang Da Dao 1095
430030 Wuhan, China
Tel.: 86-27-69378388
Email: dmedizin@tjh.tjmu.edu.cn;
dmedizin@sina.com

Oncology and Translational Medicine (OTM) is sponsored by Tongji Hospital, Tongji Medical College, Huazhong University of Science and Technology, China (English, bimonthly).

OTM mainly publishes original and review articles on oncology and translational medicine. We are working with the commitment to bring the highest quality research to the widest possible audience and share the research work in a timely fashion.

Manuscripts considered for publication include regular scientific papers, original research, brief reports and case reports. Review articles, commentaries and letters are welcome.

About Us

- Peer-reviewed
- Rapid publication
- Online first
- Open access
- Both print and online versions

For more information about us, please visit:
http://otm.tjh.com.cn